IOWA STATE UNIVERSITY
Digital Repository

Retrospective Theses and Dissertations

Iowa State University Capstones, Theses and Dissertations

1995

The manipulation of interfacial architecture for chemical analysis

Man-Kit Ho
Iowa State University

Follow this and additional works at: https://lib.dr.iastate.edu/rtd

Part of the Analytical Chemistry Commons

Recommended Citation
Ho, Man-Kit, "The manipulation of interfacial architecture for chemical analysis " (1995). *Retrospective Theses and Dissertations*. 11059.
https://lib.dr.iastate.edu/rtd/11059

This Dissertation is brought to you for free and open access by the Iowa State University Capstones, Theses and Dissertations at Iowa State University Digital Repository. It has been accepted for inclusion in Retrospective Theses and Dissertations by an authorized administrator of Iowa State University Digital Repository. For more information, please contact digirep@iastate.edu.

المنارة للاستشارات

www.manaraa.com

INFORMATION TO USERS

This manuscript has been reproduced from the microfilm master. UMI films the text directly from the original or copy submitted. Thus, some thesis and dissertation copies are in typewriter face, while others may be from any type of computer printer.

The quality of this reproduction is dependent upon the quality of the copy submitted. Broken or indistinct print, colored or poor quality illustrations and photographs, print bleedthrough, substandard margins, and improper alignment can adversely affect reproduction.

In the unlikely event that the author did not send UMI a complete manuscript and there are missing pages, these will be noted. Also, if unauthorized copyright material had to be removed, a note will indicate the deletion.

Oversize materials (e.g., maps, drawings, charts) are reproduced by sectioning the original, beginning at the upper left-hand corner and continuing from left to right in equal sections with small overlaps. Each original is also photographed in one exposure and is included in reduced form at the back of the book.

Photographs included in the original manuscript have been reproduced xerographically in this copy. Higher quality 6" x 9" black and white photographic prints are available for any photographs or illustrations appearing in this copy for an additional charge. Contact UMI directly to order.

UMI

A Bell & Howell Information Company
300 North Zeeb Road, Ann Arbor, MI 48106-1346 USA
313/761-4700 800/521-0600

The manipulation of interfacial architecture for chemical analysis

by

Man-Kit Ho

A Dissertation Submitted to the
Graduate Faculty in Partial Fulfillment of the
Requirements for the Degree of
DOCTOR OF PHILOSOPHY

Department: Chemistry
Major: Analytical Chemistry

Approved:

Signature was redacted for privacy.

In Charge of Major Work

Signature was redacted for privacy.

For the Major Department

Signature was redacted for privacy.

For the Graduate College

Iowa State University
Ames, Iowa

1995

UMI Number: 9610960

UMI Microform 9610960
Copyright 1996, by UMI Company. All rights reserved.

This microform edition is protected against unauthorized
copying under Title 17, United States Code.

UMI
300 North Zeeb Road
Ann Arbor, MI 48103

TABLE OF CONTENTS

ACKNOWLEDGMENT v

GENERAL INTRODUCTION 1

Dissertation Organization 1

Introduction 1

CHAPTER 1. SPONTANEOUSLY ADSORBED MONOLAYERS OF THIOL-CONTAINING α- AND β- CYCLODEXTRIN DERIVATIVES AT GOLD SURFACES: FORMATION, STRUCTURE, AND GUEST-HOST INTERACTIONS 6

ABSTRACT 6

INTRODUCTION 7

EXPERIMENTAL SECTION 9

RESULTS AND DISCUSSION 17

CONCLUSIONS 52

APPENDIX--DETERMINATION OF INFRARED SPECTROSCOPIC BAND ASSIGNMENTS FOR THIOL-CONTAINING CYCLODEXTRIN DERIVATIVES (**6** AND **7**) 53

ACKNOWLEDGMENT 55

REFERENCES 55

CHAPTER 2. THIOL-DERIVATIZED METALLOPORPHYRINS: MONOMOLECULAR FILMS FOR THE ELECTROCATALYTIC REDUCTION OF DIOXYGEN AT GOLD ELECTRODES 60

ABSTRACT 60

RESULTS AND DISCUSSION 61

ACKNOWLEDGMENT 72

REFERENCES AND NOTES 73

CHAPTER 3. ELECTROCHEMICAL OXIDATION OF AMINE-CONTAINING COMPOUNDS: A ROUTE TO THE SURFACE MODIFICATION OF GLASSY CARBON ELECTRODES 77

ABSTRACT 77

INTRODUCTION 78

EXPERIMENTAL 80

RESULTS AND DISCUSSION 84

CONCLUSIONS 104

ACKNOWLEDGMENTS 105

REFERENCES AND NOTES 105

CHAPTER 4. SURFACTANT MODIFIED EMLC
PART I: EFFECT OF CATIONS ON SEPARATION 108

ABSTRACT 108

INTRODUCTION 109

EXPERIMENTAL SECTION 113

RESULTS AND DISCUSSION 114

CONCLUSIONS 122

ACKNOWLEDGMENT 123

REFERENCES 123

CHAPTER 5. SURFACTANT MODIFIED EMLC PART II: MANIPULATION OF CHIRAL SEPARATION SELECTIVITY 125

ABSTRACT 125

INTRODUCTION 126

EXPERIMENTAL SECTION 127

THEORY/MODEL 128

RESULTS AND DISCUSSION 131

CONCLUSIONS 143

ACKNOWLEDGMENT 144

REFERENCES 145

SUMMARY, DISCUSSION, AND PERSPECTIVE 147

REFERENCES 152

ACKNOWLEDGMENT

I would like to express my gratitude to my major professor, Prof. Marc D. Porter, for his guidance, advice, and encouragement throughout the years. Also, I would like to thank the Porter group members, both past and present, for providing so many enjoyable moments. Thanks is also extended to Dr. Alan Schwabacher, Dr. Chinkap Chung, Dr. Keith Woo, Dr. Jerzy Zak, and Dr. Hongping Yuan for their helpful discussions. Last and most important, I would like to thank my parents, sisters and brother for their support, help and priceless love over the years.

This work was supported by US D.O.E. at Iowa State University under Contract No. w-7405-eng-82.

GENERAL INTRODUCTION

Dissertation Organization

This dissertation explores the role and manipulation of the interfacial structure in chemical analysis. The introduction section, which precedes five papers, provides a brief overview of the research described in each chapter. Chapter 1 discusses the design and fabrication of thiol-derivatized cyclodextrin monolayers at gold for the studies of molecular recognition properties. Chapter 2 investigates the effect of the interfacial structure on the catalytic potency of metalloporphyrin monolayers at gold. Chapter 3 discusses a new route for the modification of glassy carbon surfaces. Finally, Chapters 4 and 5 investigate a novel approach to modify the selectivity of electrochemically modulated liquid chromatography (EMLC)-based separations by using the deposition of surfactant-like molecules at the stationary phase. The dissertation concludes with a general summary and discussion of the results, possible future research directions, and lists the references cited in the introduction.

Introduction

The fabrication and manipulation of interfacial architectures are of importance to many research areas in analytical chemistry [1-3]. The importance stems from the critical role of liquid- and gas-solid interfaces in a host of transduction mechanisms that rely on the specificity and extent of the interactions between an analyte and a modified surface. For example, the modification of an electrode surface can transform a comparatively nonselective electron-transfer process to one with an enhanced specificity based on the identity [4], size [5-10], and hydrophobicity/hydrophilicity [11] of an electroactive species. Similar advances have been realized through the manipulation of the molecular architecture at the surface of piezoelectric [12-13] and fiber optic-based sensors [14] and of chromatographic stationary phases [15].

Studies of the design and fabrication of surfaces with specific interfacial architectures are the focus of Chapter 1 and 2. Several recent studies have shown that organosulfur compounds spontaneously form well-organized, compact monolayers at gold surfaces [16-20]. This approach provides an excellent pathway for the construction of interfaces with specific structures and chemical and physical properties. This approach also has been used for constructing model systems for the studies of a variety of fundamental issues pertaining to interfacial processes including wetting [21-22] and heterogeneous electron transfer [23-24]. As part of an effort to study and to gain control of interfacial reactivity at the molecular level, the papers in Chapters 1 and 2 discuss the fabrication of interfaces for specific analytical functions using “thiols on gold” chemistry. The paper in Chapter 1 targets the creation of an interfacial structure that will exhibit selectivity via a molecular recognition process. Fabrication of monolayers with molecular recognition properties has been the subject of several recent studies [4-8, 25-31]. The work presented in this chapter focuses on the construction of monolayers with well-defined binding cavities for the complexation of sterically acceptable molecules. The strategy is to transfer the well-known host-guest chemistry of cyclodextrins to gold surfaces by the synthesis of thiol-derivatives of α- and β-cyclodextrins. As discussed, the derivatives were designed to yield a monolayer with the cavity of the immobilized cyclodextrin oriented along the surface normal, to enhance accessibility with the analytes. A variety of surface sensitive techniques were employed to characterize the structure of these monolayers. The results from preliminary tests of the molecular specificity of these monolayers, conducted using the quartz crystal microbalance experiments and hexane and tetrachloroethylene as probe molecules, are discussed.

Chapter 2 investigates the effects of the interfacial structure of metalloporphyrin monolayers on their catalytic potency for the reduction of dioxygen in a collaborative project with Dr. Keith Woo and Dr. Hongping Yuan. The electrocatalytic reduction of dioxygen via immobilized metallomacrocycles has been suggested as an attractive reaction for use in fuel cells [32-35]. To date, research in this area has focused primarily on investigating the effect of variations in the internal molecular structure of the metallomacrocycle molecules on their catalytic potency [36, 37]. Although these studies have provided the framework of a model that can be used to predict catalytic potency based on molecular structure, the effects of the interfacial structure of the metallomacrocycle at the electrode surface on its catalytic potency has not been addressed. Such a study, which is fundamentally needed for the development of modified electrodes with increased potency, is the focus of the research in this chapter. To address this important issue, two different thiol-derivatives of cobalt-porphyrin with different "expected" orientations as monolayers chemisorbed at gold were synthesized. The electrocatalytic potency for the reduction of dioxygen of the two types of monolayers was assessed using voltammetry. Correlations between the interfacial structures of the monolayers and electrocatalytic potency are discussed in the paper.

Chapter 3 describes a new route for the modification of the surface of glassy carbon electrodes by the electrochemical oxidation of amine-containing compounds. By using X-ray photoelectron spectroscopy to assess relative coverages, the factors requisite for optimizing surface coverage were delineated by using a wide variety of primary, secondary, and tertiary amine-containing compounds. Possible applications for the fabrication of electrocatalytic and biosensor electrode architectures are discussed. Furthermore, the approach can be potentially used for immobilization of redox active molecules onto carbonaceous stationary phases for the development of novel separation schemes in electrochemically modulated liquid chromatography (EMLC), which is the focus of the next portion of this discussion.

Another area of analytical chemistry in which interfacial processes play an important role is modern liquid chromatography (LC) [15]. However, one of the limitations of LC is the fixed composition of the stationary phases. To circumvent this problem several research groups [38-42], including our own [43-46], have been exploring the viability of a new form of LC. The heart of the technique, which we have dubbed electrochemically-modulated liquid chromatography (EMLC), is the transformation of the LC column into an electrochemical cell. Thus, electrochemically-induced alterations in the composition of a conductive stationary phase can be exploited for the manipulation of the efficiency of a separation. Chapters 4 and 5 will discuss another novel variant of EMLC. The approach is based on the control of the adsorption/desorption of surfactant-like additives to the mobile phase by the application of an applied potential to the stationary phase. Chapter 4 will demonstrate the idea through affecting the electrosorption of three alkylaniline compounds using different supporting electrolytes in the mobile phase. The differences in the resulting separations are attributed to the differences in the double layer structure in each supporting electrolyte. Chapter 5 further demonstrates the capability of this technique by modifying a carbonaceous stationary phase to facilitate the separation of optical isomers using the chiral selector. It will be demonstrated that the chiral selectivity of the separation can be manipulated by controlling the amount of β-cyclodextrin immobilized at the stationary phase through the changes in the potential applied to the stationary phase. A mechanism is proposed that qualitatively explains the basis of the observed separations.

CHAPTER 1. SPONTANEOUSLY ADSORBED MONOLAYERS OF THIOL-CONTAINING α- AND β- CYCLODEXTRIN DERIVATIVES AT GOLD SURFACES: FORMATION, STRUCTURE, AND GUEST-HOST INTERACTIONS

A paper to be submitted to the Journal of American Chemical Society

Mankit Ho, Chinkap Chung, Alan Schwabacher, and Marc D. Porter

ABSTRACT

Thiol-containing α- and β-cyclodextrin (CD) derivatives have been synthesized as precursors for the preparation of the analogous monolayers chemisorbed at gold surfaces. The derivatives were formed by the complete replacement of the primary hydroxyl groups at the bottom of the CD cavities of the two oligomers with -$S(CH_2)_2SH$ groups. The long term goals of this effort is the creation of interfacial structures that exhibit the well known guest-host selectivity of the many solution-soluble forms of CDs. Both solvent and immersion studies of the formation of monolayer have been characterized by infrared reflection spectroscopy, optical ellipsometry, contact angle measurements, x-ray photoelectron spectroscopy, and electrochemistry. The results confirm the formation of monolayers for the adsorbates when DMF was used as the solvent. These results further indicated that both forms of the CD-derivatives adopt an orientation whereby the principle axis of the CD cavity is oriented towards the surface normal. Our findings also reveal that when ethanol or tetrahydrofuran are used as the solvents, multilayer structures are formed that are connected

by hydrogen-bonding interactions between the secondary hydroxyl groups at the top rim of the CD cavity.

The molecular recognition properties of the monolayers were demonstrated by the preliminary results of QCM experiments using hexane and tetrachloroethylene as the probe molecules. The same responses were observed for both α- and β-cyclodextrin coated crystals. On the other hand, β-cyclodextrin coated crystals have a higher response for tetrachloroethylene than that of α-cyclodextrin coated crystals. These can be explained by the size selectivity of the cyclodextrin monolayers.

INTRODUCTION

It is now well established that organosulfur compounds adsorb spontaneously onto noble metals such as gold (Au) [1-6] and silver (Ag) [7] to form monolayers. The monolayers formed from n-alkanethiol were characterized to be ordered and compact [3]. Theoretically, if we can carefully synthesize a molecule with specific targeted properties and functionalize it with a sulfur moiety, we can fabricate a monolayer with a specific function. Therefore, monolayers formed by spontaneous adsorption offer unique opportunities as model systems for organic surface research such as corrosion [8], adhesion [9-11], electron-transport phenomena [12-20], catalysis [21, 23] and sensor fabrication [23, 24]. Fabrication of self-assembled monolayers at gold surfaces with molecular recognition abilities constitutes the focus of this report.

Cyclodextrins are a family of oligomers that are composed of an α-(1, 4)-linkage of a different number (6 for α, 7 for β, 8 for γ and so on) of D(+)-glucopyranose units joined together to form donut-shaped molecules. The unique arrangement of hydrophobic cavity and hydrophilic ring of cyclodextrins make them able to form inclusion complexes with a wide range of organic molecules [25]. Moreover, depending on the size and shape of the molecules, cyclodextrins have different complexation constants towards the molecules. In light of the special properties of cyclodextrins, we decided to synthesis cyclodextrin derivatives with sulfur moieties so that we can form cyclodextrin monolayers at gold. The main goal of the projects is to take advantage of the selective host-guest interaction ability of the cyclodextrins and to translate them onto the surfaces to fabricate monolayers with molecular recognition properties, and hence, fabricate new kinds of sensor devices.

In our previous work [26, 27], we have synthesized different kinds of sulfur-bearing cyclodextrin derivatives. However, characterization using different techniques indicated the monolayers formed from the derivatives show disorder features which affected the molecular recognition properties of the monolayers. We suspected the disorder nature of the monolayers due to the fact that all the sulfur moiety sites of these cyclodextrin derivatives are directly attached to the cyclodextrin, which imposed strains for the sulfur moieties to find the binding sites. Therefore, two new cyclodextrin derivatives, hexakis(6-ethylenethio-6-deoxy)-α-cyclodextrin (**6**) and heptakis(6-ethylenethiol-6-deoxy)-β-cyclodextrin (**7**), have been synthesized. Both of them contain a mercaptal functional group as the binding site onto the gold surface. An additional feature of the derivatives is an ethylene spacer group between the cyclodextrin and the thiol group. The ethylene spacer will provide more flexibility for the thiol group to bind onto the gold surface. Scheme I shows the target interfacial structure of the cyclodextrin derivatives at gold. We want all the cyclodextrins orientated with the cavities facing outside; in this way the host-guest interaction can be maximized. This paper reports the studies of monolayer fabrication from these two derivatives. There are three main objectives of the report: firstly, to examine the conditions for the monolayer formation; the influence of solvents and immersion time on the interfacial structures of the monolayers will be examined. Secondly, the interfacial structures of the cyclodextrin monolayers will be deduced with the help of a variety of surface sensitive techniques (ellipsometric film thickness measurement, contact angle, X-ray photoelectron spectroscopy (XPS) and infrared reflection spectroscopy). Finally, preliminary studies using a quartz crystal microbalance (QCM) to demonstrate the host-guest interaction of the monolayers will be presented.

EXPERIMENTAL SECTION

A. Reagents. Deionized water was prepared using a Milli-Q purification system (Millipore Products). Absolute ethanol (EtOH) (punctilious grade) was from Quantum. Acetone, ammonium chloride, chloroform, dimethylformamide (DMF), diethylether, hexane, hydrochloric acid, hydrogen peroxide, methanol (MeOH), sodium sulfate, sodium hydroxide, sulfuric acid, tetrahydrofuran (THF), toluene, and zinc (powder) were from Fisher. Sodium hydride (Aldrich, 60% in oil suspension) was rinsed with hexane several times immediately

Scheme I. The strategy for the fabrication of cyclodextrin monolayers at gold.

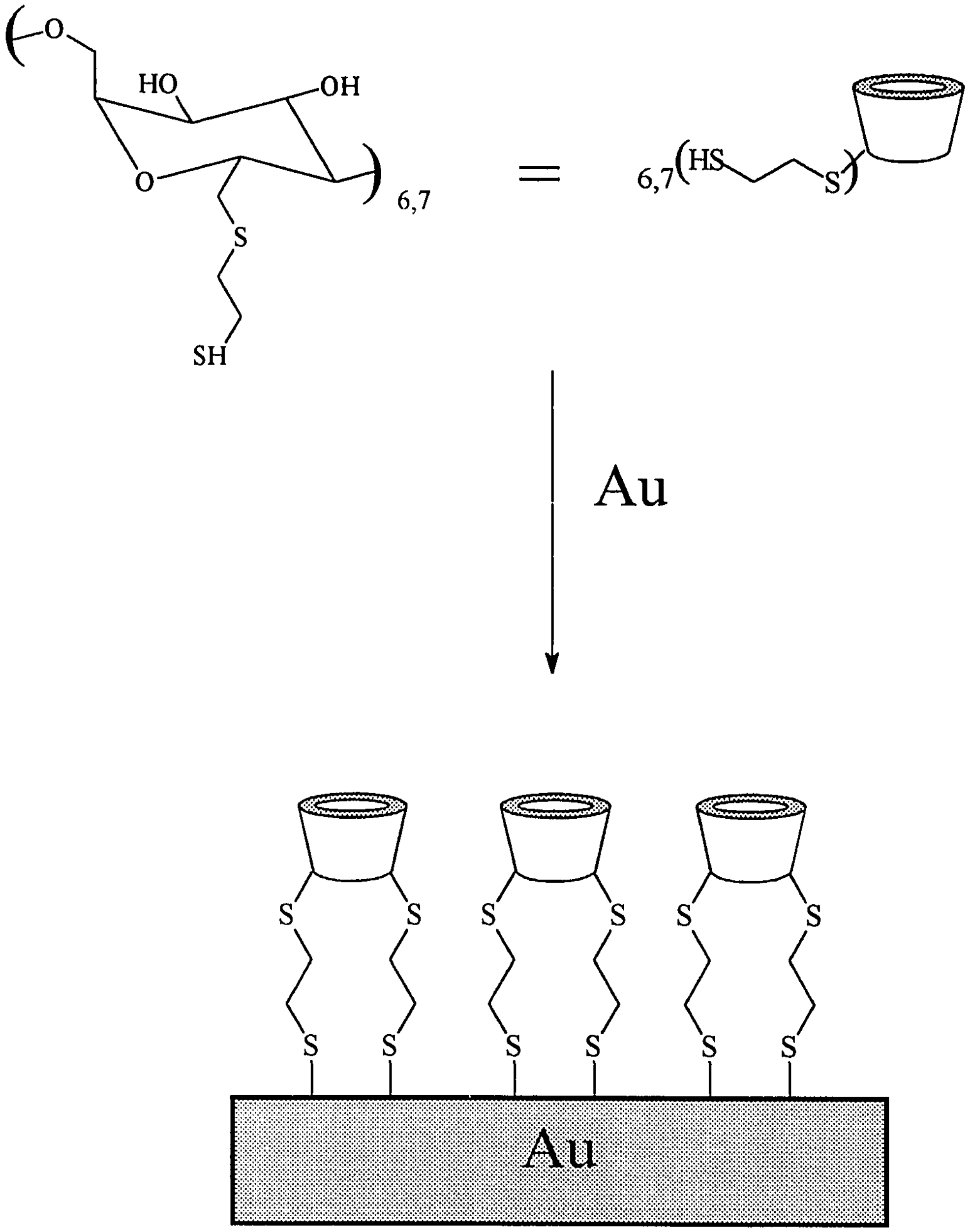
O
HO
OH
O
S
SH
6,7
6,7
HS
S
Au
S
Au

prior to use. The α- and β–cyclodextrins were a gift from American-Maize Products. Hexanethiol (Eastman Kodak) was purified by passing through a neutral alumina column. Octadecanethiol (Aldrich) was recrystallized twice from absolute ethanol. Mercaptoethanol, methanesufonylbromide, 1,2-ethylenedithiol, benzyl bromide, sodium methoxide, methanesulfonyl chloride, and tetrachloroethylene (TCE) were from Aldrich. 11-Mercapto-1-undecanol and methanesulfonyl bromide were synthesized according to literature procedures [28]. Ammonia gas (anhydrous) was from Air Products. All chemicals were used as received unless otherwise specified.

B. Synthesis of Thiol-Derivatized Cyclodextrins.

(i) 4-Phenyl-3-thiabutane-1-thiol (1) [29]. A solution of 8.1 g (0.15 mole) of sodium methoxide in 50 mL of methanol was added to a stirred suspension of 20 mL (0.2 mole) of 1,2-ethylenedithiol in 35 mL of methanol. Next, 12 mL (0.14 mole) of benzylbromide in 50 mL of methanol was added dropwise to the stirred solution. The resulting mixture was refluxed for 4 h. After refluxing, methanol was removed by rotary evaporation, and the residue was distributed between 100 mL of 3 M NaOH (aqueous) and 100 mL of diethyl ether. After discarding the ether phase, the aqueous phase was acidified with 6 M HCl and extracted with a fresh (100 mL) portion of diethyl ether. The organic phase was dried with Na_2SO_4 and the solvent was removed by rotary evaporation. The product was purified using flash chromatography with hexane:toluene (1:3) as the eluent. ^1H NMR: δ 7.29 (m, 5H), 3.71 (s, 2H), 2.63 (m, 4H), 1.65 (m, 1H).

(ii) 6-heptabromo-heptadeoxy analogs of α- and β-cyclodextrin (2 and 3) [30]. While stirring, 6 mL (170 mmole) of methanesufonylbromide was added dropwise to a stirred solution of 2.27 g (2 mmole) of α- or β-CD in 25 mL of DMF. The solution was stirred for 24 h at 65 °C. The solvent was then removed by rotary evaporation to yield a pale yellow oil which was subsequently dissolved in methanol and neutralized with 3 M sodium methoxide in methanol. The addition of ice induced the formation of a white precipitate, which was collected by filtration and washed with water and methanol to yield **2** or **3**. **2**: ^{13}C NMR (DMSO-d_6): δ 101.84, 84.20, 72.49, 71.62, 70.63, 34.81. **3**: ^{1}H NMR (DMSO-d_6): δ 6.00 (d,1H, OH), 5.88 (s, 1H, OH), 4.97 (s, 1H, H-1), 4.00 (m, 1H), 3.63 (m, 2H), 3.35 (m, 2H); ^{13}C NMR (DMSO-d_6): δ 102.09, 84.62, 72.28, 72.06, 70.63, 34.43.

(iii) 6-hepta-(4-Phenyl-3-thiabutane-1-mercapto)-6-deoxy analogs of α- and β-cyclodextrin (4 and 5). While under a nitrogen atmosphere, 3 eq of **1** was added to a stirred solution of 1.5 eq of NaH in dry DMF, followed by the dropwise addition of 1 eq of **2** or **3** in DMF. The mixture was stirred at room temperature for 24 h, with the formation of a white precipitate subsequently induced by the addition of ice water. The precipitate was collected by filtration and washed with deionized water and acetone. The crude product was then recrystallized twice from a methanol-chloroform mixture to yield **4** or **5**.

4: ^{1}H NMR (DMSO-d_6): 7.23 (m, 5H), 5.703 (d, 1H), 5.530; ^{13}C NMR (DMSO-d_6): δ 138.46, 128.80, 128.35, 126.82, 101.91, 85.02, 72.83, 71.89, 71.42, 35.16, 33.39, 32.56, 31.20; elemental analysis: $(C_{90}H_{120}O_{24}S_{12})\cdot 2H_2O$, calculated: C 54.36, H 6.18 S 19.35; found:

C 54.04, H 6.12, S 19.25. **5**: ^{1}H NMR (DMSO-d$_6$): 7.26 (m, 5H), 5.93 (d, 1H), 5.87 (s, 1H), 4.87 (s 1H), 3.69 (s 2H), 3.64 (m, 1H), 3.33 (m 4H), 3.05 (d, 1H), 2.76 (m 2H), 2.49 (m, 2H); ^{13}C NMR (DMSO-d$_6$): δ 138.47, 128.67, 128.42, 126.86, 102.01, 84.89, 72.57, 72.20, 71.57, 35.22, 33.19, 32.50, 31.04; elemental analysis: $(C_{105}H_{140}O_{28}S_{14})\cdot 2H_2O$, calculated: C 54.02, H 6.22 S 19.19; found: C 53.79, H 6.19, S 19.35.

(iv) 6-hepta-ethylenedithiol-6-deoxy analogs of α- and β-cyclodextrin (6 and 7). Liquid ammonia was first condensed into a 3-neck round bottom flask under nitrogen, followed by the addition of 1 g of **4** or **5** to form a suspension. Then, 0.2 g of metallic sodium was added until the blue color had persisted for 2 h, after which the reaction was quenched with 2 g of ammonium chloride. Ammonia was subsequently evaporated under nitrogen. Ice water was added to induce the formation of a white precipitate, which was collected by filtration and washed with deionized water and acetone to yield **6** or 7. **6**: ^{13}C NMR (DMSO-d$_6$): δ 101.91, 85., 72.91, 71.85, 71., 36.57, 33.33, 24.38; elemental analysis: $(C_{48}H_{84}O_{24}S_{12})\cdot H_2O$, calculated: C 39.82, H 5.99, S 26.57; found: C 40.17, H 5.98, S 26.73. 7: ^{1}H NMR (DMSO-d$_6$): δ 5.94 (d, 1H), 5.84 (s, 1H), 4.88 (s), 3.76 (m), 3.57 (m), 3.11 (d), 2.76 (m, 2H), 2.70 (m 2H); ^{13}C NMR (DMSO-d$_6$): δ 101.83, 84.98., 72.50, 72.80, 71.14, 36.44, 33.10, 24.38; elemental analysis: $(C_{56}H_{98}O_{28}S_{14})\cdot 2H_2O$, calculated: C 39.48, H 6.04, S 26.30;found: C 39.5, H 5.94, S 26.36.

C. Sample Preparation. Substrates were prepared by the resistive evaporation of 15 nm of chromium (0.1 nm/s), followed by 300 nm of gold (0.3 nm/s) onto glass slides. The glass slides were precleaned in microsolution (Cole-Parmer) for ~3 h, rinsed thoroughly with deionized water and methanol, and dried under a stream of nitrogen before being loaded into the evaporator. The pressure in the cryopumped E360A Edwards Coating System before the evaporation was <1 x 10^{-6} torr. After ~45 minutes of cooling time, the evaporator was back-filled with purified nitrogen, and the substrates were removed. The substrates for the quartz crystal microbalance measurements (polished AT-cut quartz, 9 MHz (Velpy-Fisher)) were prepared similarly.

Layers from the cyclodextrin precursors, **6** and **7**, and from $CH_3(CH_2)_{10}SH$ and $HO(CH_2)_{10}SH$ were formed from dilute solutions onto freshly evaporated gold substrates. Concentrations for deposition were varied and are specified for each experiment in the text. Upon removal from the deposition solutions, the samples were first rinsed with the solvent used for formation and absolute ethanol, and dried on a photoresist spin-coater.

D. Instrumentation.

(i) Ellipsometric Measurements of Film Thickness. Film thicknesses were determined using a computer-controlled Gaertner Model L-116B Auto Gain ellipsometer at 632.8 nm. Analyzer and polarizer angles were measured at three or more separate locations on each substrate for determinations of the optical function of each uncoated substrate as well as for the film thicknesses. The thickness calculations used a refractive index of 1.39 for **6** and 1.32 for **7**. These values were developed by an analysis using Bruggeman effective medium theory to account for the effects of the void volume of inclusion cavities of both α- and β-CDs. This analysis is based on a determination of the volume fractions and refractive indices of the organic and void components of the CDs. The refractive index of sucrose (n_D = 1.54 [31]) used as an approximation the refractive index of the organic fraction of a CD molecule (changes in the refractive indices for both precursors of ±0.03 resulted in thickness differences of ~3%).

(ii) Contact Angle Measurements. Advancing contact angles (θ_a) were measured in the laboratory ambient using a Rame-Hart Model 100-00 goniometer. For these measurements, 2-mL droplets were formed on the substrate with the needle of the syringe in the droplet; θ_a was determined as the volume of the droplet was slowly increased.

(iii) Infrared Spectroscopy. Infrared spectra were acquired with a Nicolet 750 FT-IR spectrometer. The spectrometer was purged with boil-off from liquid nitrogen. Spectra were obtained by coaddition of 1024 sample and 1024 background scans at 2 cm^{-1} resolution (zero filled) after Happ-Genzel apodization. Liquid-N_2-cooled MCT detectors were used to measure the intensity of the IR radiation. Transmission spectra were collected by the dispersion of the adsorbate precursors **6** and **7** in KBr. Surface spectra were acquired using p-polarized light incident at 80° from the surface normal. These spectra are reported as -log(R/R_O), where R is the reflectivity of the sample and R_O is the reflectivity of a perdeuterated octadecathiolate-coated gold substrate.

(iv) X-ray Photoelectron Spectroscopy (XPS). The XPS data were acquired with a Physical Electronics Industries Model 5500 surface analysis system equipped with a hemispherical analyzer, monochromator, and multichannel detector. Monochromatic Al K_α radiation (1486.6 eV) at 300 W was used for excitation. The photoelectrons were collected at 45° from the surface normal. Binding energies were referenced to the gold($4f_{7/2}$) emission band at 84.0 eV. The base pressure of the ion-pumped ultrahigh vacuum chamber was less than 1×10^{-9} Torr during analysis.

(v) Electrochemical Measurements. Electrochemical measurements were carried out in a conventional three-electrode cell, with a Pt-coil counter electrode, and a Ag/AgCl(sat'd NaCl) reference electrode. An inert elastomer gasket defined the geometric area of the working electrode (0.6 cm^2). The applied potential was controlled by a Princeton Applied Research Model 173 galvanostat/potentiostat and Model 175 universal programmer. Voltammograms were recorded on a Houston Instruments Omnigraphic 2000 x-y recorder.

(vi) Quartz Crystal Microbalance Measurements. One-port scattering parameters (S-parameters) were measured using either a Hewlett-Packard 8753 network analyzer. The S-parameters relate the voltage waves incident on the port of those reflected from the port. Data acquisition and analysis used Hewlett-Packard 85165A resonator measurement software running on either HP-236 computer workstation or an HP-8234A measurement co-processor. The software transforms the scattering parameters to electrical admittance values by using the Butterworth-Van Dyke equivalent circuit model to fit the data to an admittance circle and then to calculate the series resonance frequency, F_s. Results reported as changes in the resonance frequency, F_r, were measured at the frequency at which the susceptance is zero.

RESULTS AND DISCUSSION

A. Synthesis of Cyclodextrin Derivatives with Alkyl Thiol Appendages. As summarized in Scheme II and detailed in the Experimental Section, the synthesis of the thiol-derivatized CDs was designed such that the mercaptal appendages were tethered to the bottom, or more narrow portion, of the CD cavity. In contrast to our earlier designs [27], an ethylene spacer group was placed between the mercaptal functionality and the bottom of the cavity to enhance the flexibility of the appendage and the subsequent dexterity for optimal binding to the gold surface. In brief, the primary hydroxyl groups of the CDs were activated by the formation of the bromide derivatives **2** and **3** using methanesulfonyl bromide [28]. After protection of one of the mercaptal groups of 1,2-ethylenedithiol with benzylbromide to form **1**, the bromide groups of **2** and **3** were displaced by **1** in the presence of NaH, yielding **4** and **5**. Both **4** and **5** were then purified via recrystallization. Removal of the benzyl protecting groups from **4** and **5** resulted in the thiol-containing cyclodextrin derivatives **6** and **7**. The combined results of the structural analyses indicate a virtually complete transformation of the primary hydroxyl groups of the two starting materials to the appendaged structures **6** and **7**.

Scheme II. The synthetic pathway for the synthesis of **6** and **7**.

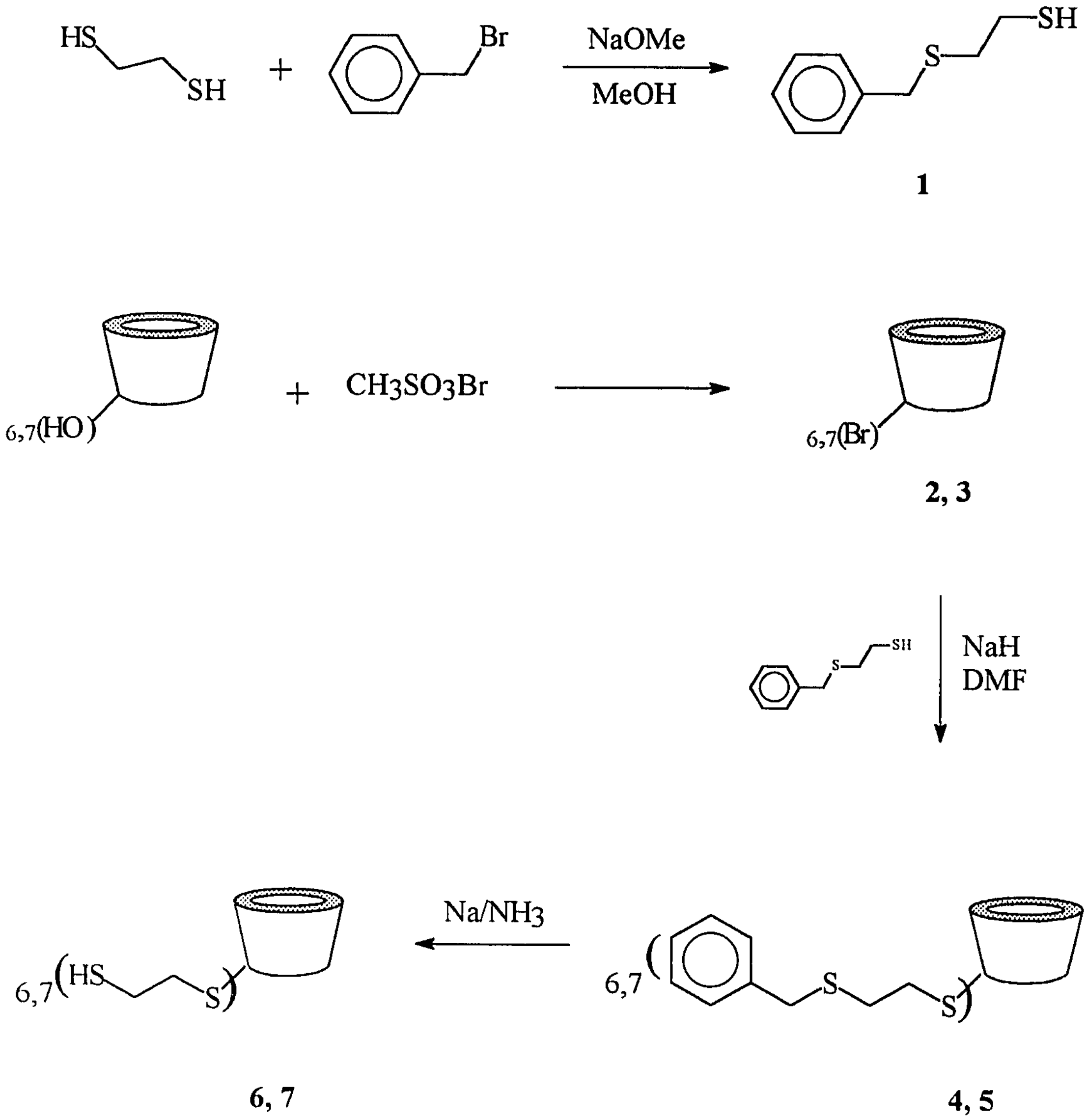
HS
SH
+
Br
NaOMe
MeOH
S
SH
1
6,7(HO)
+
CH3SO3Br
6,7(Br)
2, 3
S
SH
NaH
DMF
Na/NH3
6,7(HS
S)
6,7(
S
S)
6, 7
4, 5

B. Formation of Films from 6 and 7 at Gold Surfaces. In this section, the formation conditions of monolayers from **6** and **7** will be discussed. The main objective is to establish the best conditions for the assembling the targeted interfacial structures as shown in Scheme I.

(i) Films of 6 and 7 from different solvents. To assess the feasibility for the formation of monolayers at gold from **6** and **7**, infrared reflection absorption spectroscopy (IRRAS) was used to monitor the evolution of the surface structure. Experiments first evaluated formation for ~18 h immersion time from solvents (i.e., H_2O, DMF, EtOH, and THF) in which **6** and **7** exhibited a wide range of solubilities. Comparatively, **6** and **7** have the lowest solubility in H_2O, are sparsely soluble in EtOH and THF, and are highly soluble in DMF. As a consequence, saturated solutions of **6** and **7** were used for formation from H_2O, EtOH, and THF, and ~20 μM solutions from DMF. The concentration in EtOH and THF are well below 20 μM. Under these conditions, the presence of **6** and **7** was detected at gold substrates immersed in the EtOH-, THF-, and DMF-solutions, but not at those immersed in the H_2O-solution. We attribute the latter finding to the comparatively low solubility of both **6** and **7** in H_2O.

Figures 1 and 2 present the results of the IRRAS characterizations for the layers formed from **6** and **7** at gold from the DMF-, EtOH-, and THF-solutions. Two spectral regions were shown in the figures (between 3800-2700 cm^{-1} and 1700-900 cm^{-1}). Spectra of the precursors, after dispersion in KBr, are given for comparison. Qualitatively, the close correspondence in the bands for the layers formed from the three solvent systems and those

Figure 1: IR spectra of: (a) **6** dispersed in KBr; (b)-(d) **6** at gold assembled from DMF, EtOH and THF, respectively. The immersion time for the film formation was 18 h. $S = 5.0 \text{ x } 10^{-2}$ and $5.0 \text{ x } 10^{-4}$ A.U. for KBr and at gold spectra respectively.

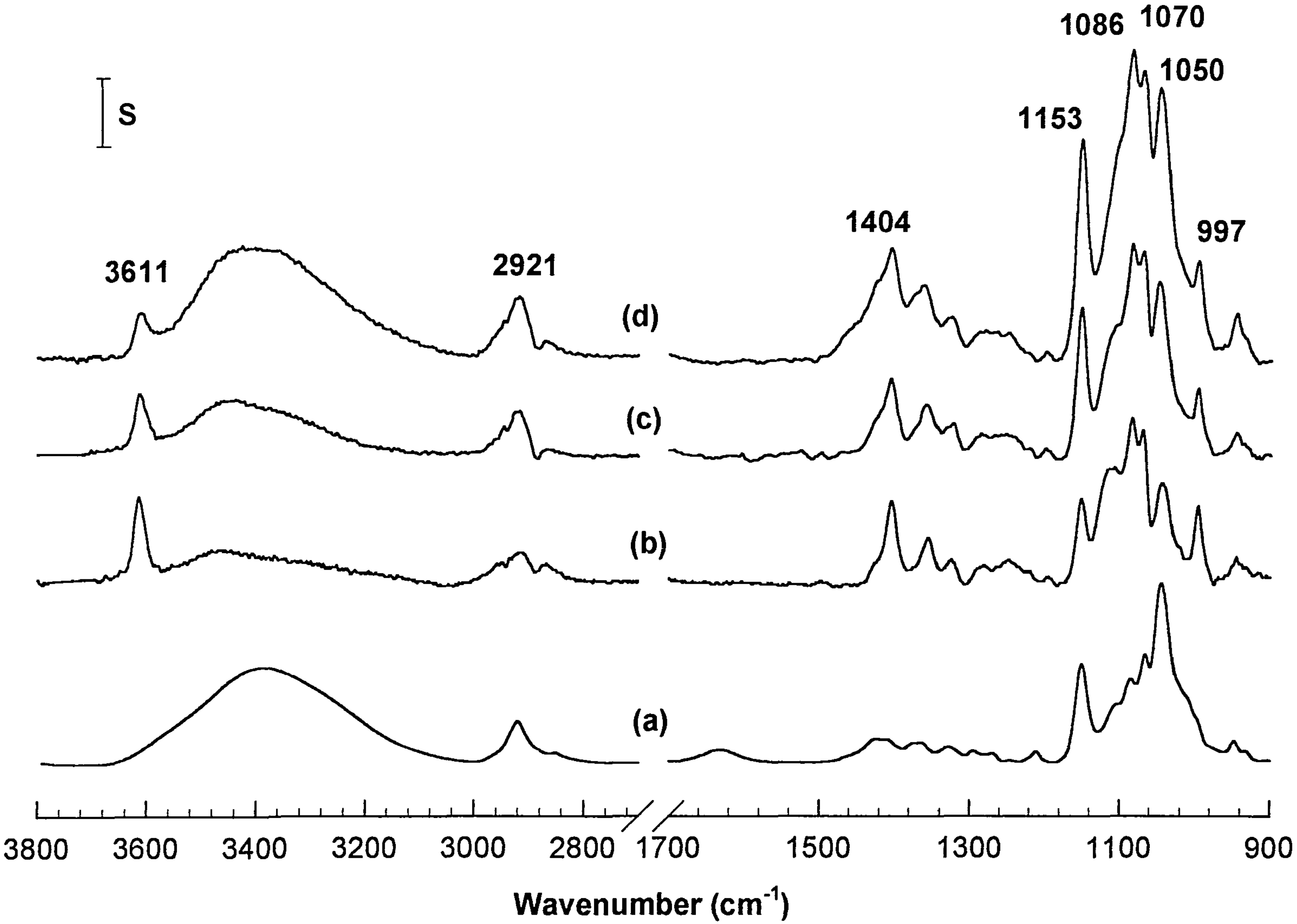
S
3611
2921
1404
1153
1086
1070
1050
997
(d)
(c)
(b)
(a)
3800
3600
3400
3200
3000
2800
1700
1500
1300
1100
900
Wavenumber (cm^{-1})

Figure 2: IR spectra: (a) **7** dispersed in KBr; (b)-(d) **7** at gold assembled from DMF, EtOH and THF, respectively. The immersion time for the film formation was 18h. S = 5.0×10^{-2} and 5.0×10^{-4} A.U. for KBr and at gold spectra respectively.

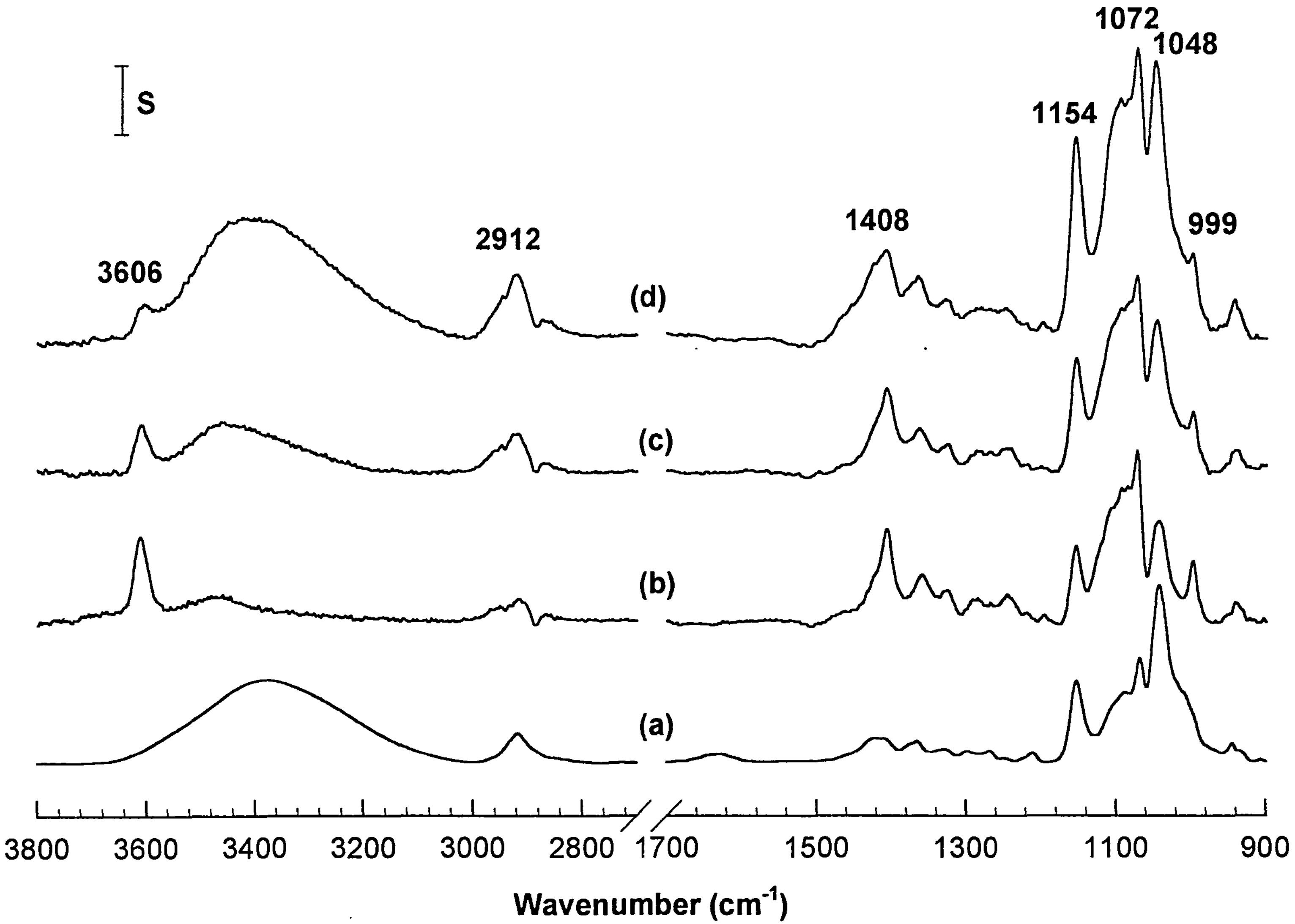
S
3606
2912
1408
1154
1072
1048
999
(d)
(c)
(b)
(a)
3800
3600
3400
3200
3000
2800
1700
1500
1300
1100
900
Wavenumber (cm^{-1})

for the precursors in KBr confirm the presence of immobilized forms of **6** and **7**. There are, however, notable differences in the absolute and relative magnitudes of the bands for the layers from the three solvents as well with those of the precursors, which indicate that the layers formed from each of the solvents are structurally different. The band assignments are listed in Table I. (See the appendix for the discussion of band assignments.)

The detailed analysis of the changes in relative magnitude of the bands can be used to gain insight into the orientation of the CD-cavities with respect to the surface normal. This analysis is based on the infrared "surface selection rule" [32, 33], an effect that arises from the strong anisotropy of the electric field upon the reflection of infrared light from a metal surface. Thus, only vibrational modes that have components of their dipole derivatives perpendicular to the surface will be observed. In ideal cases, an average orientation can be deduced by a comparison of the observed IRRAS spectrum with that calculated for an isotropic array of adsorbate precursors of equivalent thickness. However, the extensive overlap of the spectral features precludes such an analysis. We can nevertheless qualitatively develop an orientational description by comparisons of the observed IRRAS spectra to those of the precursors dispersed in KBr, the latter of which are representative of isotropic distributions of **6** and **7**.

The low energy of the IR spectral region (1700-900 cm^{-1}) contains a large number of diagnostic bands, including ν(C-O-C), ν(C-O), ν(C-C), δ(C-H), and δ(O-H) [34-39]. Of the many possible vibrational modes that could be used for an assessment of orientation, an orientational analysis based on ν_s(C-O-C) and ν_{as} (C-O-C) of the glucosidic linkages are the

Table I. Peak Positions and Band Assignments of Cyclodextrin Derivatives (**6**, **7**) in KBr and at Gold

Band Assignments	**6** / KBr	**6** / Au (DMF)	**6** / Au (EtOH)	**6** / Au (THF)	**7** / KBr	**7** / Au (DMF)	**7** / Au (EtOH)	**7** / Au (THF)
ν(O-H) (intramolecular H-bonded)	---	3613	3613	3611	---	3612	3610	3606
ν(O-H) (intermolecular H-bonded)	3390	3468	3447	3408	3381	3468	3451	3409
$\nu(CH_2)$	---	2954	22947	2947		2950	2949	2947
$\nu(CH_2)$	2920	2915	2921	2921	2918	2918	2922	2922
$\nu(CH_2)$	---	2873	2867	2970	---	2865	2870	2868
	2852	---	---	---	2835	---	---	---
ν (S-H)	2550	---	---	---	2550	---	---	---
adsorbed H_2O	1632	---	---	---	1634	---	---	---
$\delta(CH_2)$	1425	1427	1427	1426	1422	1423	---	1425
δ(C-H)	1408	1405	1406	1404	1410	1406	1406	1408
	1376	---	---	---	1366			
δ (O-H)	1363	1355	1358	1361		1359	1364	1364
ω(C-H)	1329	1326	1323	1327	1329	1324	1324	1325
ω(C-H)	1298	---	---	---	1300	---	---	---
δ (O-H)	1271	1285	1287	1285	---	1288	1285	
δ (O-H)	1211	1200	1200	1200	---	1211	---	1199
ν_a (C-O-C), glucosidic linkages	1151	1151	1152	1153	1154	1154	1153	1154
	1115	1116	---	---	---	---	---	---
ν_a(C-O-C), glucosidic ring	---	1107	1107	---	---	---	---	---
ν (C-O), 2° OH	1086	1086	1086	1086	1089	---	1094	1094
ν_s(C-O-C), glucosidic ring	1067	1070	1070	1070	1069	1072	1072	1072
ν_s (C-O-C), glucosidic linkages	1045	1044	1049	1050	1043	1044	1046	1048
ν (C-O), 2° OH	997	997	997	997	---	997	998	999
ring vibration	948	948	948	948	946	942	941	943

most tractable. With both modes, the plane of the dipole moment changes are nearly perpendicular to the principal axis of the CD cavity (based on the crystal structure of α-CD, the average intersect angle between the plane of the C-O-C vibrationals for the glucosidic linkage is ~60° [40]). Whereas the corresponding vibrational modes for the glucosidic units are more along the axis (the average intersection angle is ~20° [40]). Thus, a comparison of the absorbance of the band at ~1045 cm^{-1} of glucosidic linkage to that for the ν_s(C-O-C) of the glucosidic units at ~1067 cm^{-1} (i.e., A_{1045}/A_{1067}) can be used as a general orientational diagnostic. For example, if the cyclodextrin oriented at the surface similar to what is shown in Scheme I, the A_{1045}/A_{1067} will be decreased when compared to the KBr spectrum. As shown in Figures 1 and 2, the relative magnitudes of both bands of (C-O-C) of glucosidic linkage are significantly lower at the surface than those in the KBr spectra for all three solvents. Table II tabulated the A_{1045}/A_{1067} values from the KBr and films spectra. The decrease in relative magnitudes of the band at 1045 cm^{-1} therefore argues that the immobilized layers from **6** and **7** are preferentially oriented with the axis of their cavities, perpendicular to the surface. However, when comparing the films from different solvents, the films exhibit slightly different orientations at gold. Based on the diagnostic of the A_{1045}/A_{1067} values, films from DMF have the lowest value, which argues the films are the most ordered ones. THF, however, produced the most disordered films (highest A_{1045}/A_{1067} values). Furthermore, careful examination the absolute magnitudes of the bands indicates that more cyclodextrins deposited onto the surface when THF was used. This may suggest that the extra material deposited on the surface contributes to the disorderliness of the films.

Table II. Ratio of absorbance of the IR bands at 1045 cm^{-1} to 1070 cm^{-1} (A_{1045}/A_{1070})

Sample (solvent)	A_{1045}/A_{1070}
6 / KBr	1.67
7/KBr	1.70
6/Au (DMF)	0.64
7/Au (DMF)	0.59
6/Au (EtOH)	0.85
7/Au (EtOH)	0.78
6/Au (THF)	0.95
7/Au (THF)	0.96

For the high energy region, the ν(O-H) of the secondary hydroxyl groups at the rim of the cavity can also provide structural information about the films. There are two types of ν(O-H) are observed: the intermolecular H-bonded ν(O-H) (the sharp band at 3610 cm^{-1}) and the intermolecular H-bonded ν(O-H) (the broader and lower energy band). The relative magnitudes of the two bands exhibit a clear solvent dependence. When DMF is used as the solvent, the high energy band is predominant. The pattern is reversed when THF and EtOH are used as solvents, with the band for the intermolecularly H-bonded species formed from THF much larger than that from EtOH. Moreover, the positions of the bands for the samples from THF are lower in energy (**6**: 3408 cm^{-1}, **7**: 3409 cm^{-1}) than those from EtOH (**6**: 3447 cm^{-1} , **7**: 3451 cm^{-1}). Both observations are diagnostic of the formation of a more extensively hydrogen-bonded system for the layers from THF, which is consistent (though not experimentally confirmed) with expectations from considerations of the solubilities of **6** and **7** in both solvents. Since the intermolecular H-bonding is usually an energetically favorable process, the lack of intermolecular H-bonding of the hydroxyl groups in the case of DMF must be due to the structural constraint of the films at surface. The structural arrangement of the cyclodextrins shown in Scheme I can be used to account for the self-association without intermolecular H-bonding of the secondary hydroxyl groups. Whereas for THF-formed and EtOH-formed films the more intermolecular H-bonding of the secondary hydroxyl group also indicates more disordered films were formed.

The above IR data show that both **6** and **7** can be immobilized onto gold substrates with the three solvents. The changes of the relative intensity of the bands suggested **6** and **7** immobilized at gold with a preferential orientation. However, the films from different solvents exhibited different interfacial structures. Among the solvents studied, films from DMF show the highest degree of ordering but the least amount of cyclodextrin. In the following section, we will investigate the origin of the differences between the films.

(ii) Immersion time dependence of film formation. To gain further insight into these differences, an IRRAS characterization of the effects of immersion time was conducted. Based on the data in Figures 1 and 2, this set of studies focused on using DMF and EtOH as the solvents for layer formation. Figures 3 and 4 present the respective results with DMF as the solvent for **6** and **7**, and Figures 5 and 6 the respective results with EtOH as the solvent. In all cases, IRRAS data were acquired for immersion times of 1, 5, 18, 30, and 144 h. As evident in the spectra from DMF, any changes of the bands are virtually undetectable. Importantly, the changes in the bands for the intramolecularly hydrogen-bonded structures are effectively invariant with immersion time. Furthermore, both absolute and relative intensities of the bands are unchanged. These data also suggest that the film formation process is effectively complete in about 1h and there is little change in the interfacial structure for longer immersion times. Studies at shorter immersion times are planned.

In contrast to the interfacial structures of the films formed from DMF, those from EtOH exhibited a strong dependence on immersion time. From the IRRAS data in Figure 5 and 6, at short immersion times (e.g., 1 h), the spectra for both types of layers are comparable to those formed when DMF is used as the solvent. That is, the secondary hydroxyl groups are primarily intramolecularly H-bonded and the magnitudes of ν_s(C-O-C) and ν_{as}(C-O-C)

Figure 3a-e: IRRA spectra of **6** at gold assembled from DMF with immersion times of 1 h, 5 h, 18 h, 30 h, and 144 h, respectively.

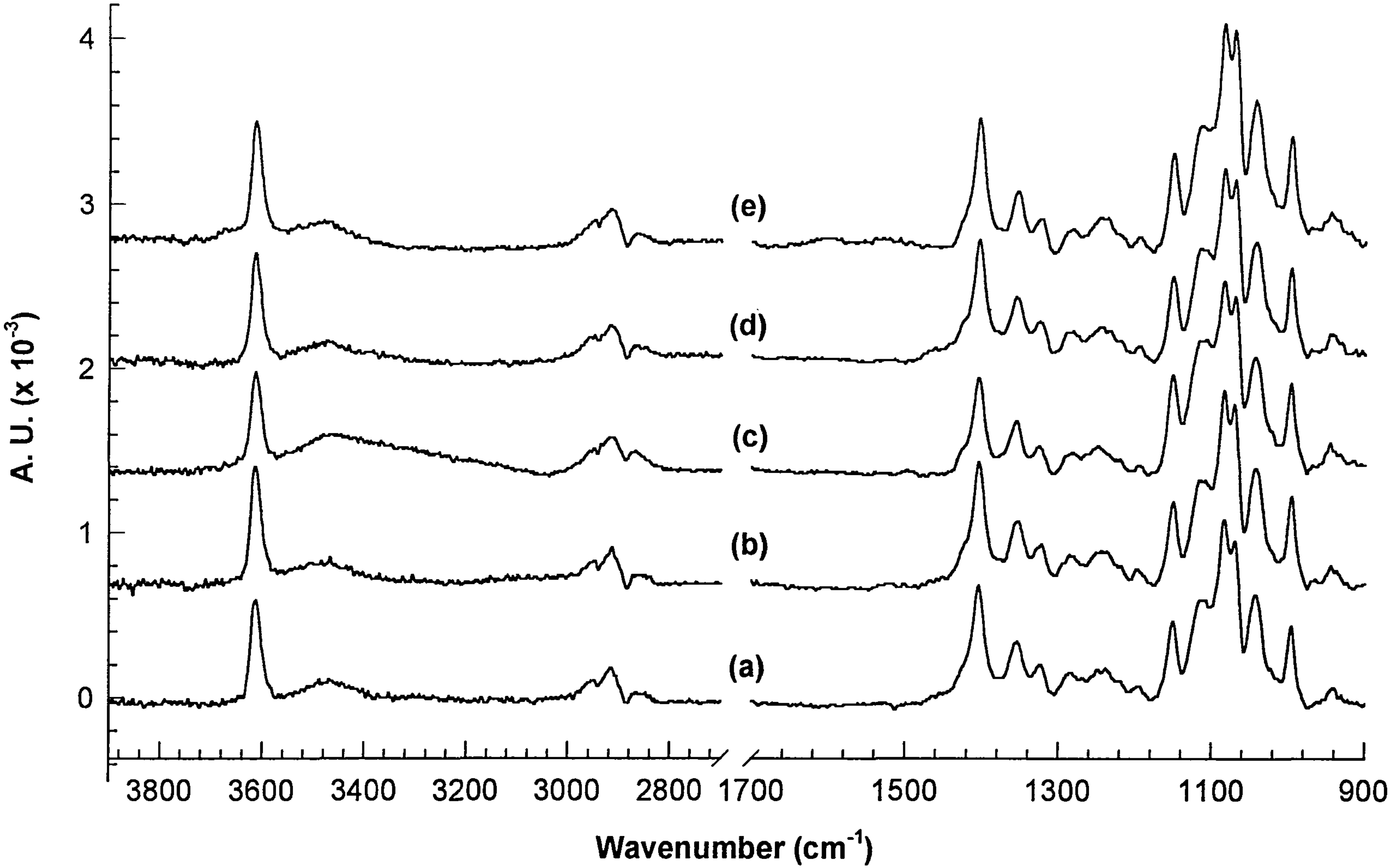
A. U. (x 10^{-3})
0
1
2
3
4
(e)
(d)
(c)
(b)
(a)
3800
3600
3400
3200
3000
2800
1700
1500
1300
1100
900
Wavenumber (cm^{-1})

Figure 4a-e: IRRA spectra of 7 at gold assembled from DMF with immersion times of 1 h, 5 h, 18 h, 30 h, and 144 h, respectively.

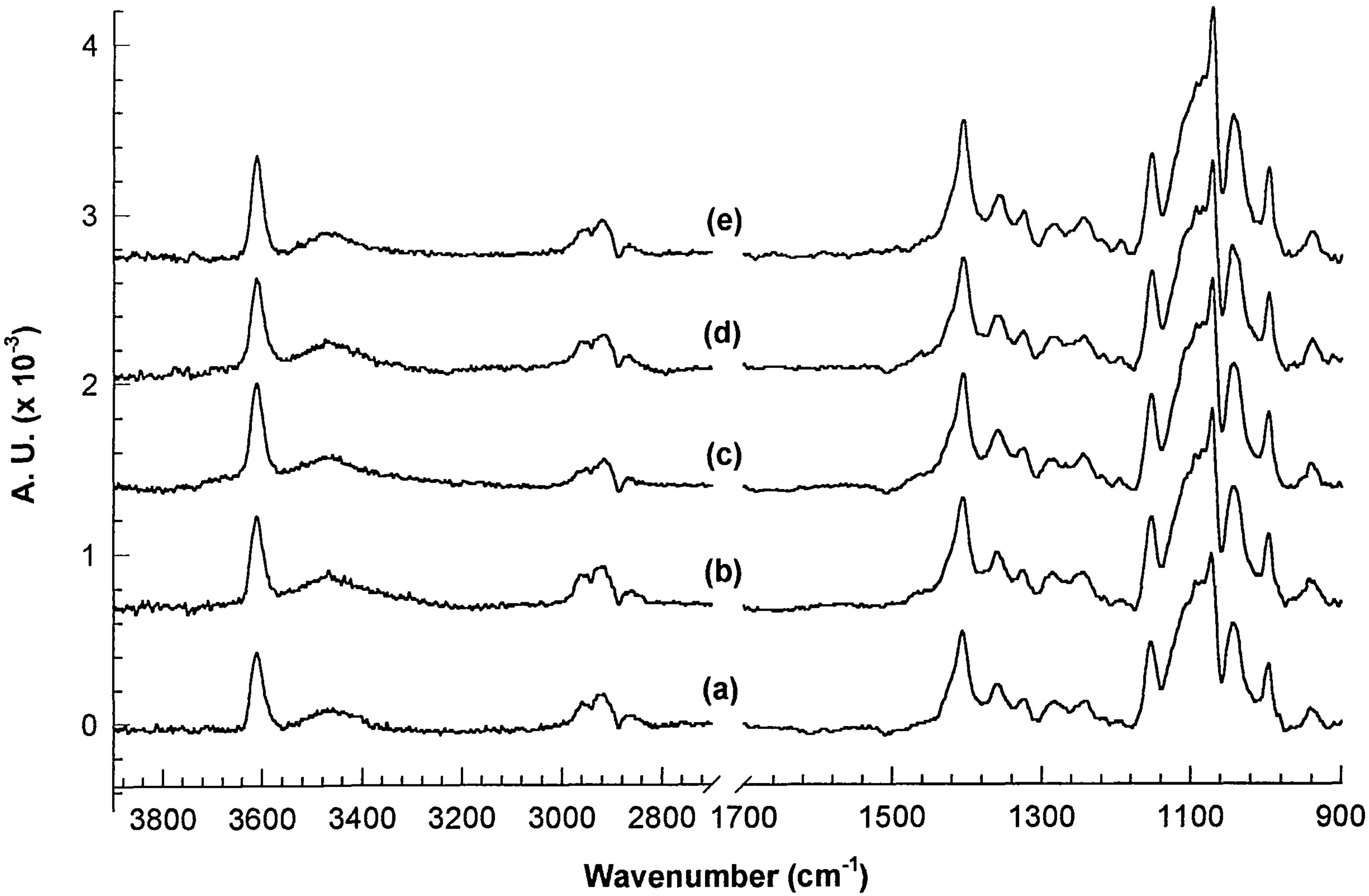
A. U. (x 10^{-3})
0
1
2
3
4
(a)
(b)
(c)
(d)
(e)
3800
3600
3400
3200
3000
2800
1700
1500
1300
1100
900
Wavenumber (cm^{-1})

Figure 5a-e: IRRA spectra of **6** at gold assembled from ETOH with immersion times of 1 h, 5 h, 18 h, 30 h, and 144 h, respectively.

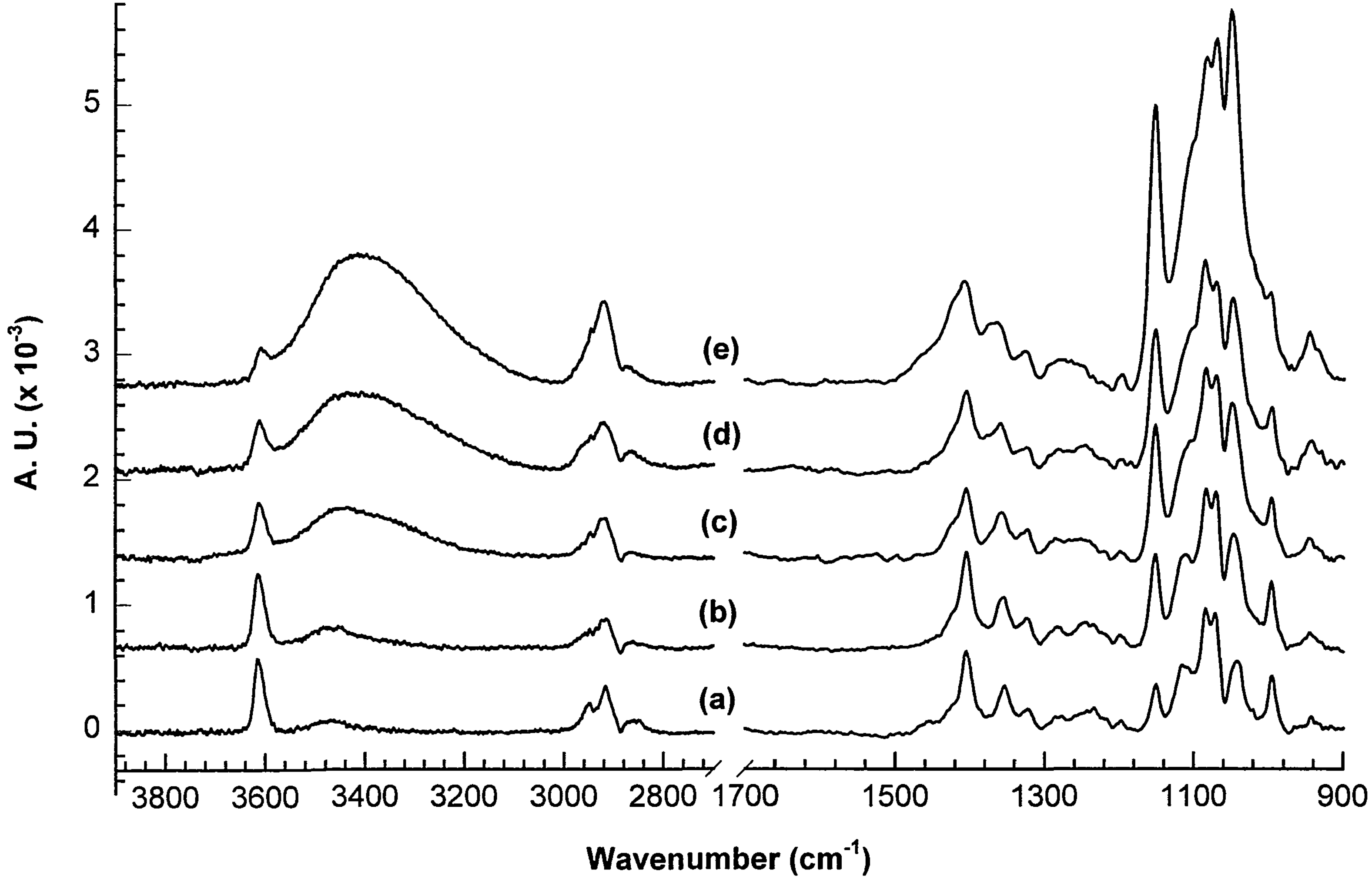
A. U. (x 10^{-3})
0
1
2
3
4
5
(e)
(d)
(c)
(b)
(a)
3800
3600
3400
3200
3000
2800
1700
1500
1300
1100
900
Wavenumber (cm^{-1})

Figure 6a-e: IRRA spectra of 7 at gold assembled from ETOH with immersion times of 1 h, 5 h, 18 h, 30 h, and 144 h, respectively.

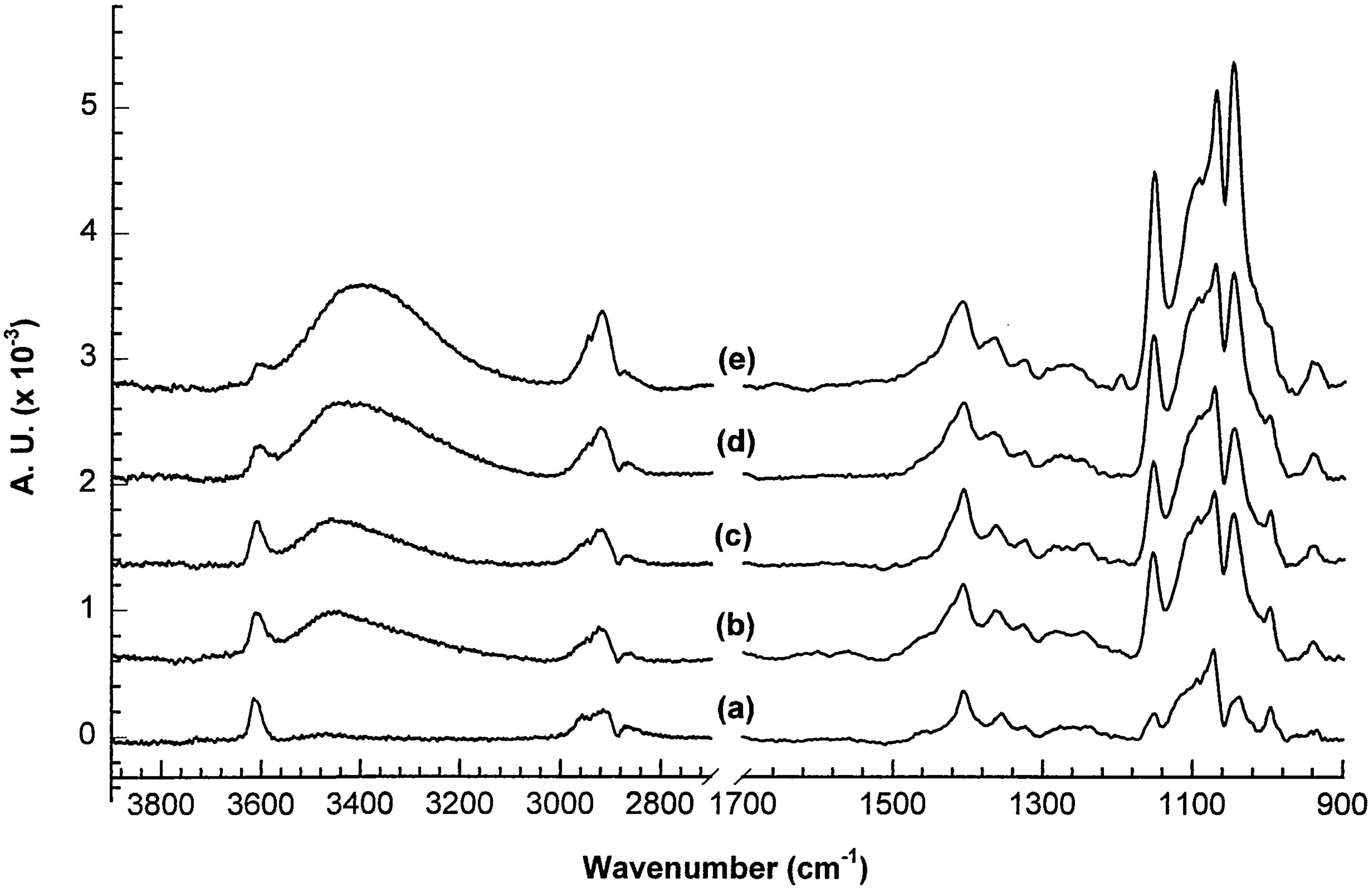
A. U. (x 10^{-3})
0
1
2
3
4
5
(e)
(d)
(c)
(b)
(a)
3800
3600
3400
3200
3000
2800
1700
1500
1300
1100
900
Wavenumber (cm^{-1})

for the glucosidic linkages are small. This similarity argues that the interfacial structures that were formed at short immersion times from both solvents are qualitatively the same. However, as immersion time increases, the spectra change dramatically. The intramolecular hydrogen-bonding is displaced by the intermolecular hydrogen-bonding. For the lower frequency region, both ν_{as}(C-O-C) and ν_s(C-O-C) of the glucosidic linkage gradually increase in their relative magnitudes (e.g., at 18 h immersion times, A_{1045}/A_{1070} for **6** and **7** equals 0.85 and 0.78; and at 144 h, the respective values equal 1.31 for **6** and 1.1 for **7**), suggesting that the average orientation of **6** and **7** at gold is evolving. At the same time, the absolute magnitudes of all of the bands (with the exception of the intramolecularly hydrogen bonded ν(OH)) are gradually increased, which confirms that the CD-layers form a multilayer structure with increased immersions time. We interpret these observations to the formation of a H-bonded multilayer film at long immersion. Furthermore, since the overlayer is not chemisorbed at gold, the multilayer exhibits a more disordered structure.

In conclusion, the above IR structural and immersion time studies show that DMF is the best solvent for the monolayer formation of **6** and **7** at gold. With DMF as the solvent, the monolayer formation process is basically complete in an immersion time of about 1 hour, and the interfacial structures of the films will not change at longer immersion times. The relative intensity changes of the bands also argue that the films are more ordered and with a preferential orientation with the axis that pass through the cyclodextrin cavity perpendicular to the gold surface. To further confirm the interfacial structures of the films, we employ more surface sensitive techniques to analyze different aspects of the films. The following sections will discuss the analysis.

C. More Evidence for Interfacial Structures of 6 and 7 at Gold. This section examines the interfacial structures of **6** and **7** at gold based on characterizations by several different surface sensitive techniques: the nature of the thiol-appendages with gold using XPS, the wettability of the surface as related to the identity of the surface functional groups, the film thickness from optical ellipsometry, and surface coverage by electrochemistry.

(i) Optical ellipsometry thickness and contact angle measurements. To further assess details of the interfacial structures of **6** and **7** at gold, optical ellipsometry and contact angle measurements were used to characterize thicknesses and wettabilities. Table III summarizes the results, and includes data for comparative interfacial structures. The ellipsometric analysis yielded thicknesses of ~12 Å for both structures. Based on considerations of molecular models [41], the theoretical thicknesses for both monolayers with the appendages fully extended is ~15 Å. Thus, within the limitations of our analysis of the data, the similarities of the observed and predicted thicknesses point to the formation of films that are one molecular layer in thickness.

Advancing contact angle (θ_a) measurements were used to probe the wettability of these monolayers; with water and hexadecane as probe liquids. As shown in Table III, the values of θ_a are about 32° for **6** at gold and 31° for **7** at gold for water, and are effectively immeasurable (<10°) for hexadecane. By comparison, the wettabilities of both **6** and **7** at gold are *intermediate* of those for methyl-terminated ($\theta_a(H_2O) = 115°$) and hydroxyl-

Table III. Ellipsometric Thicknesses and Advancing Contact Angles (θ_a) and for **6** and **7** and comparative interfacial structures at gold surfaces[a]

Monolayers	Ellipsometric Thickness (Å)	θ_a (degrees)		Reference
		H_2O	$C_{16}H_{34}$	
6 (DMF)	12	32	< 10	this work
7 (DMF)	12	31	< 10	this work
$CH_3(CH_2)_5SH$	9	109	< 10	this work
$HO(CH_2)_{12}SH$: $CH_3(CH_2)_{11}SH$				
1:0	--	< 10	< 10	b
3:1	--	32	< 10	b
6:7	--	54	< 10	b
1:3	--	68	15	b
1:4	--	81	25	b
1:16	--	102	39	b
0:1	--	115	43	b

(a) Data for 18 h immersion times. (b) Bain C. D. et al., *J. Am. Chem. Soc.* **1989**, *111*, 7155-64.

terminated ($\theta_a(H_2O) < 10°$) monolayers with a polymethylene chain containing eleven methylene groups [42]. That is, **6** and **7** at gold exhibit a wettability that is neither that of a "pure" hydroxyl-terminated monolayer or of a "pure" methyl-terminated monolayer. We attribute this observation primarily to the presence of the hydrophobic cavity in the cyclodextrin structure which results in an interfacial structure composed of a both hydrophilic (i.e., secondary hydroxyl groups on the rim of the cavity) and hydrophobic cavity. This conclusion is consistent with the results of recent studies of the wettability of two-component monolayers [43], a summary of which is included in Table III. In these studies, the effect of altering the relative amount of a hydrophobic (methyl-terminated) and hydrophilic (hydroxyl-terminated) functionality at the interface was tested. Monolayers of only a methyl-terminated monolayer or a hydroxyl-terminated monolayers exhibited properties of the single component. Monolayers of mixed composition displayed intermediate wettabilities that are similar to those observed for our cyclodextrin monolayers. Together, the ellipsometric thicknesses and wettability data are in-line with the properties expected of the targeted arrangement of the monolayers from **6** and **7**.

(ii) XPS Studies of the nature of S-Au interaction. To examine the bonding between the thiol-appendages of **6** and 7 and gold, XPS studies were conducted. Figures 7a and b present the results in the S(2p) region, and include the findings of a curve fitting analysis. The individual data points represent the experimental data and the solid curves the fitted data. As expected from the structures of **6** and 7, these can be fit with two sets of bands.

Figure 7 : XPS spectra of (a) **6** at gold; (b) **7** at gold. Both were assembled from DMF with an immersion time of 20 h. The dots were the experimental data points. The solid lines were the curve-fitted lines.

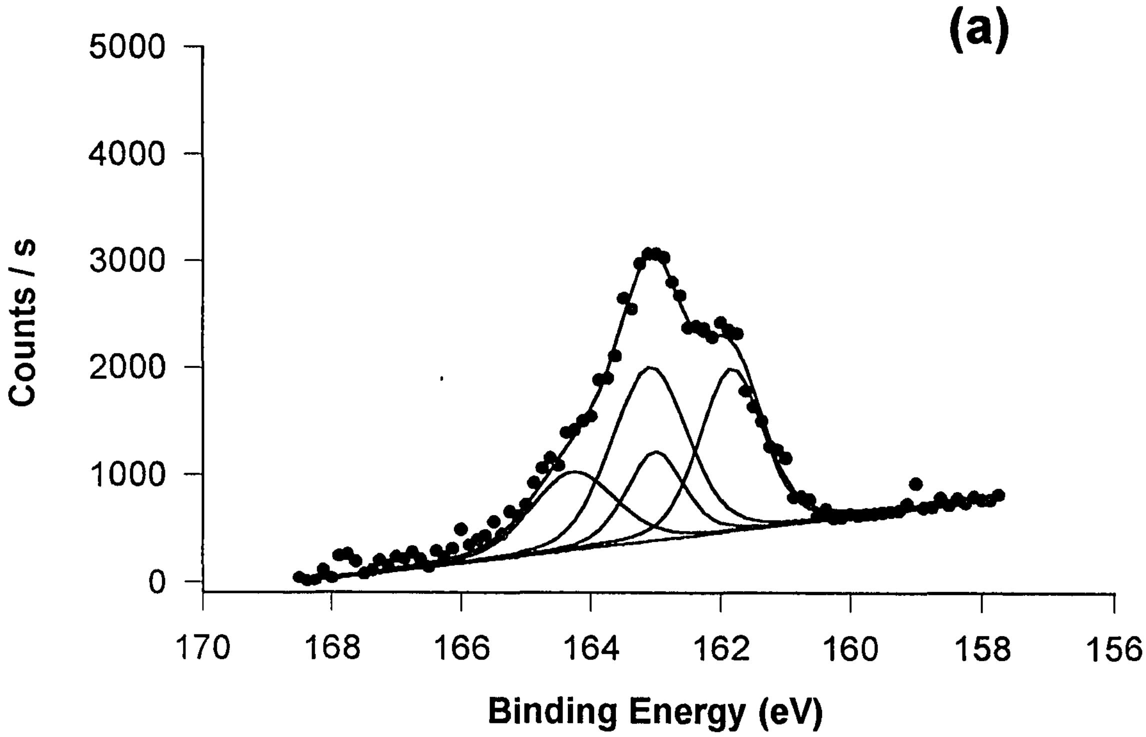
(a)
Counts / s
5000
4000
3000
2000
1000
0
170
168
166
164
162
160
158
156
Binding Energy (eV)

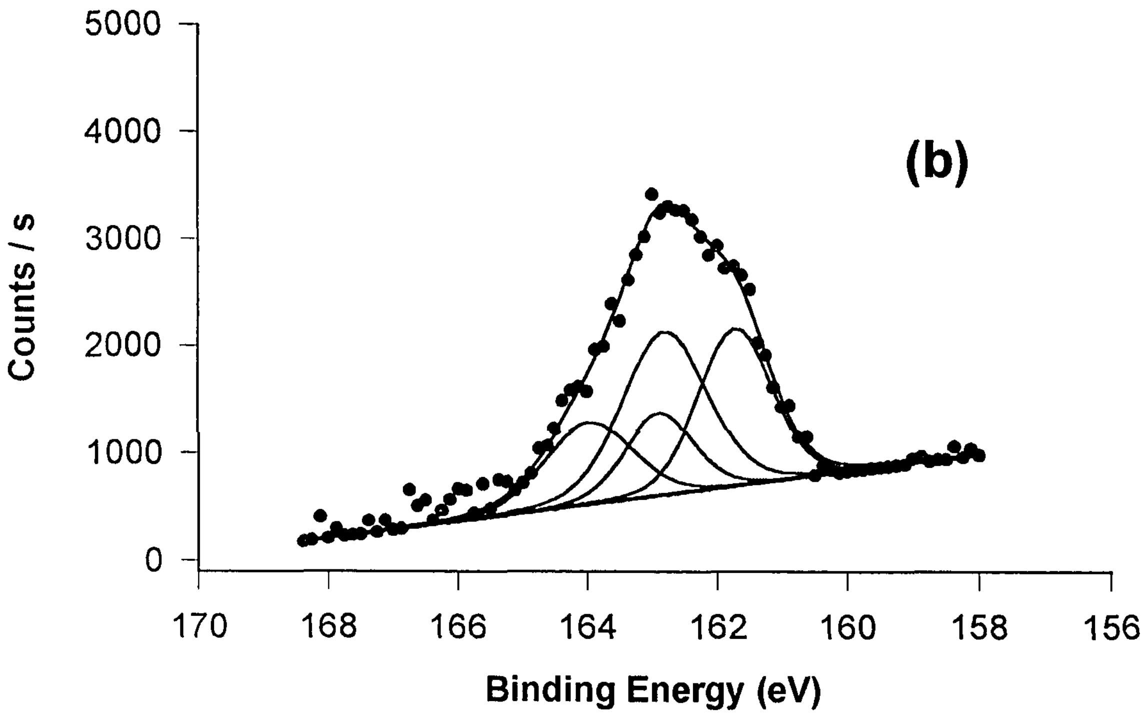
(b)
Counts / s
5000
4000
3000
2000
1000
0
170
168
166
164
162
160
158
156
Binding Energy (eV)

The first set has S($2p_{3/2}$) at 161.9 eV and S($2p_{1/2}$) at 163.1 eV, and the second set has S($2p_{3/2}$) at 163.0 eV and S($2p_{1/2}$) at 164.2 eV. Based on earlier studies, thiol and thioether functional groups have similar binding energies in this region (S($2p_{3/2}$) ~163.0 eV and S($2p_{1/2}$) ~164.2 eV [24]), whereas the bands for gold-thiolates are about 1 eV lower in energy (S($2p_{3/2}$) ~161.9 eV and S($2p_{1/2}$) ~163.1 eV [44-47]). Thus, the results from the curve fitting data are consistent with the formation of the thiolate monolayers from **6** and **7** at gold. Furthermore, the ratio of the intensity of the two sets of bands are ~1:1, which also indicates that the interfacial structures of **6** and **7** at gold are the same as in Scheme I.

(iii) Electrochemical Assessment of Surface Coverage. The layers formed by **6** and **7** from DMF were also characterized by an electrochemical assessment of surface coverage. This analysis is based on our studies of the electrode reactions of these systems, which have shown that the alkanethiolate monolayers at gold can be desorbed in alkaline solution via Reaction 1 [48, 49]. Integration of the charge under the desorption wave, after

$$\text{RS-Au} + e^{-} \rightarrow \text{RS}^{-} + \text{Au} \qquad [1]$$

accounting for surface roughness and after using a straight capacitive-baseline approximation for charging current, is therefore diagnostic of the surface coverage.

Figure 8 presents the current-potential curves for linear sweep voltammograms for the DMF-formed layers from **6** and **7** at gold. In both cases, the large cathodic wave at -0.95 V (vs. Ag/AgCl (sat'd KCl)) reflects Reaction 1. Integration of charge under each of the waves translates to surface coverages (Γ_{exp}) of 0.85 x 10^{-10} mol/cm^2 for the layer from **6** and

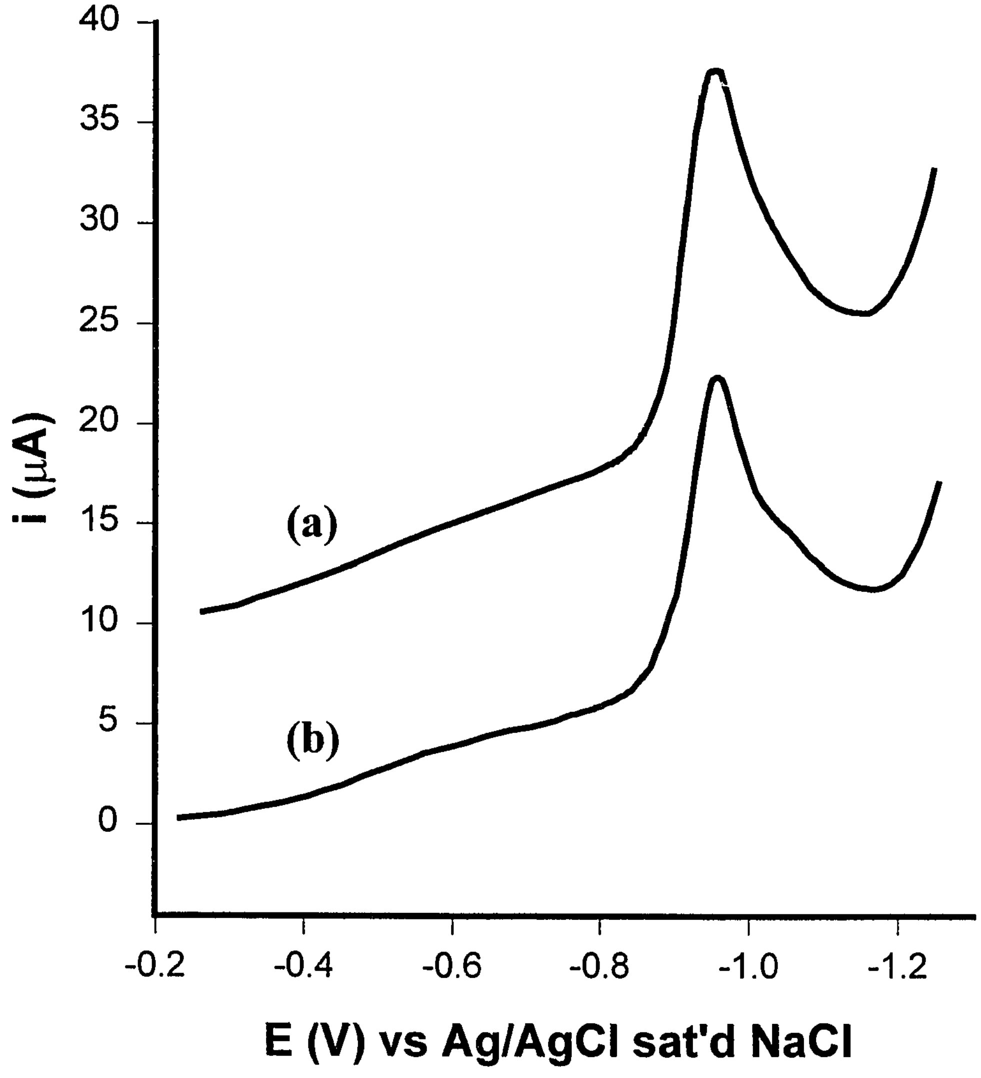

Fig 8. Voltammograms of (a) **6** at gold; (b) **7** at gold in 0.5 M KOH(aq). Scan rate is 50 mV/s.

0.61×10^{-10} mol/cm^2 for the layer from **7**. These coverages, as summarized in Table IV, are roughly 25% lower than those based on the theoretical closest packed coverages for both systems.

Together, the data from the surface sensitive techniques provide important details of different aspects of **6** and **7** at gold as formed from DMF. We conclude that the films of **6** and **7** assembled from DMF are of monomolecular thickness. The interfacial structures of the monolayers are the same as shown in Scheme I, i.e., with the axis passing through the cyclodextrin cavities perpendicular to the surface. In this arrangement, all the cavities of the cyclodextrin should be facing outside and hence the host-guest interaction can be maximized. Therefore, the monolayers were used for the test of molecular recognition in a later section.

Table IV. Electrochemical Desorption Data for **6** and **7** Chemisorbed at Gold from DMF

Sample	E_p (V)	Γ_{theory} (10^{-11} mole/cm^2)	Γ_{expt}* (10^{-11} mole/cm^2)	% of Coverage
6/Au	-0.95	10.22	8.54	84
7/Au	-0.95	8.19	6.07	74

* The roughness factor for Au/Cr/glass is 1.3.

D. Molecular Recognition Properties of The Cyclodextrin Monolayers. After understanding the condition for the monolayer formation of **6** and **7** at gold, QCM was used to test the molecular recognition properties of the monolayers. For the formation of monolayers at quartz crystals, DMF was used as the solvent with an immersion time of ~18 h. Preliminary studies for the responses of the **6** and **7** coated quartz crystal when exposed to different analytes in the gas phase were examined. Third harmonic of the fundamental resonance frequency was used to increase the sensitivity of the response [50]. Hexane and tetrachloroethylene were chosen to be the probe molecules. Dickert and Bauer [51] have demonstrated the α- and β-cyclodextrin polymers coated quartz crystals showed different responses towards tetrachloroethylene (with higher response for β-cyclodextrin). The difference in response can be attributed to size effect. They attributed the observation to the fact that the tetrachloroethylene is too big to fit into the α-cyclodextrin's cavity.

Figures 9a and b are the QCM responses using hexane as the probe molecules. Essentially, there is no difference for **6** and **7** monolayers towards different concentrations of hexane in gas. Difference in selectivity was observed for the tetrachloroethylene as the probe molecules. Figures 10a and b shown the QCM responses for **6** and **7** coated surface to tetracholroethylene. The results clearly show that there is a greater response for the β-cyclodextrin coated surface. This observation was in agreement with the results that Dickert and Bauer's have reported. Therefore, we have demonstrated that we can alter the selectivity of monolayers by creating different cavity sizes at the surface with different cyclodextrins.

Figure 9: QCM responses of (a) **6** at gold; (b) **7** at gold when exposed to different concentrations of analyte in the gas phase. The analyte was hexane..

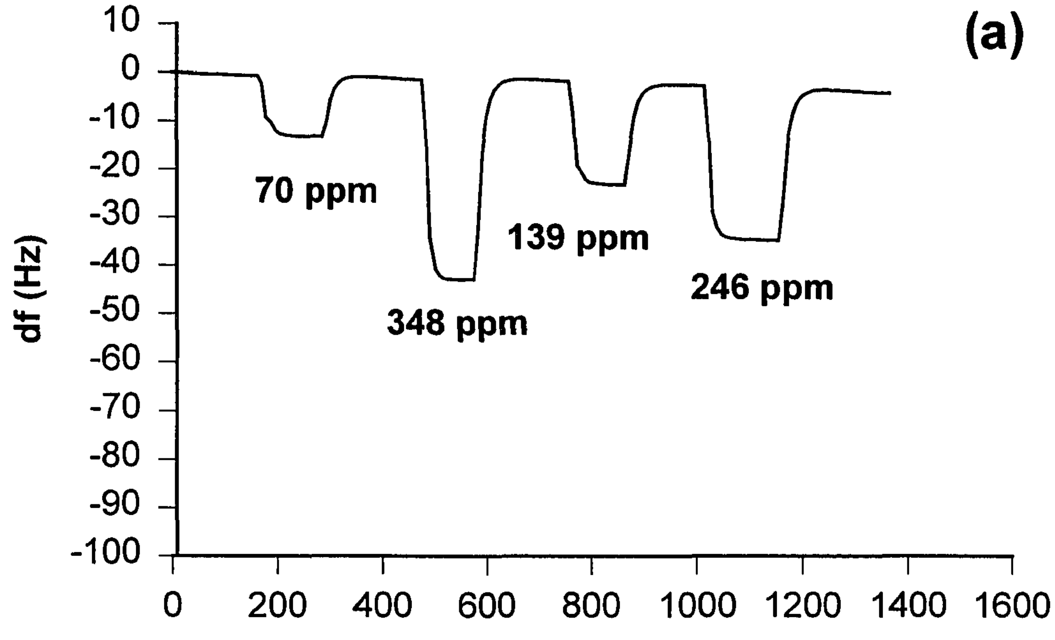
(a)
df (Hz)
10
0
-10
-20
-30
-40
-50
-60
-70
-80
-90
-100
70 ppm
348 ppm
139 ppm
246 ppm
0
200
400
600
800
1000
1200
1400
1600
Time (sec)

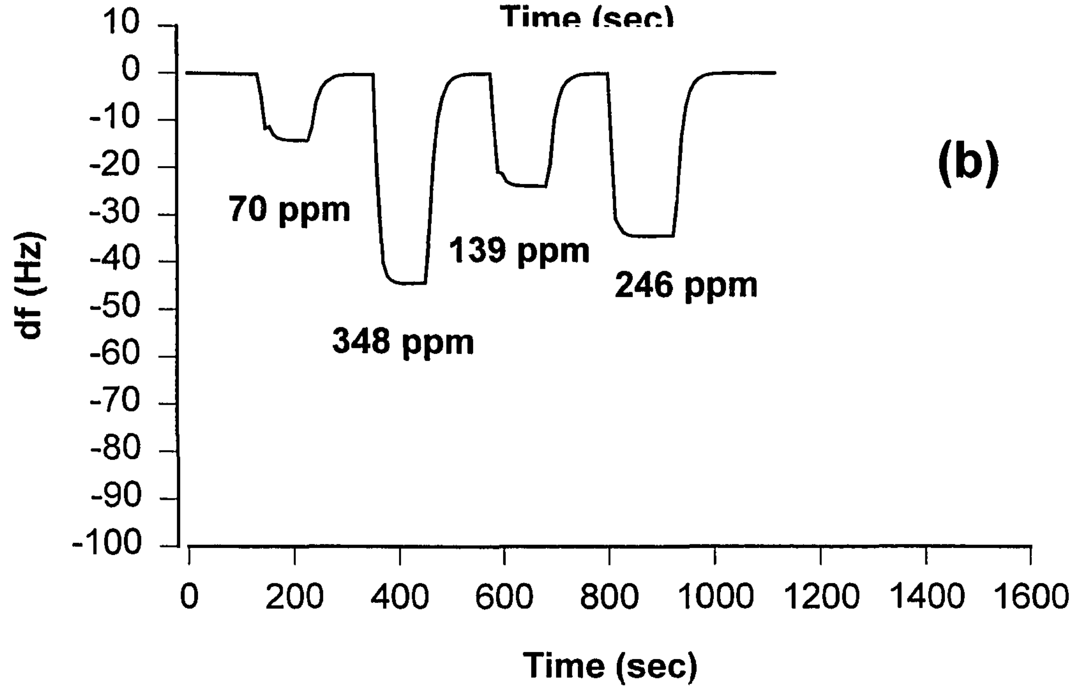
(b)
df (Hz)
10
0
-10
-20
-30
-40
-50
-60
-70
-80
-90
-100
70 ppm
348 ppm
139 ppm
246 ppm
0
200
400
600
800
1000
1200
1400
1600
Time (sec)

Fig. 10: QCM responses of (a) **6** at gold; (b) **7** at gold when exposed to different concentrations of analyte in the gas phase. The analyte was tetrachloroethylene.

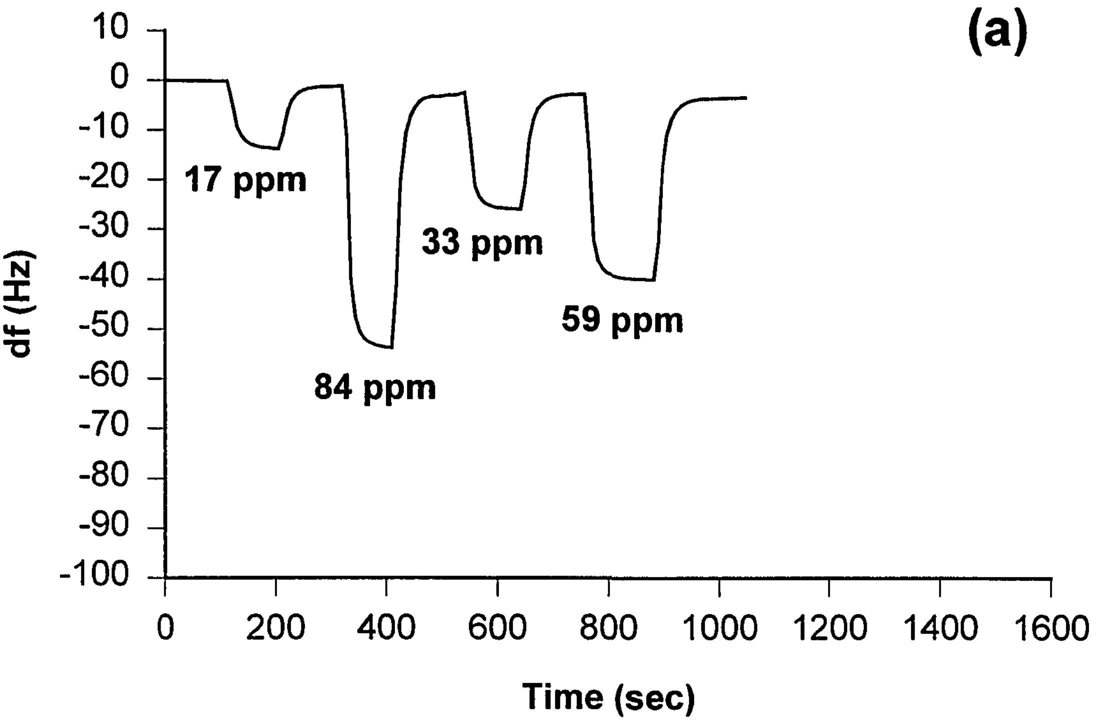
(a)
10
0
-10
-20
-30
-40
-50
-60
-70
-80
-90
-100
df (Hz)
17 ppm
84 ppm
33 ppm
59 ppm
0
200
400
600
800
1000
1200
1400
1600
Time (sec)

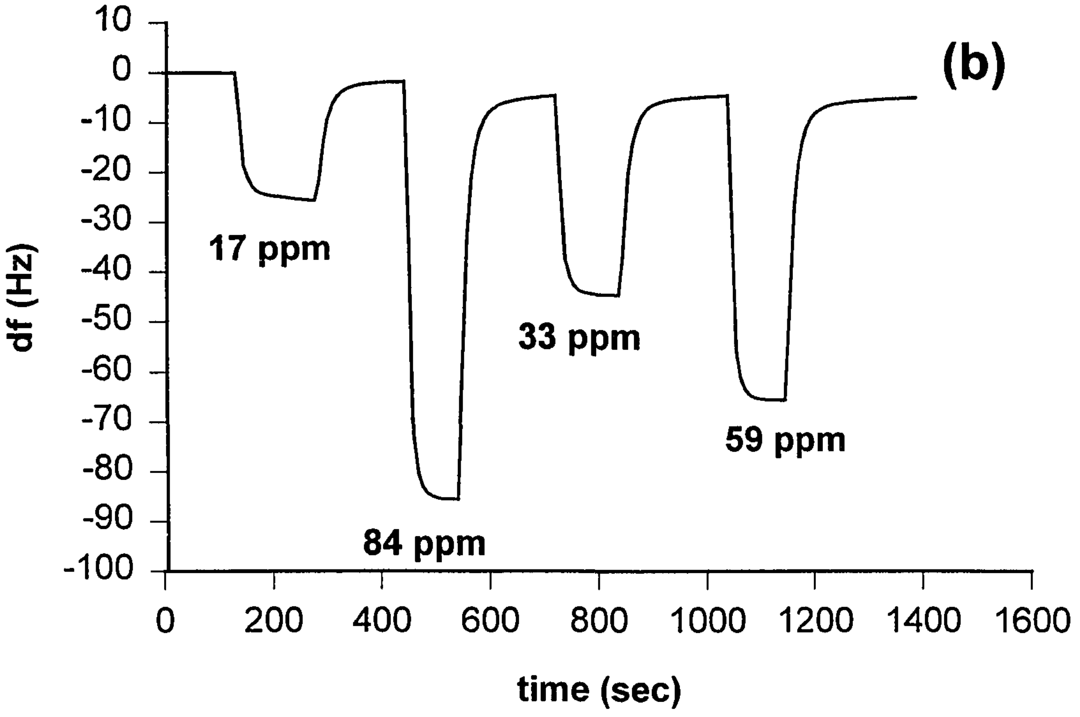
(b)
10
0
-10
-20
-30
-40
-50
-60
-70
-80
-90
-100
df (Hz)
17 ppm
84 ppm
33 ppm
59 ppm
0
200
400
600
800
1000
1200
1400
1600
time (sec)

CONCLUSIONS

We have synthesized two new thiol-containing α- and, β-cyclodextrins derivatives (**6**, **7**). The unique feature of the derivatives is ethylene spacer groups, which increase the flexibility for the thiol moieties to find binding sites at gold surfaces. Detailed studies to assess the effect of solvents and immersion time on the monolayer formation were carried out. Data shown that monolayers of **6** and **7** at Gold can be formed when DMF was used as the solvent. Characterization of the monolayers by different surface sensitive techniques showed that the cyclodextrin orientation at surfaces were the same as shown in Scheme I. However, when EtOH or THF are used as the solvents for assembling, mutilayers will be formed at long immersion times. The molecular recognition properties of the monolayers were demonstrated by QCM experiments using hexane and tetrachloroethylene as the probe molecules. Both **6** and **7** coated crystals have the same responses for hexane. Greater responses were obtained for **7** coated crystals when tetrachloroethylene was used. This can be explained by the better fitting of molecules for β-cyclodextrins due to size effect.

APPENDIX--DETERMINATION OF INFRARED SPECTROSCOPIC BAND ASSIGNMENTS FOR THIOL-CONTAINING CYCLODEXTRIN DERIVATIVES (6 AND 7)

A detailed description of the assignment of IR spectral bands of **6** and **7** are presented in this section. These assignments are based on earlier reports [34-39] and on our experimental observations.

The low energy spectral region (Figures 1 and 2) contains a large number of diagnostic bands, including ν(C-O-C), ν(C-O), ν(C-C), δ(C-H), and δ(O-H) [34-36]. The assignments in this region are complicated by extensive band overlap and the presence of mixed vibrational modes.

The envelope between 1200 and 950 cm^{-1}, which contains at least five clearly identifiable bands, arises primarily from ν(C-O-C) of the glucosidic linkages and the glucose rings and ν(C-O) of the secondary hydroxyl groups. The ν(C-O-C) of the glucosidic linkages has two components: ν_{as}(C-O-C) and ν_s(C-O-C). We have assigned the band at 1045 cm^{-1} to ν_s(C-O-C) based on the findings of a recent IRRAS study of Langmuir-Blodgett films of oriented, amphiphilic CDs [52]. The assignment of ν_{as}(C-O-C), which is ascribed to the band at ~1150 cm^{-1}, is more controversial. Labeling experiments have shown that this band decreases in magnitude upon deuteration [36]. Based on the general trends in the literature, we, however, believe that such a decrease is more accurately attributed to a coupling with the ν(C-O) or δ(O-H) of the secondary hydroxyl groups.

For the remaining bands in this envelope, we ascribe the bands at 1086 cm^{-1} and 997 cm^{-1} to ν(C-O) of the secondary hydroxyl groups. This assignment is based on the results of the spectroscopic changes as judged from our preliminary attempts to acylate the secondary hydroxyl groups of the layers from **6** and **7** [53]. Finally, the bands at 1107 cm^{-1} and 1070 cm^{-1} are attributed to ν_a(C-O-C) and ν_s(C-O-C) of the glucose monomers, respectively, and the band at 1405 cm^{-1} to δ(C-H) coupled with either δ(O-H) or ν(C-O).

In the high energy region, two different ν(O-H) are observed for the layers from **6** and **7**: a sharp band at 3611 cm^{-1} and a much broader band about 150 cm^{-1} lower in energy. As expected from the structures of **6** and **7**, neither of the bands are indicative of a "free" secondary ν(O-H) of sugar derivatives. The ν(O-H) bands of "free" secondary alcohols are typically found between 3620 and 3640 cm^{-1} [39]. We attribute the two bands to the presence of the secondary alcohols **6** and **7** that have differing extents of hydrogen-bonding. In general, as the extent of hydrogen-bonding increases, the position of ν(O-H) decreases and its width increases [38]. The sharp band at ~3610 cm^{-1} is therefore assigned to ν(O-H) of the *intramolecularly* hydrogen-bonded secondary hydroxyl groups that are present at the rim of large end of the CD-cavities. This assignment is based largely on the findings of an extensive study of the solvent-dependence of the infrared spectra of a variety of O-methyl derivatives of glucose [39]. Importantly, a single band at 3611 cm^{-1} was observed in a nonhydrogen-bonding solvent for 4,6-di-O-methyl-β-D-glucoside, a compound that is structurally similar to the monomer unit of both **6** and **7**. In non-hydrogen-bonding solvents, a single sharp band was observed at 3611 cm^{-1}.

Following the above analysis, we ascribe the broader, lower energy ν(O-H) to *intermolecularly* hydrogen-bonded hydroxyl groups. This assignment is based on two key observations: 1) only the lower energy ν(O-H) is present in the KBr spectra (**6**: 3390 cm^{-1}; **7**: 3381 cm^{-1}), and 2) both modes are evident to differing extents in the spectra for each type of sample. We believe the former reflects the phase segregation of **6** and **7** when dispersed in KBr, resulting in an intermolecular hydrogen-bonding interaction between the secondary hydroxyl groups of **6** and **7**.

ACKNOWLEDGMENT

The authors express their appreciation to C. J. Zhong for expert assistance with the QCM experiments and J. W. Anderegg for acquisition of the XPS spectra. The Ames Laboratory is operated for U.S. Department of Energy by Iowa State University under Contract No. w-7405-eng-82. This work was supported by the Office of Basic Energy Sciences, Chemical Science Division.

REFERENCES

1. Ulman, A. *An Introduction to Ultrahigh Organic Films: From Langmuir-Blodgett to Self-Assembly*; Academic Press: Boston, **1991**.
2. Nuzzo, R. G.; Allara, D. L. *J. Am. Chem. Soc.* **1983**, *105*, 4481.

3 Porter, M. D.; Bright, T. B.; Allara, D. L.; Chidsey, C. E. D. *J. Am. Chem. Soc.* **1987**, *109*, 3559.

4. Bain, C. D.; Troughton, E. B.; Tao, Y. -T; Evall, J.; Whitesides, G. M.; Nuzzo, R. G. *J. Am. Chem. Soc.* **1989**, *111*, 321.

5. Biebuyck, H. A.; Whitesides, G. M. *Langmuir* **1993**, *9*, 1766.

6. Zhong, C. J.; Porter, M. D. *J. Am. Chem. Soc.* **1994**, *116*, 11616.

7. Walczak, M. M.; Chuang, C.; Stole, S. M.; Widrig, C. A.; Porter, M. D. *J. Am. Chem. Soc.* **1991**, *113*, 2378.

8. Notoya, T.; Poling, G. W. *Corrosion* **1979**, *35*, 193.

. Allara, D. L.; Heburd, A. F.; Padden, F. J.; Nuzzo, R. G.; Falcon, D. R. *J. Vac. Sci. Technol. A* **1983**, *1*, 376.

9. Stewart, K. R.; Whiitesides. G. M.; Godfried, H. P.; Silvera, I. F. *Rev. Sci. Instrum.* **1986**, *57*, 1381.

10. Ulman, A.; Tillman, N. *Langmuir* **1989**, *5*, 1418.

11. Czanderna, A. W.; King, D. E.; Spaulding, D. *J. Vac. Sci. Technol. A* **1991**, *9*, 2607.

12. Li, T. -T.; Weaver, M. J. *J. Am. Chem. Soc.* **1984**, *106*, 6107.

13. Chidsey, C. E. *Science* **1991**, *251*, 919.

14. Miller, C.; Cuedent, P.; Graetzel, M. *J. Phys. Chem.* **1991**, *95*, 877.

15. Finklea, H. O.; Hanshew, D. D. *J. Am. Chem. Soc.* **1992**, *114*, 3173.

16. Carter, M. T.; Rowe, G. K.; Richardson, J. N.; Tender, M.; Terrill, R.H.; Murray, R. W. *J. Am. Chem. Soc.* **1995**, *117*, 2896.

17. Smith, C. P.; White, H. S., *Anal. Chem.* **1992**, *64*, 2398.

18. Finklea, H.O.; Robinson, L. R.; Blackburn, A.; Richter, B., *Langmuir* **1986**, 2, 239.

19. Rowe, G. K.; Creager, S. E. *Langmuir* **1991**, *7*, 2307.

20. De Long, H. C., Buttry, D. A., *Langmuir* **1992**, *8*, 2491.

21. Hutchison, J. E.; Postlethwaite, T. A.; Murray. R. W. *Langmuir* **1993**, *9*, 3277.

22. Zak, J.; Yuan, H. P.; Ho, M.; Woo, L. K.; Porter, M. D. *Langmuir* **1993**, *93*, 2772.

23. Wang, J.; Wu, H.; Angnes, L. *Anal. Chem.* **1993**, *65*, 1893.

24. Kepley, L. J.; Crooks, R. M.; Ricco, A. J. *Anal. Chem.* **1992**, *64*, 3191.

25. Bender, M. L.; Komiyama, M. Cyclodextrin Chemistry, Springer-Verlag, 1978.

26. Porter, M. D. *Chem. Eng. News* **1989** (May 1), 32.

27. Chinkap Chung *Ph.D. Dissertation*, Iowa State University, **1990**

28. Sieber, G. *Ann.* **1960**, *631*, 180.

29. Armstrong, W. H.; Youinou, M.-T.; Palermo, R. E. *Inorganica Chimica Acta* **1984**, *88*, 21.

30. Takeo, K.; Sumimoto, T.; Kuge *Staerke* **1974**, *26*, 111.

31. Weast, R. C. *Handbook of Chemistry and Physics*, CRC, HL, **1981**

32. Greenler, R. G. *J. Chem. Phys.* **1969**, 50, 310.

33. Porter, M. D. *Anal. Chem.* **1988**, *60*, 1143A.

34. Casu, B.; Reggiani, M.; Gallo, G. G.; Vigevani, A. *Carbohyd. Res.*, **1970**, *12*, 171.

35. Casu, B.; Reggiani, M.; Gallo, G. G.; Vigevani, A. *Tetrahedron* **1968**, *24*, 803.

36. Casu, B.; Reggiani, M. *Die Starke* **1966**,218.

37. Higgins, H. G.; Stewart, C. M.; Harrington, K. J. *J. Polymer Sci.* **1961**, *51*, 59.

38. Casu, B.; Reggiani, M.; Gallo, G. G.; Vigevani, A. *Tetrahedron* **1966**, *22*, 3061.

39. Michell, A. J.; Higgins, H. G. *Tetrahedron* **1965**, *21*, 1109.

40. Manor, P. C.; Saenger, W. *J. Am. Chem Soc.* **1974**, *96*, 3630.

41. The measurement is based on the CPK model.

42. Bain, C. D.; Evall, J.; Whitesides, G. M. *J. Am. Chem. Soc.* **1989**, *111*, 7155.

43. Lindberg, B. J.; Hamrin, K.; Johansson, G.; Gelius, U.; Fahlman, A.; Nordling, C.; Siegbahn, K. *Physi. Sci.* **1970**, *1*, 286.

44. Nuzzo, R. G.; Zegarski, B. R.; Dubois, L. H. *J. Am. Chem. Soc.* **1987**, *109*, 733.

45. Bain, C. D.; Biebuyck, H. A.; Whitesides, G. M. *Langmuir* **1989**, *5*, 723.

46. Laibinis, P. E.; Whitesides, G. M.; Allara, D. L.; Tao, Y.-T.; Parik, A N.; Nuzzo, R. G. *J. Am. Chem. Soc.* **1991**, *113*, 7152.

47. Weisshaar, D. E.; Walczak, M. M.; Porter, M. D. *Langmuir* **1993**, *9*, 323.

48. Widrig, C. A.; Chung, C.; Porter, M. D. *J. Electroanal. Chem.* **1991**, *310*, 335.

49. Walczak, M. M.; Popenoe, D. D.; Deihammer, R. S.; Lamp, B. D.; Chung, C.; Porter, M. D. *Langmuir* **1991**, *7*, 2687.

50. Zhong, C. J.; Porter, M. D. Manuscript in preparation.

51. Dickert, F. L.; Bauer, P. A. *Adv. Mater.* **1991**, *9*, 436.

52. Kawabata, Y.; Matsumoto, M.; Nakayoshi, T., Tanaka, M.; Manda, E. *Thin Solid Films* **1988**, *159*, 353.

53. The studies were performed by the reaction of **6** or **7** at gold with gas phase acetyl chloride.

CHAPTER 2. THIOL-DERIVATIZED METALLOPORPHYRINS: MONOMOLECULAR FILMS FOR THE ELECTROCATALYTIC REDUCTION OF DIOXYGEN AT GOLD ELECTRODES

A paper published in Langmuir[1]

Jerzy Zak[2], Hongping Yuan, Mankit Ho, L. Keith Woo, and Marc D. Porter

ABSTRACT

This paper describes preliminary results in the design, construction, and characterization of cobalt(II) porphyrins derivatized with alkyl thiol appendages. The use of the thiol appendages leads to the formation of a chemisorbed monolayer of the corresponding thiolate at gold electrodes. This approach provides a beginning for fabricating electrocatalytic monolayers with a preselected architecture through the manipulation of the number and location of the appendages. Voltammetric data indicate that monolayers from both **I(Co)** and **II(Co)** at gold catalyze the two-electron reduction of O_2 to H_2O_2. The monolayer from **I(Co)**, however, has a lower electrocatalytic activity. Infrared, X-ray photoelectron, and visible spectroscopic data are presented that argue the difference in reactivity arises from a difference in interfacial architecture.

---

[1] Reprinted with permission from *Langmuir* **1993**, *9*, 2772-2774. Copyright © 1994 the American Chemical Society.

[2] Permanent address: The Silesian Technical University, Department of Chemistry, 44-100 Gliwice Poland.

Findings are also reported that indicate the preparation of mixed monolayers (e.g., two-component monolayers from **I(Co)** and $CH_3(CH_2)_3SH$) may prove valuable to this area of research.

RESULTS AND DISCUSSION

Recent findings point to the electrocatalytic reduction of O_2 via immobilized metallomacrocycles as an attractive reaction for use in fuel cells [1-7]. We report herein the creation and characterization of monolayers formed by the chemisorption [8-10] of the thiol-derivatized cobalt(II) porphyrins **I(Co)** and **II(Co)** at gold electrodes. A key feature of **I(Co)** and **II(Co)** is the number and location of the thiol-containing "legs". Our findings suggest that this approach can serve as an effective starting point for controlling the spatial orientation and coverage of the adsorbates (Chart I). We show that monolayers from **I(Co)** and **II(Co)** exhibit different electrocatalytic properties. Results from infrared (IRS), X-ray photoeletron (XPS), and visible (VS) spectroscopic data as well as from various chemical manipulations of the surface structure indicate that the differences in activity arise from differences in their interfacial architecture.

Preparation of the free-base thiol-derivatized porphyrins **I(H_2)** and **II(H_2)** followed modifications of earlier procedures [11-12]. Of paramount importance is the placement of both thiol appendages of **II(H_2)** on the same side of the porphyrin plane. This was achieved

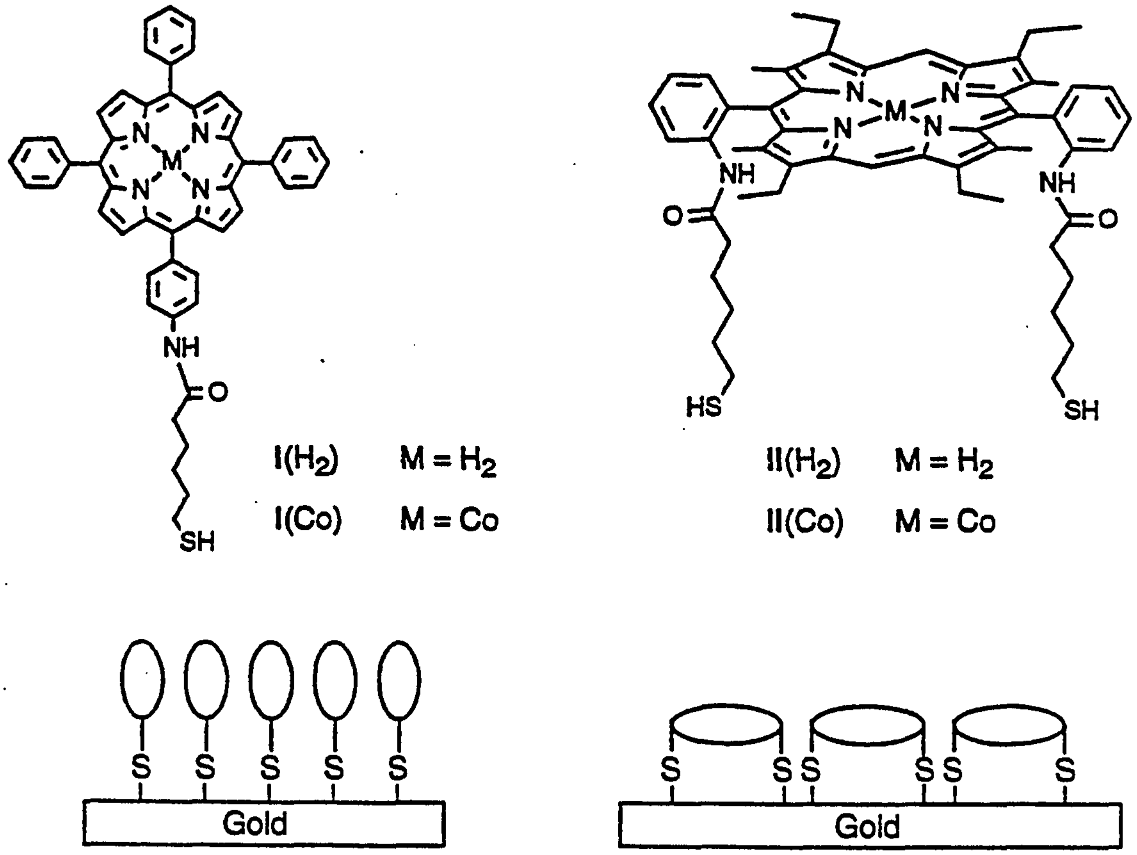

I(H_2) M = H_2

I(Co) M = Co

II(H_2) M = H_2

II(Co) M = Co

NH
O
SH
N
M
HS
S
Gold

Chart I. The Structures of the Thio-containing porphyrin derivatives and their "Expected" Orientation at Gold using the *cis*-amine isomer of 5,15-bis[*o*-aminophenyl]etioporphyrin as the precursor, which was separated from its *trans*-amine isomer using chromatography [13]. Alkylation of the *cis*-amine isomer with 6-(tritylthio)hexanoyl chloride, followed by removal of the trityl protecting groups with $Hg(OAc)_2$ and H_2S [14], produced 5α,15α-bis[*o*-(6-mercaptohexylamido)phenyl]etioporphyrin, **II(H$_2$)**. Meso-[*p*-(6-mercaptohexylamido)phenyl]triphenylporphyrin, **I(H$_2$)**, was prepared in a similar manner from (*p*-aminophenyl)triphenylporphyrin [15]. The metal complexes, **I(Co)** and **II(Co)**, were synthesized by insertion of Co(II) before removal of the trityl groups [16]. Monolayers were constructed by the immersion of annealed mica-supported gold [17, 18] into 10 mM CH_2Cl_2 solutions of the thiol-derivatives for ~12 h. Samples were rinsed extensively with CH_2Cl_2 and CH_3CH_2OH upon emersion. The subsequent findings are representative of the testing of more than ten samples of each type of monolayer.

Evidence of the reactivities of the monolayers from **I(Co)** and **II(Co)** is provided by the voltammograms in O_2-saturated solutions of 0.1 M $HClO_4$ in Figure 1. Curve a is for uncoated gold. Curves b and c are for **I(Co)** and **II(Co)**, respectively, as monolayers at gold. The positions and magnitudes of the curves reveal that the monolayer from **II(Co)** is a more effective electrocatalyst for the reduction of O_2 to H_2O_2 [19]. Control experiments [20], which used analogs of **I(Co)** and **II(Co)** where all of the SH groups are replaced by CH_3 groups, indicate that the differences in curves b and c do not arise from differences in the electronic structures of the adsorbate precursors. We therefore attribute our observations to

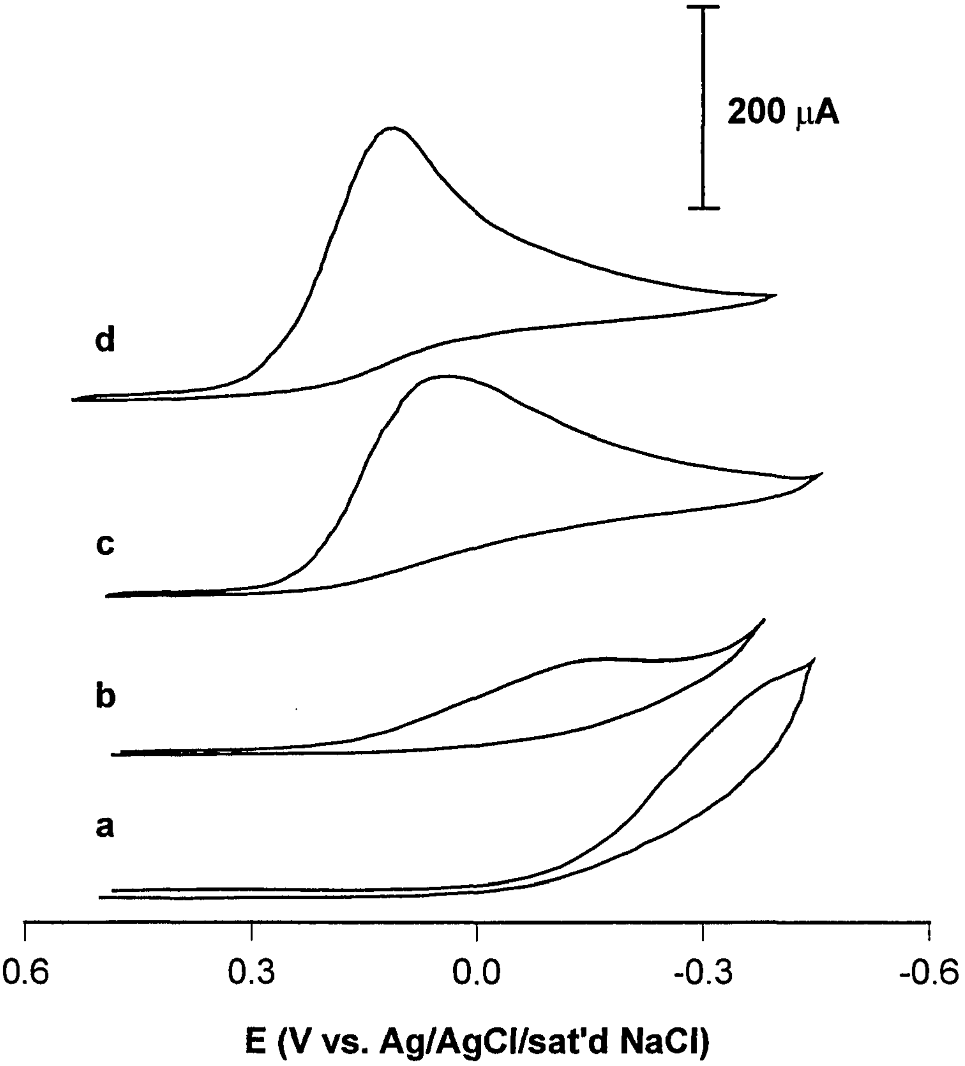

Figure 1. Voltammetric curves obtained for different Au electrodes: (a) uncoated Au, (b) **I(Co)** chemisorbed at Au, (c) **II(Co)** chemisorbed at Au, and (d) mixed monolayer from $CH_3(CH_2)_3SH$ and **I(Co)** chemisorbed at Au. The supporting electrolyte was an O_2-saturated solution of 0.1 M $HClO_4$. The scan rate was 50 mV/s; geometric electrode area was of 0.63 cm^2.

differences in the architecture of the two monolayers as directed by the chemisorption at gold via the thiol-containing appendages groups.

Figure 2 presents IRS [17, 18] data that provide insights into the structures of the two monolayers. The absolute magnitudes of the bands for **I(Co)** and **II(Co)** at gold and the similarities of their positions with respect to the precursors in KBr point to the formation of a monomolecular film of each complex. In addition, these data reveal general *qualitative* details about the architecture of the two monolayers [21]. The details develop from considerations of the infrared surface selection rule which results from the preferential excitation of vibrational modes with dipoles normal to a highly reflecting metal surface [22-24]. Thus, the differences in the relative absorbances of the bands for **I(Co)** and **II(Co)** at gold relative to in KBr are diagnostic of a preferentially, as opposed to randomly, oriented surface structure for both types of monolayers. At this time, however, an analysis of the orientation of the porphyrin ring from these data awaits completion of an in-depth band assignment study [25-28].

Characterizations using XPS, in addition to substantiating the composition of both types of monolayers, confirm chemisorption at gold through sulfur. For **I(Co)** at gold, bands only for sulfur as a gold-bound thiolate were observed: S($2p_{1/2}$) at 163.1 eV and S($2p_{3/2}$) at 161.9 eV [29-32]. Features diagnostic of unreacted SH groups and the more highly oxidized forms of sulfur (e.g., disulfides and sulfonates), which are all found at higher binding energies [33], were not detected. The XPS data for **II(Co)** is in agreement with the data for

Figure 2. Infrared spectra for **I(Co)** (A) and **II(Co)** (B) in KBr and at gold. S is 4.0×10^{-2} and 4.0×10^{-4} A.U. for the KBr and monolayer spectra, respectively. The reflection spectra were collected using p-polarized light incident at 82° with respect to the surface normal.

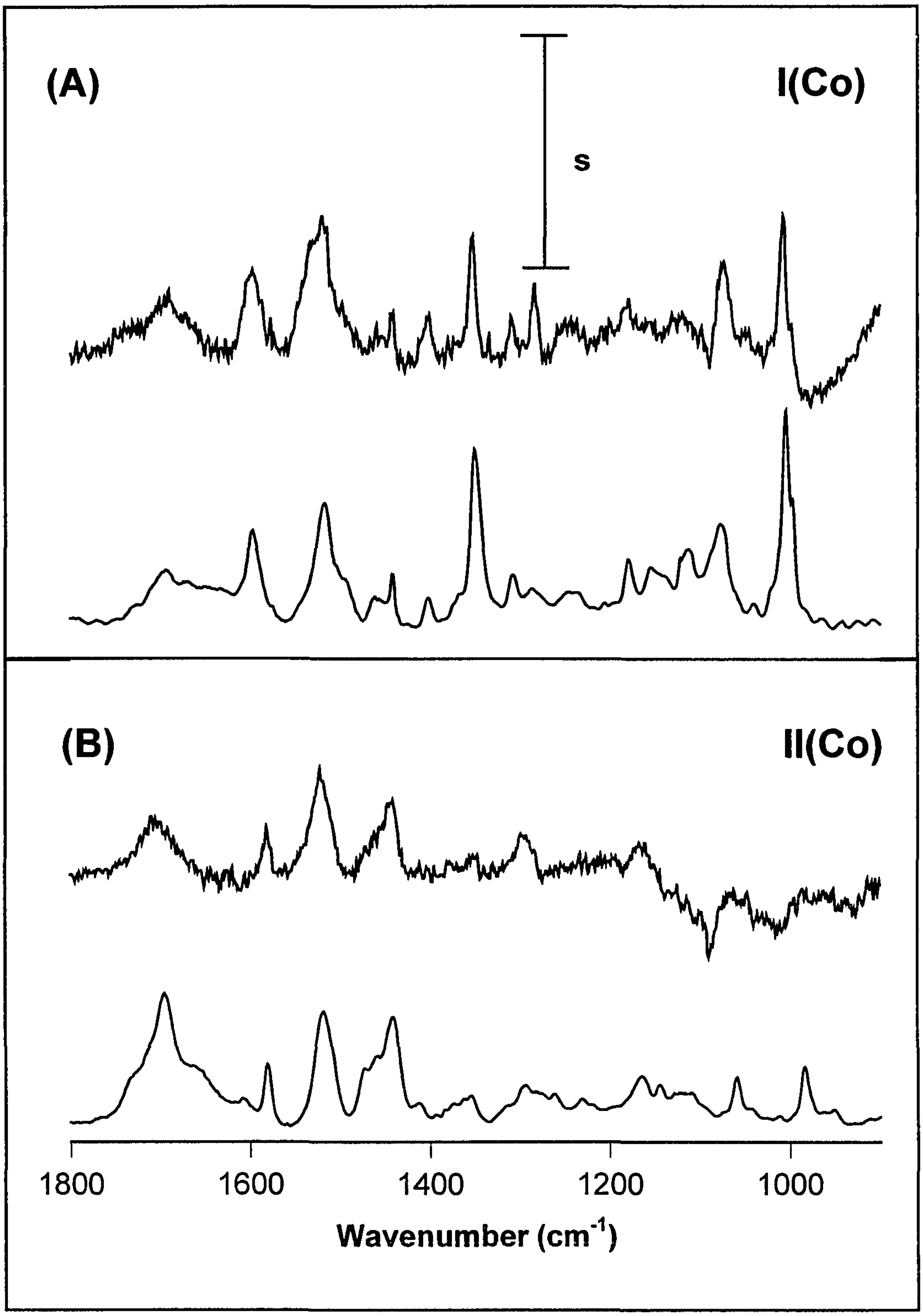
(A)
I(Co)
s
(B)
II(Co)
1800
1600
1400
1200
1000
Wavenumber (cm^{-1})

I(Co) at gold, though we are unable to rule out the presence of a trace amount of polysulfide [34].

The VS data reveal an additional aspect of the interfacial structures of these two monolayers. Upon chemisorption, the B band of **I(Co)** undergoes an exitonic splitting to yield a doublet with blue- (394 nm) and red-shifted (448 nm) components (Figure 3, spectrum e), as also found at related Langmuir-Blodgett films [35-38]. On the other hand, only a weakly absorbing red-shifted (436 nm) B band was observed upon chemisorption of **II(Co)**. The positions of the B bands in CH_2Cl_2 are 412 nm and 402 nm for **I(Co)** and **II(Co)**, respectively. These spectral changes suggest a difference in the electronic dipolar interactions between the adsorbates in the two monolayers. The red shift for the monolayer from **II(Co)** is typical of head-to-tail dipolar interactions between the π-systems of neighboring adsorbates [35-38]. This interaction is consistent with the structural description based on IRS. In contrast, the spectrum for the monolayer from **I(Co)** reveals the presence of coplanar, inclined [35] (as oppose to face-to face [39]) π-π electronic interactions between neighboring adsorbates. Based on these data, we infer that the structure of monolayer from **II(Co)** is in line with that depicted in Chart I, whereas that from **I(Co)** is more consistent with the representation in Chart II.

Figure 3. Visible spectra for **I(Co)**. (a) **I(Co)** in CH_2Cl_2. (b)-(d) mixed monolayers formed by exchanging a butanethiolate monolayer at gold with 10 mM of **I(Co)** in CH_2Cl_2: (b) butanethiolate only; (c) 2 h exchange; (d) 18 h exchange. (e) **I(Co)** at gold as a pure monolayer. S is 0.1 A.U. for (a) and 0.01 A.U. for (b)-(e). The VS measurements were made using a Hewlett-Packard 8452A diode array spectrometer. The reflection spectra were collected using p-polarized light incident at 60° with respect to the surface normal. An uncoated gold substrate served as a reference. The spectra in (b)-(e) were smoothed using an eleven-point Savitsky-Golay algorithm.

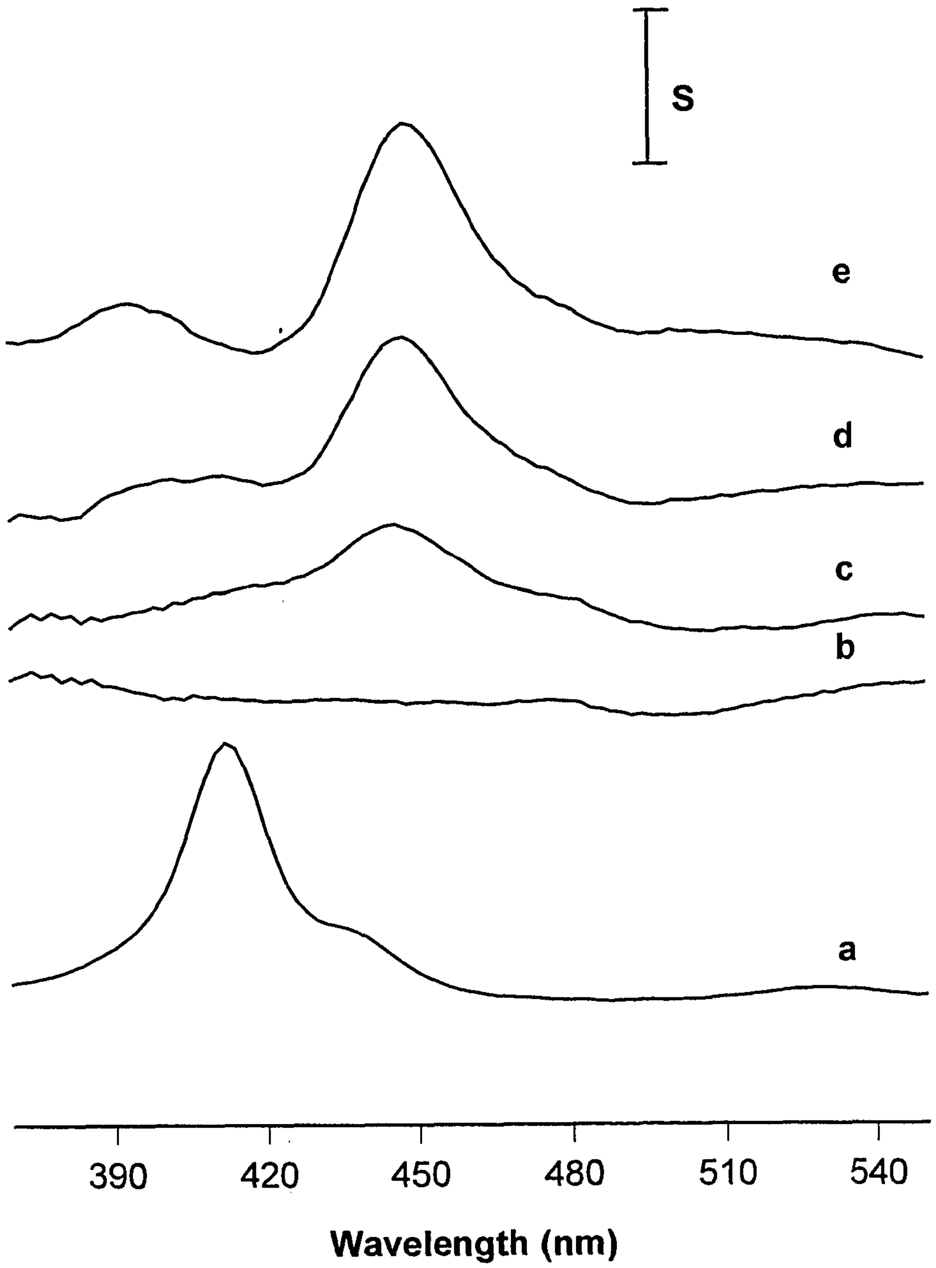
S
e
d
c
b
a
390
420
450
480
510
540
Wavelength (nm)

Chart II

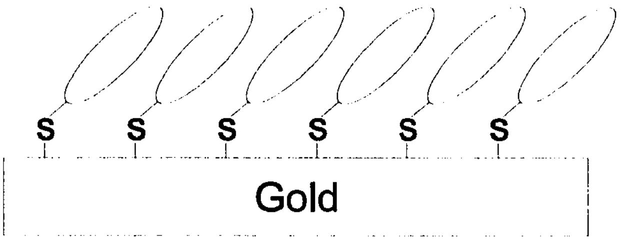

To assess the influence of the π-π interactions for the monolayer from **I(Co)**, a mixed monolayer was prepared by a partial exchange **I(Co)** with a previously formed monolayer from $CH_3(CH_2)_3SH$ [40]. Curve d in Figure 1 exemplifies the improvement in the electrocatalytic response. We attribute this to an isolation of porphyrin moieties within the matrix of the short chain thiolate. The VS data in Figure 3 confirm the effect of the short chain thiolate on the coplanar, inclined π-stacking of the monolayer from **I(Co)**. Spectrum b is for the monolayer from $CH_3(CH_2)_3SH$. The spectra in c and d are for exchange times of 2 and 18 h, respectively. Exitonic splitting of the B band is detectable only at long exchange times, consistent with the general architecture in Chart II. Voltammetric experiments at these samples reveal that electrocatalytic potency decreased upon extensive exchange. These findings argue that lower electrocatalytic current for monolayer **I(Co)** results from coplanar, inclined π-π interactions between adsorbates, which hinders accessibility to catalytic sites.

Support of our interpretation is provided by the results of attempts to metalate **I(H_2)** and **II(H_2)** using $Co(OAc)_2$ (~2 mM in CH_3OH, 1 h immersion) after monolayer formation.

With such treatment, monolayers from **II(H_2)** displayed a response like curve c in Figure 1. Similarly treated monolayers from **I(H_2)** failed to catalyze O_2 reduction at a detectable level. Finally, $Co(OAc)_2$ treatment of a mixed monolayer from **I(H_2)** and $CH_3(CH_2)_3SH$ produced an electrode with an activity similar to that in Figure 1, curve d.

Work in progress is addressing further the fundamental aspects of these types of monolayers. The goal is to establish a clear connection between the molecular architecture of interfacial structures, the resulting electrocatalytic potency, and to improve subsequent electrocatalytic performance. Of particular interest is unraveling how the interplay of the chemisorption of sulfur at gold and the π-π interactions between neighboring porphyrins controls the resulting interfacial structure.

ACKNOWLEDGMENT

Insightful discussions with M. G. Finn and the expert assistance of J. Andregg on the XPS measurements are gratefully acknowledged. LKW is a NSF Presidential Young Investigator (CHE-9057752) and a 1993 Camille and Henry Dreyfus Teacher-Scholar. The Ames Laboratory is operated for the U. S. Department of Energy by Iowa State University. This work was supported by the Office of Basic Energy Sciences, Chemical Science Division.

REFERENCES AND NOTES

1. Murray, R. W. *Electroanalytical Chemistry: A Series of Advances*; Bard, A. J., Ed., Marcel Dekker: New York, 1984; Vol. 13, p. 191.
2. Forshey, P. A.; Kuwana, T. *Inorg. Chem.* **1983**, *22*, 699.
3. Durand, R. R.; Bencosme, C.S.; Collman, J. P.; Anson, F. C. *J. Am. Chem. Soc.* **1983**, *105*, 2710.
4. Ni, C. -L.; Abdalmuhdi, I.; Chang, C. K.; Anson, F. C. *J. Phys. Chem.* **1987**, *91*, 1158.
5. Bettelheim, A.; White, B. A.; Murray, R. W. *J. Electroanal. Chem.* **1987**, *217*, 271.
6. Van Galen, D. A.; Majda, M. *Anal. Chem.* **1988**, *60*, 1549.
7. Hutchison J. E.; Postlethwaite T. A.; Murray R. W. *J. Electroanal. Chem.*, submitted.
8. Ulman, A. *An Introduction to Ultrahigh Organic Films: From Langmuir-Blodgett to Self-Assembly*; Academic Press: Boston, **1991**.
9. Whitesides, G. M.; Laibinis, P. E. *Langmuir* **1990**, *6*, 87.
10. Dubois, L. H.; Nuzzo, R. G. *Ann. Rev. Phys. Chem.* **1992**, *42*, 437.
11. Woo, L. K.; Maurya, M. R.; Tolpppi, C. J.; Jacobson, R. A.; Yang, S.; Rose, E. *Inorg. Chim. Acta* **1991**, *182*, 41.
12. Woo, L. K.; Maurya, M. R.; Jacobson, R. A.; Yang, S.; Ringrose, S. L. *Inorg. Chem.* **1992**, *31*, 913.
13. Young, R.; Chang, C. K. *J. Am. Chem.* Soc. **1985**, *107*, 898.
14. Collman, J. P.; Groh, S. E. *J. Am. Chem. Soc.* **1982**, *104*, 1391.

15. Further details of the synthesis and other preparative procedures will appear in a manuscript in preparation.
16. Fuhrhop, J.; Smith, K. M. *Laboratory Methods in Porphyrin and Metalloporphyrin Research*; Elsevier: New York, **1975**, 42.
17. Widrig, C. A.; Chung, C.; Porter, M. D. *J. Electroanal. Chem.* **1991**, *310*, 335.
18. Walczak, M. M.; Popenone, D. D.; Deinhammer, R. S.; Lamp, B. D.; Chung, C.; Porter, M. D. *Langmuir* **1991**, *7*, 2687.
19. Data supporting H_2O_2 as the electrolysis product was obtained spectroscopically using a long optical pathlength thin-layer electrochemical cell (J. Zak, Iowa State University, unpublished results).
20. Electrodes prepared by dip coating the alkyl analogs of **I(Co)** and **II(Co)** at gold exhibited similar voltammetry in O_2-saturated solutions of 0.1 M $HClO_4$: peak potentials of the **I(Co)** and **II(Co)** analogs are +0.07 V and +0.04 V (vs. Ag/AgCl (sat'd NaCl)), respectively.
21. The voltammetry of the metal centers for I(Co) and II(Co) in deoxygenated solutions is poorly defined and difficult to distinguish from the background current. This has hindered attempts to determine the surface coverage by the measurement of the charge required for the one-electron conversion of the metal centers. We are presently devising a spectrophotometric assay for collecting such information.
22. Greener, R. G. *J. Chem. Phys.* **1969**, 50, 310.
23. Porter, M. D. *Anal. Chem.* **1988**, *60*, 1143A.

24 McIntyre, J. D. E. *Advances in Electrochemistry and Electrochemical Engineering*; Delahay, P.; Tobias, C. W., Eds.; Wiley: New York, **1973**.

25. Cotton, T. M.; Schultz, S. G.; Van Duyne, R. P. *J. Am. Chem. Soc.* **1982**, *104*, 6528.

26. Nakanishi, K.; Solomon, P. H. *Infared Absorption Spectroscopy*; Holden-Day, Inc.: Oakland, 1977.

27. Sprio, T. G.; Czernuszewics, R. S.; Li, X.-Y. *Coord. Chem. Rev.* **1990**, *100*, 541

28. Alben J. O. *The Porphyrins*; Dolphin, D., Ed.; Academic Press: Boston, **1988**; Vol III, Part A.

29. Nuzzo, R. G.; Zegarski, B. R.; Dubois, L. H. *J. Am. Chem. Soc.* **1987**, *109*, 733.

30. Bain, C. D.; Biebuyck, H. A.; Whitesides, G. M. *Langmuir* **1989**, *5*, 723.

31. Laibinis, P. E.; Whitesides, G. M.; Allara, D. L.; Tao, Y.-T.; Parik, A N.; Nuzzo, R. G. *J. Am. Chem. Soc.* **1991**, *113*, 7152.

32. Weisshaar, D. E.; Walczak, M. M.; Porter, M. D. *Langmuir* **1993**, *9*, 323.

33. Lindberg, B. J.; Hamrin, K.; Johansson, G.; Gelius, U.; Fahlman, A.; Nordling, C.; Siegbahn, K. *Physi. Sci.* **1970**, *1*, 286.

34. A slight broadening at the low energy side of the S(2p$_{3/2}$) band for **II(Co)** suggests the possible presence of polysulfide. However, this feature is barely detectable above the noise of the measurement and suggests that only trace amounts of these impurities are present.

35. Schick, G. A.; Schreiman, I. C.; Wagner, R. W.; Lindsey, J. S.; Bocian, D. F. *J. Am. Chem. Soc.* **1989**, *111*, 1344.

36. Bulkowski, J. E.; Bull, R. A.; Sauerbrunn, S. R. *ACS Symp. Ser.;* Nazik, A. J. Ed.; American Chemical Soc.: Washington, D. C., **1981**; Vol. 146, 279.

37. Bull, R. A.; Bulkowski, J. E. *J. Colloid Interface Sci.* **1983**, *92*, 1.

38. Cantor C. R.; Schimmel P. R. *Biophysical Chemistry*; W. H. Freeman: San Francisco 1980; Part II, p. 395

39. Face-to-face π-π electronic interactions between porphyrins exhibit only a blue-shifted B band (see, for example, Gouterman, M; Hanson, L. K.; Khalil, G.-E.; Buchler, J. W.; Rohbock, K.; Dolphin, D. *J. Am. Chem. Soc.* **1975**, *97*, 3142.)

40. The mixed monolayer structure was prepared by forming a layer from 1 mM $CH_3(CH_2)_3SH$ in ethanol, followed by a partial exchange with 10 mM of **I(Co)** in CH_2Cl_2 for ~4 h.

CHAPTER 3. ELECTROCHEMICAL OXIDATION OF AMINE-CONTAINING COMPOUNDS: A ROUTE TO THE SURFACE MODIFICATION OF GLASSY CARBON ELECTRODES

A paper published in Langmuir[1]

Randall S. Deinhammer, Mankit Ho, James T. Anderegg, and Marc D. Porter[2]

ABSTRACT

A method for the modification of glassy carbon electrodes (GCEs) with amine-containing compounds for electrocatalytic and biosensor purposes is investigated. The method utilizes the electrooxidation of amines to their analogous cation radicals to form a chemically stable covalent linkage between the nitrogen atom of the amine and edge plane sites at the GCE surface. Using X-ray photoelectron spectroscopy (XPS) for coverage assessment, the capability of this route is demonstrated by the immobilization of a simple primary amine at the GCE surface. An investigation of the influence of substituents on the nitrogen atom (e.g., primary, secondary, tertiary amines) revealed that the surface coverage of primary amines was ~3 times higher than that of secondary amines, whereas tertiary amines were not immobilized at a detectable level. This behavior is attributed to a strong steric effect whereby bulky substituents on the nitrogen atom hinder accessibility of the reactive

---

[1] Reprinted with permission from *Langmuir* **1994**, *10*, 1306-13. Copyright © 1994 the American Chemical Society.

[2] Author to whom correspondence should be addressed.

amine cation radical to surface binding sites. Amine salts and amides also showed no detectable coverage by XPS. The utility of the method for creation of a GCE with electrocatalytic activity is demonstrated by the immobilization of dopamine (DA) at the GCE surface. The DA-modified GCE is used to facilitate oxidation of β-NADH via a surface EC mechanism. These examples illustrate the facility of this route for simplifying and shortening dramatically the processing required for immobilization using other synthetic methods. A mechanism for the immobilization process is also briefly discussed.

INTRODUCTION

Over the past several years, there has been a continued interest in the use of carbon-based materials for electrochemical purposes [1-3]. The impetus for this interest is the potential of such materials as replacements for precious metal electrodes. Often, however, these materials require some form of surface pretreatment [4-9] or bulk material processing (e.g., doping of carbon with noble metals [10]) to overcome sluggish electron-transfer kinetics or to enhance selectivity for electroanalysis. Such processing in the former case can involve a lengthy sequence of steps, including oxidative [4-6] and coupling agent [4,7-9] pretreatments that are followed by the immobilization of a target moiety through linkage with the coupling agent. Therefore, in view of the importance of these types of materials to electrosynthesis [7,8], electrocatalysis [11-14], and biosensor [15-19] technologies, it is of fundamental importance to develop new, less complex routes for the modification of carbon surfaces.

Recently, a novel route has been devised for modifying carbon fibers as components in composite materials [20]. This route is based on the electrooxidation of amine-containing compounds, and is generalized in Scheme I. As proposed, the process proceeds initially via the one-electron oxidation of an amine functionality to its corresponding cation radical, which subsequently forms a carbon-nitrogen linkage at the carbon surface. In the composite materials application, ω-diamines are used to enhance the mechanical toughness of the composite whereby one of the amine groups of the diamine is linked to the surface of the carbon fiber and the other to reactive groups in an epoxy resin.

Scheme I

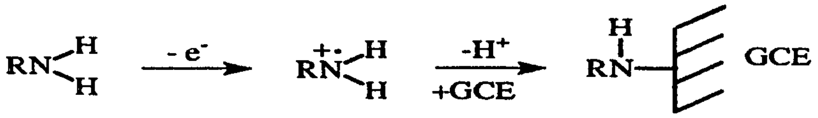

Based on our interests in the surface modification of carbon-based materials as stationary phases for new forms of chemical separations [21,22], we have explored the extension of Scheme I as a facile means for altering the interfacial architecture of glassy carbon electrodes (GCEs). In the following sections, we describe the results of an investigation of the range and scope of Scheme I as a route for the creation of chemically modified GCEs. Our investigation included an assessment of: (1) the extent of the immobilization of different types of amine-containing compounds (i.e., primary, secondary, and tertiary alkylamines); (2) the ability to create an electrocatalytic GCE via the immobilization of dopamine; and (3) the ability to create a biotinylated GCE surface capable of binding the protein avidin. The focus of the latter effort, which was demonstration of the utility of Scheme I for the fabrication of a platform for anchoring enzymes at carbonaceous materials for biosensor purposes [17-19], is described elsewhere [23]. In each of our assessments, particular attention was given to defining the experimental conditions that resulted in a maximal modifier coverage. X-ray photoelectron spectroscopy (XPS) was used as the primary tool for coverage assessment. The coverage of the dopamine-modified GCE was also determined electrochemically. Finally, an extension of the immobilization mechanism is proposed that is based, in part, on our results from attempts to modify the basal plane of highly oriented pyrolytic graphite (HOPG) electrodes using Scheme I.

EXPERIMENTAL

Reagents and Chemicals.

N-acetylethylenediamine, N-propylacetamide, butylamine, N-methylbutylamine, N-ethylbutylamine, N,N-dimethylbutylamine, and 3-hydroxytyramine hydrochloride (dopamine hydrochloride) were from Aldrich. Triethylamine was from Eastman. Table I gives the chemical structures for each of these compounds. Catechol, disodium hydrogen phosphate, sodium chloride, and perchloric acid (70%) were from Fisher. β-nicotinamide

Table 1. Chemical Structures, Anodic Peak Current Voltages (E_p), and N/C Values for Various Nitrogen-Containing Compounds.

Chemical Name	Chemical Structure	Conditions	E_{pa} (V)	100 (N/C)
N-acetylethylenediamine	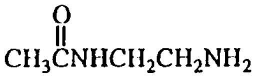 $CH_3\overset{\overset{O}{\|}}{C}NHCH_2CH_2NH_2$	1 voltage cycle 2 voltage cycles	+1.30 V	6.4 6.5
N-propylacetamide	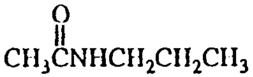 $CH_3\overset{\overset{O}{\|}}{C}NHCH_2CH_2CH_3$	1 voltage cycle	------	trace
Butylamine	$CH_3(CH_2)_3NH_2$	1 voltage cycle 1 voltage cycle (HOPG)	+1.25 V +1.35 V	3.7 trace
N-methylbutylamine	$CH_3(CH_2)_3NHCH_3$	1 voltage cycle 2 voltage cycles	+1.03 V	1.4 1.4
N-ethylbutylamine	$CH_3(CH_2)_3NHCH_2CH_3$	1 voltage cycle	+1.02 V	0.9
N,N-dimethylbutylamine	$CH_3(CH_2)_3N(CH_3)_2$	1 voltage cycle 2 voltage cycles	+0.88 V, +1.02 V	trace trace
Triethylamine	$(CH_3CH_2)_3N$	1 voltage cycle	+0.86 V	trace
Dopamine	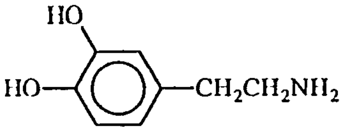	1 voltage cycle injection method	+1.25 V	1.3 3.5
N-(5-aminopentyl) biotinamide	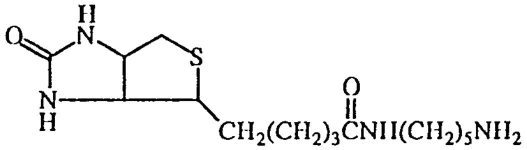	1 voltage cycle 2 voltage cycles	+1.25 V	6.4 7.5

adenine dinucleotide (β-NADH) was from Sigma, and was stored at $0^{o}C$. Sodium dihydrogen phosphate was from Mallinckrodt. Lithium perchlorate (anhydrous) was from G. Frederick Smith. Alpha-alumina (1.0 μm) was from Buehler. Absolute ethanol (punctilious grade) was from Quantum Chemical Co. The liquid amine-containing compounds were purified by distillation before use. All other chemicals were used as received. House distilled water was further processed using a Millipore Milli-Q water purification system, and was used in all solution and electrode preparations. The phosphate buffer solution (pH ~7) consisted of 0.1 M NaCl, 10 mM Na_2HPO_4, and 10 mM Na_2HPO_4. The amino group of dopamine hydrochloride was deprotonated by addition of triethylamine.

Carbon Substrate Preparation.

The GCEs (Tokai Carbon, grade GC-20) were prepared by polishing first with silicon carbide powder (600 grit) followed by 1.0 μm alumina on a polishing pad (Buehler). The GCEs were sonicated in water for 15 min after each polishing step. After the initial polishing, the GCEs were resurfaced using 1.0 μm alumina only. All GCEs were sonicated for 15 min in water, rinsed with water and ethanol, and dried with a stream of high purity nitrogen immediately before use. After electrochemical treatment in the amine-containing electrolytic solutions, the GCEs were rinsed with ethanol and water and sonicated for 15 min in pH 7 phosphate buffer. This process was used to remove any physisorbed, unreacted materials from the electrode surface. Samples were then characterized using XPS or electrochemical techniques. The HOPG electrodes (Union Carbide, grade ZYB) were prepared by removal of a thin top-layer of the material with adhesive tape to expose a fresh surface.

Electrochemistry.

Electrochemical experiments were performed using a CV-27 potentiostat (Bioanalytical Systems) and a Houston Instruments Omnigraphic 2000 XY recorder. Voltage steps were generated using a PAR 175 Universal Programmer that was connected to the potentiostat. A conventional three-electrode cell was used with the geometric area of the electrode defined by the circular opening in an inert elastomer gasket (0.40 cm^2). A Pt coil auxiliary electrode and a Ag/AgCl/sat'd $LiClO_4$ reference electrode (-34 mV vs SCE) were used; all voltages are given with respect to this reference. All electrolysis solutions were 0.1 M $LiClO_4$ in absolute ethanol.

X-Ray Photoelectron Spectroscopy.

The XPS data were acquired with a Physical Electronics Industries Model 5500 multi-technique surface analysis system equipped with a hemispherical analyzer, a monochromator, and a multichannel detector. Monochromatic Al Kα-radiation (1486.6 eV) at 300 W was used for excitation. The photoelectrons were collected at 10^{o} from the surface parallel to maximize surface detection sensitivity [24]. Binding energies were referenced to the C(1s) emission band at 284.3 eV. Acquisition times for the survey spectra were typically 2 min, and those for the high resolution spectra were between 2-7 min for the N(1s) region.

The base pressure of the ion-pumped UHV chamber was less than 1 x 10^{-9} Torr during analysis. The elemental nitrogen-to-carbon ratio, (N/C), was used as the major parameter for assessing the extent of modifier coverage. Values for N/C were calculated by dividing the total number of counts under the N(1s) band by that under the C(1s) band and multiplying the result by 100, after accounting for differences in sensitivity factors [25]. The N/C values are reported as averages of 2-6 samples, and varied by ~10-15 % between similarly prepared samples.

RESULTS AND DISCUSSION

Feasibility of Immobilizing Amine-Containing Molecules at GCEs via Scheme I.

To assess the range and scope of Scheme I as a route for the modification of carbon surfaces, we began with an examination of the immobilization of several simple, structurally-related alkylamines at the GCE surface. These studies, presented in this and the next section, provide a general picture of the utility of this immobilization method, the stability of the modified surface, and insights into the types of nitrogen-containing functional groups that can be used for the modification.

Figure 1 shows a typical cyclic voltammetric (CV) curve obtained at a GCE in an ethanolic solution containing 1 mM N-acetylethylenediamine and 0.1 M $LiClO_4$ (solid line). The voltage scan was initiated at 0.00 V and reversed at an upper limit of +1.40 V. The scan

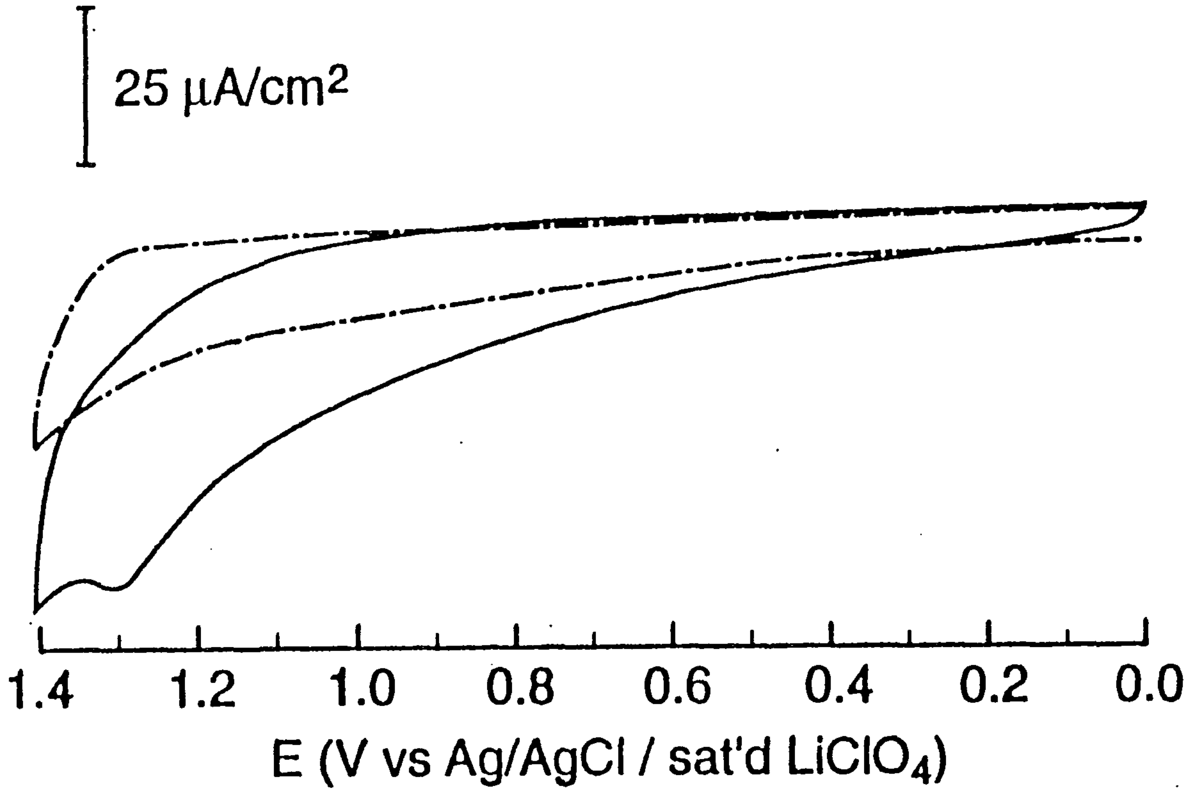

Figure 1. Cyclic voltammogram obtained at a freshly polished GCE in an ethanolic solution containing 1 mM N-acetylethylenediamine (solid curve). The dashed curve was obtained in supporting electrolyte only. The sweep rate was 10 mV/s.

rate was 10 mV/s. A broad, chemically irreversible oxidation wave is apparent, with a peak-current voltage (E_p) of +1.30 V. A comparison with a scan at a GCE in only supporting electrolyte (dashed curve) suggests the onset of an oxidative process near +0.30 V. We attribute this wave to the one-electron oxidation of the amine group to its corresponding cation radical. This interpretation is based both on the earlier literature for the oxidation of amines at carbon-based electrodes [20,26,27] and on the absence of the oxidative wave in scans at a GCE in an electrolytic solution containing N-propylacetamide. We have also found, in agreement with the literature, that basic aqueous solutions [26] (pH > pK_a of amine) as well as other nonaqueous solvent supporting electrolyte combinations (e.g., acetonitrile and tetrabutylammonium salt) support this process [20]. We, however, utilized ethanol because of the higher solubility of the amine-containing biomolecules dopamine and biotin in this solvent.

To verify that the electrooxidation of the amine functionality is requisite for immobilization, XPS was used to follow the changes in the relative nitrogen content at the GCE surface as a function of the anodic voltage limit in a single sweep CV experiment. Figure 2 presents the findings of the XPS characterization in the N(1s) region using the above N-acetylethylenediamine solution. N-acetylethylenediamine instead of a simpler primary amine was used as a probe molecule for these experiments because the two nitrogens in its molecular structure provided increased detection sensitivity. Figure 2a is the result for a GCE immersed in solution with the applied voltage (E_{app}) held at 0.00 V for 5 min. Figures 2b-d are data for GCEs cycled between 0.00 V and different upper voltage limits: +0.70 V

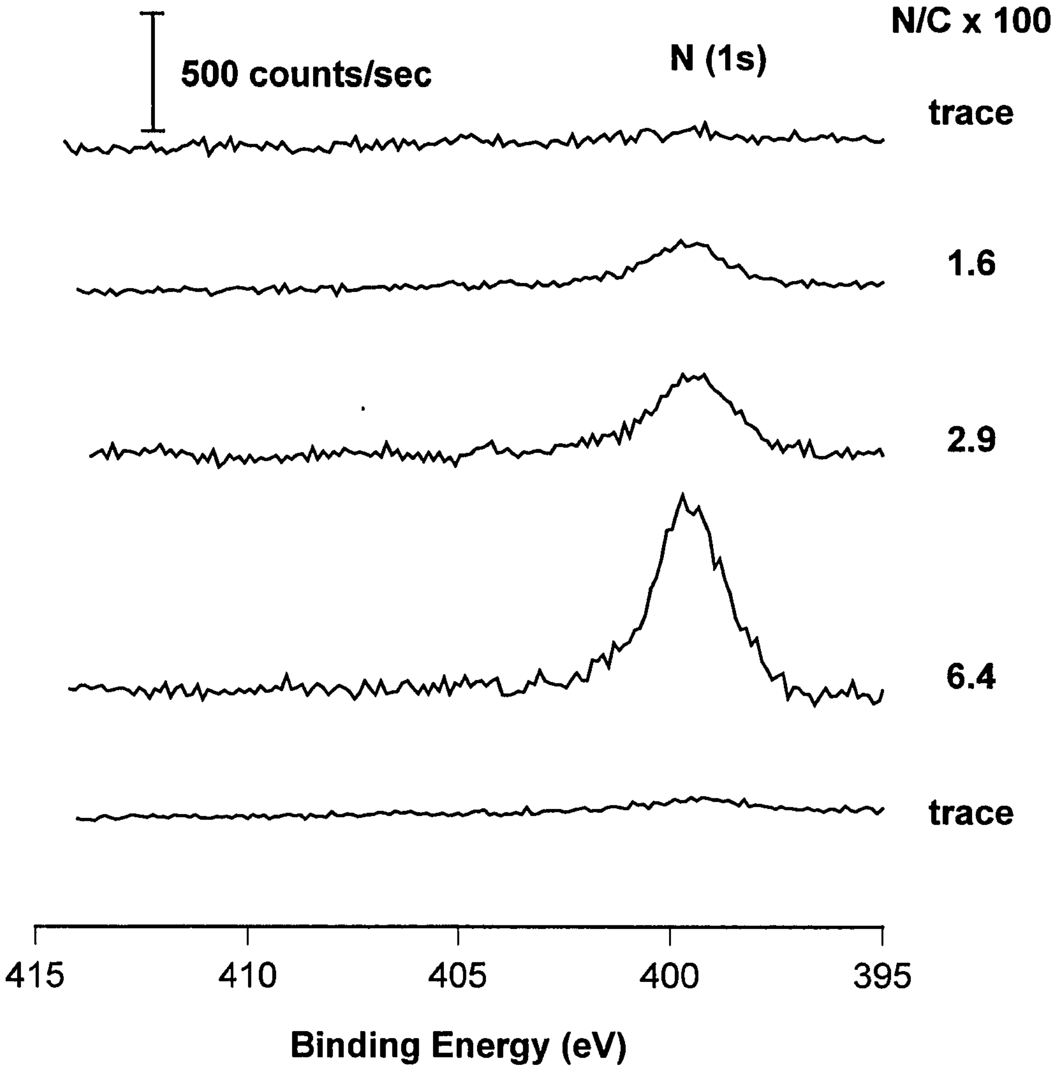

Figure 2. X-ray photoelectron spectra in the N(1s) region for freshly polished GCEs immersed in an ethanolic solution containing 1 mM N-acetylethylenediamine and held at 0.00 V for 5 min (a), or cycled once at 10 mV/s between 0.00 V and (b) +0.70 V, (c) +1.00 V, and (d) +1.40 V. The spectrum in (e) was obtained from an "as polished" GCE.

(Figure 2b), +1.00 V (Figure 2c), and +1.40V (Figure 2d). These voltage limits were chosen to span the range of the anodic wave in Figure 1. Figure 2a therefore represents the result for a GCE treated prior to the onset of amine oxidation, and Figures 2b-d the results for increases in the extent of amine oxidation. Figure 2e shows the XPS spectrum in the N(1s) region for a freshly polished but untreated GCE for comparison. The XPS spectrum for a GCE immersed into solution at open circuit is effectively the same as in Figures 2a and 2e. At best, trace levels of nitrogen are detected at the GCEs in Figures 2a and 2e. In contrast, scanning to an upper limit of +0.70 V (Figure 2b) leads to the detection of a nitrogen-containing species at the GCE surface (N/C=1.6). Upon scanning to the two more positive voltage limits, the nitrogen content at the GCE surface increases further, reaching N/C values of 2.9 at +1.00 V (Figure 2c) and 6.4 at +1.40 V (Figure 2d). These data show that oxidation of the amine functionality is requisite for immobilization at the GCE surface, as suggested in Scheme I [28].

Repetitive cycling between 0.00 V and +1.40 V or scanning to an E_{app} more positive than +1.40 V (e.g., +1.60 V) did not significantly increase the N/C value, indicating that the maximal coverage can be obtained with a single voltage cycle between 0.00 V and +1.40 V at this sweep rate. In addition, the N/C value did not significantly increase if 5 mM instead of 1 mM solutions of N-acetylethylenediamine were used. More detailed studies of the sweep rate and concentration dependence are planned.

Further support for the immobilization scheme derives from the XPS data and from tests of chemical stability. From the XPS data, the position of the peak maximum (399.3 eV) is consistent with the formation of a carbon-nitrogen bond between the amine cation radical and an aromatic moiety of the GC surface. Comparatively, the N(1s) binding energies for aliphatic primary amines are near ~ 398.0 eV [29]. Although this conclusion is complicated by the presence of the amide group of the N-acetylethylenediamine, the position of the bands for simpler, immobilized amines such as N-butylamine (see next section) are similar.

Tests of the stability of immobilization also support the formation of a covalent linkage. For instance, N-acetylethylenediamine-coated GCEs that were prepared by scanning to +1.40 V were sonicated for ~15 min (in addition to the 15 min sonication as part of the general preparation protocol; see Experimental Section) in a variety of solutions, including water, ethanol, and pH 7 phosphate buffer. In all cases, the XPS spectra in the N(1s) region were not observably different from that in Figure 2d. Importantly, sonication was found to be very effective in removing physisorbed aromatic amines (see below) from the GCE surface. For example, the surface coverage of strongly physisorbed dopamine decreased by ~95% after a 15 min sonication in the pH 7.0 phosphate buffer.

As an additional test of stability, the butylamine-modified GCE was immersed in 0.1 M H_2SO_4 for 24 hr. Examination by XPS showed no observable decrease in the surface coverage of this amine after soaking. This result, in addition to demonstrating the excellent stability of the amine-GCE linkage under harsh exposure conditions, supports the formation of a hydrolytically stable nitrogen-carbon bond. Other types of immobilized species such as amides or salts formed with acidic surface oxides would be highly unstable under these acidic conditions. These findings support the formation of an immobilized species that is covalently bonded to the GCE surface, and is consistent with the process detailed in Scheme I.

To test the stability of the amine-GCE linkage under conditions of potential cycling, a butylamine-modified GCE (see next section for preparation) was cycled between +0.20 V and +0.80 V in aqueous 0.1 M $HClO_4$. Examination by XPS after 100 cycles indicated a ~ 10% decrease in the N/C ratio. A dopamine-modified GCE (see "Immobilization of Dopamine..." section for preparation) that was subjected to the same testing exhibited a much larger decrease in the N/C ratio (~23%). We suspect this decrease arises primarily from an increased destabilization of the surface linkage from the redox process.

Immobilization of Various N-Substituted Alkylamines at the GCE Surface.

To examine the generality of Scheme I, we probed the feasibility of immobilizing primary, secondary, and tertiary amines at the GCE surface. Figures 3a-e show CV curves obtained at a GCE in ethanolic 0.1 M $LiClO_4$ solutions containing either 1 mM of butylamine (Figure 3a), N-methylbutylamine (Figure 3b), N-ethylbutylamine (Figure 3c), N,N-dimethyl-butylamine (Figure 3d), or triethylamine (Figure 3e). Chemically irreversible oxidation waves are apparent for all five of the amine-containing compounds. The negative shift in the E_p values (c.f. Table I) and sharpening of the oxidation peak observed as alkyl substituents are added to the amine group is consistent with the stabilization of the amine cation radical

Figure 3. Cyclic voltammograms obtained at freshly polished GCEs in ethanolic 0.1 M $LiClO_4$ solutions containing 1 mM of (a) butylamine, (b) N-methylbutylamine, (c) N-ethylbutylamine, (d) N,N-dimethylbutylamine, and (e) triethylamine. The sweep rate was 10 mV/s in each case.

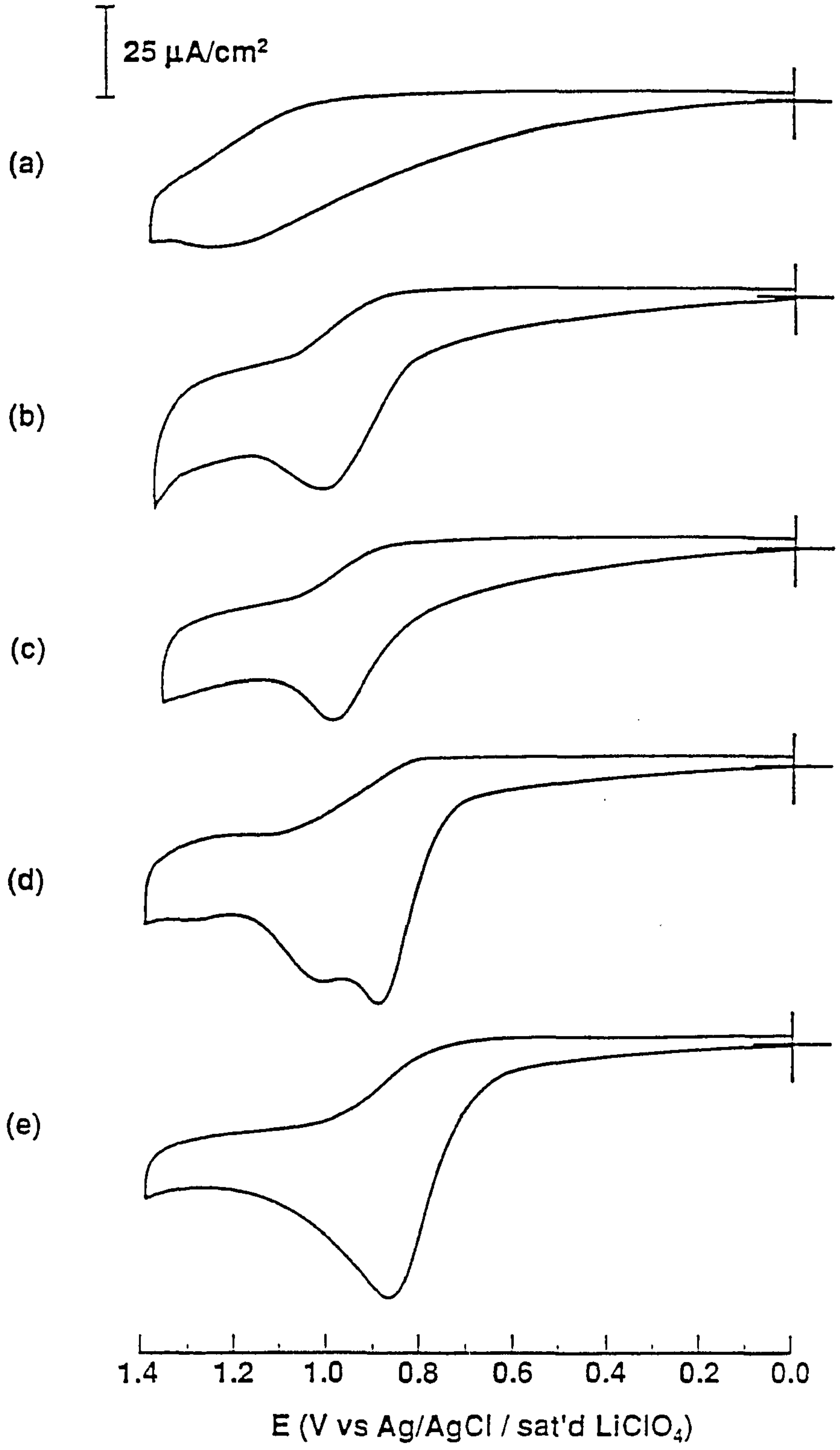
25 μA/cm²
(a)
(b)
(c)
(d)
(e)
1.4
1.2
1.0
0.8
0.6
0.4
0.2
0.0
E (V vs Ag/AgCl / sat'd LiClO$_4$)

form by the alkyl groups [26,27]. Therefore, generation of the amine cation radical is most facile for tertiary amines, and least facile for primary amines.

Interestingly, a single oxidative wave was observed in the CV curves in all cases except for N,N-dimethylbutylamine. The curve for the latter species contains two clearly observable anodic waves. We do not at present understand the origin of the multiple wave character for this species. Initially, we had suspected the presence of an electroactive impurity. Both waves, however, persisted even after purifying the compound carefully via distillation. Nevertheless, this disparity in voltammetric behavior does not translate to an observable difference in the results from testing the ability of tertiary amines to bind at the GCE surface (see below).

Figures 4a-d show XPS spectra in the N(1s) region for GCEs cycled once between 0.00 V and +1.40 V in ethanolic 0.1 M $LiClO_4$ solutions containing 1 mM of either butylamine, N-methylbutylamine, N-ethylbutylamine, or N,N-dimethylbutylamine, respectively. The XPS spectrum for a scan in a 1 mM electrolytic solution of triethylamine is also represented by Figure 4d. As expected from the data for the primary amine N-acetylethylenediamine in Figure 2, Figure 4a indicates that butylamine is immobilized with an N/C value of 3.7, a value reasonably consistent with the differences in the number of nitrogens in the two compounds. Comparisons of Figure 4a to Figures 4b-d show, however, that the extent of immobilization is strongly influenced by the presence of substitutents on the nitrogen atom. For example, the surface coverage of the methyl-substituted secondary amine (N/C=1.4) is less than half that of the primary amine (N/C=3.7). In contrast, both of

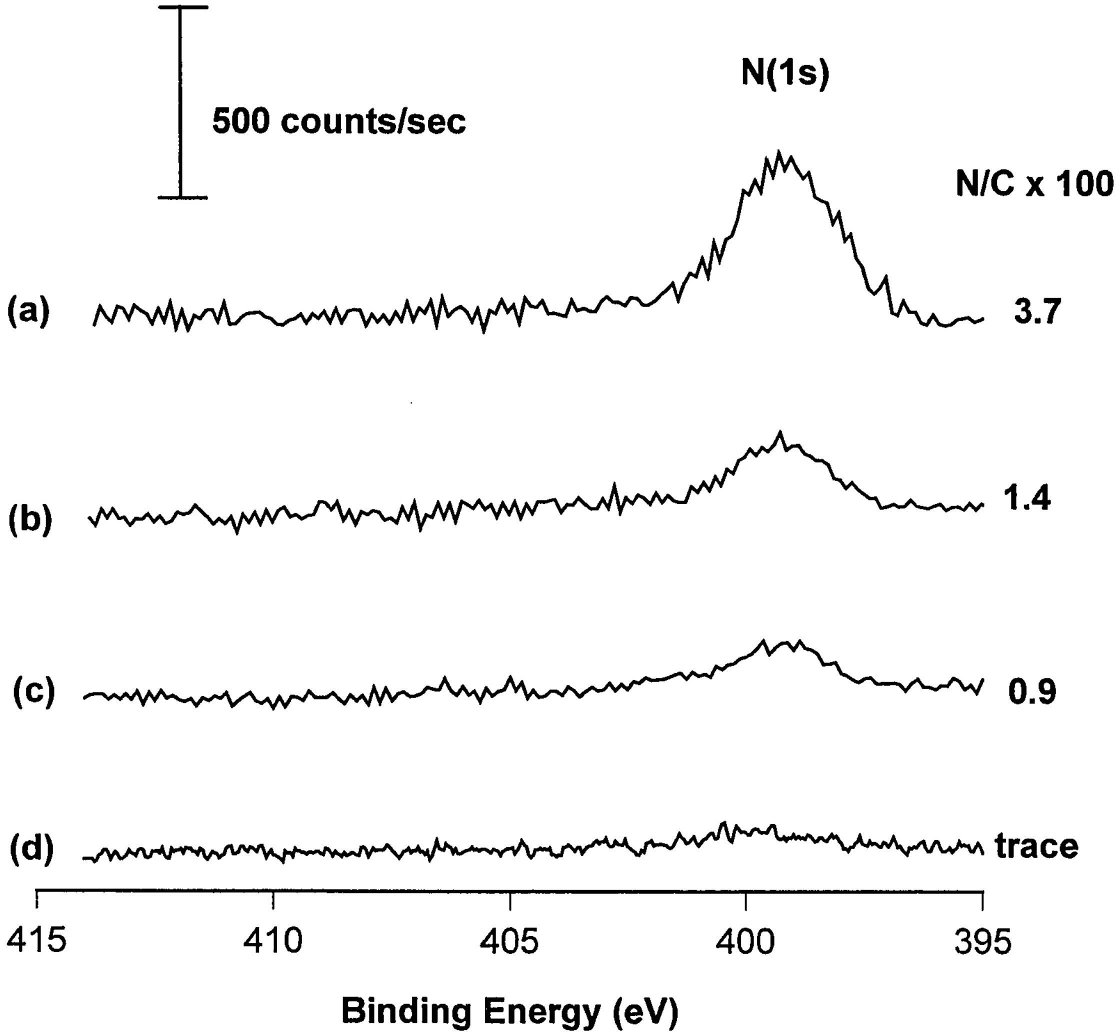

Figure 4. X-ray photoelectron spectra in the N(1s) region for freshly polished GCEs immersed in an ethanolic solution containing (a) 1 mM butylamine, (b) 1mM N-methylbutylamine, (c) 1 mM N-ethylbutylamine, and (d) 1 mM N,N-dimethylbutylamine. The applied voltage was cycled once between 0.00 V and +1.40 V at 10 mV/s in each case.

the tertiary amines, N,N-dimethylbutylamine and triethylamine, are not immobilized at the GCE surface at a detectable level, exhibiting XPS spectra effectively the same as that in the control experiments (i.e., Figure 2e).

These results show that, in spite of the more facile and more extensive oxidation of secondary and tertiary amines, their corresponding cation radicals cannot bind effectively to the GCE surface. We attribute this difference to a steric effect whereby the presence of the additional substituents on the amine functionality hinders accessibility to active sites at the GCE surface. This conclusion is supported further by the lower surface coverage (N/C=0.9) obtained for the immobilization of N-ethylbutylamine (Figure 4c), a more sterically hindered secondary amine than N-methylbutylamine, at the GCE surface.

To ensure that the differences in the extent of immobilization were not a result of differences in the reactivity of the primary, secondary, and tertiary amine cation radicals toward the GCE surface, we attempted to increase the surface coverage of the secondary and tertiary amines by cycling repetitively between 0.00 V and +1.40 V at 10 mV/s. For these experiments, E_{app} was cycled twice at a GCE in electrolytic ethanolic solutions containing 1 mM of either N-methylbutylamine or N,N-dimethylbutylamine. Although this procedure exposes the GCE surface to significantly larger amounts of secondary and tertiary amine cation radicals during the second voltage cycle, there were no observed differences in surface coverages (see Table I). These results support the existence of a strong steric effect in the immobilization step. We note that the inability to immobilize tertiary amines at the GCE surface may also reflect a dependence of the reaction mechanism on the loss of a proton from the amine cation radical (c.f. Scheme I) [20].

Immobilization of Biotin at the GCE Surfaces.

Several recent reports have employed the immobilization of biotin at the surface of carbon-based electrodes as a step in the fabrication of biosensors [17, 19]. In several of these studies, surface-bound biotin functioned as a platform for anchoring a variety of enzymes to carbon fibers via biotin-avidin complexation [30]. The construction of this type of biosensor, however, often entails a lengthy synthetic effort, a large part of which involves the immobilization of biotin. This section presents the results of our testing of Scheme 1 as a route to a more facile preparation of biotin-modified GCE.

For this test, we chose to use the amine-containing biotin derivative N-(5-aminopentyl)biotinamide. Figure 5 shows the CV curves obtained at a GCE in an enthanolic solution containing 1 mM of this derivative and 0.1 M LiClO4; the first sweep is given by the solid curve and the second by dashed curve. Although the Ep for the oxidation of the amine group (+1.25 V) is similar to that obtained for oxidation of butylamine (Figure 3a), the charges passed during the first oxidation cycle is significantly smaller. Examination by XPS of GCEs coated with biotin derivative using one voltage cycle showed a lower surface coverage of biotin (N/C = 6.4) than expected (N/C 14.8) from an extrapolation of the XPS data for butylamine and a consideration of the number of nitrogen atoms contained in the biotin derivative. To increase the surface coverage of biotin, we attempted to generate more

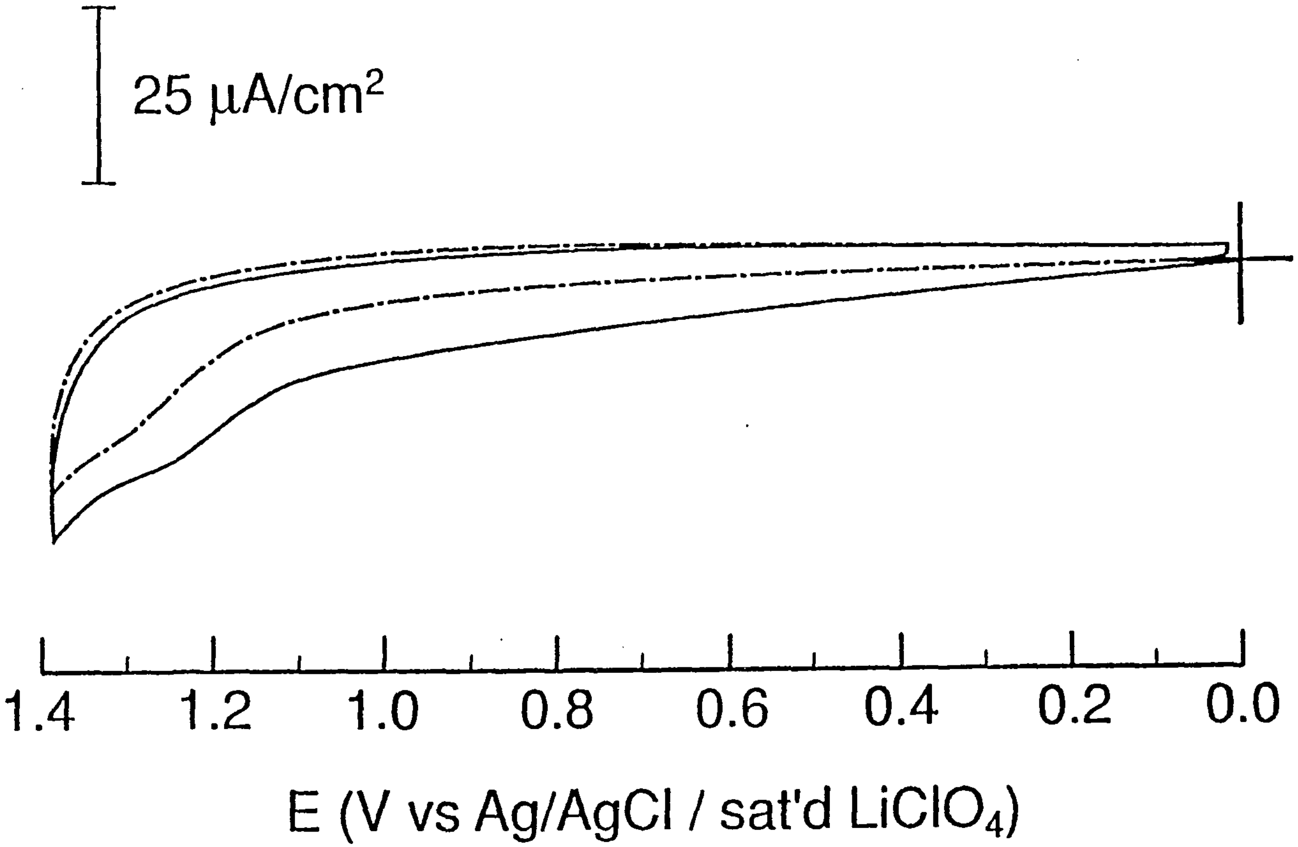

Figure 5. Cyclic voltammogram obtained at a freshly polished GCE in an ethanolic solution containing 1 mM of the biotin derivative and 0.1 M LiClO4. The dashed curve represents the sencond voltage cycle at the same GCE. The sweep rate was 10 mV/s.

biotin amine cation radicals by cycling the voltage twice between 0.00 V and + 1.40 V in the biotin-containing solution. This procedure resulted in an increase in the biotin surface coverage (N/C = 7.5, Figure 6a). Further voltage cycling did not increase the surface coverage appreciably. The necessity for two voltage cycles to obtain the maximal surface coverage of biotin is in contrast to the conditions for butylamine and N-acetylethylenediamine, which required only one voltage cycle. This difference, as well as the unexpectedly low maximal surface coverage of biotin [31], suggests that diffusional rates as well as steric effects can affect the efficiency of immobilization at the GCE surface.

Figure 6a shows the XPS survey spectrum of a GCE that was cycled twice between 0.00 V and +1.40 V in an ethanolic solution containing 1 mM of the biotin derivative. The insert in Figure 6 shows an expanded view of the N(1s) region for the samples in Figure 6. The survey spectrum reveals the presence of nitrogen and sulfur, as expected from the chemical makeup of the biotin derivative. Comparison of the intensities of the nitrogen and sulfur peaks from this spectrum to those for biotin adsorbed at the GCE by immersion of a sample in the same solution (Figure 6b) shows that a significant amount of biotin can be immobilized at the GCE via Scheme 1. Based on comparison of the N/C values for biotin and dopamine, we roughly estimate a biotin surface coverage of 1.1 x 10^{-10} mol/cm^2. Further, the relative strengths of the XPS signals for sulfur to nitrogen (1 to 4 from survey scans) argues that the biotin moiety is structurally intact upon immobilization at the GCE surface. Since this bonding procedure requires only a few minutes for completion, a platform for the construction of this general form of biosensor can be rapidly and easily prepared and

Figure 6. X-ray photoelectron survey spectra for freshly polished GCEs (a) immersed in an ethanolic solution containing 1 mM of the biotin derivative and cycled twice between 0.00 V and +1.40 V at 10 mV/s and (b) immersed in the biotin solution at open circuit for 5 min. The spectra in parts c and d of Figure 6 were obtained by immersing the GCE from Figure 6a and a freshly polished GCE into avidin-containing buffer solution at 4 °C for 16 h, respectively. The insert in the figure shows an expansion of the N(1s) region for clarity.

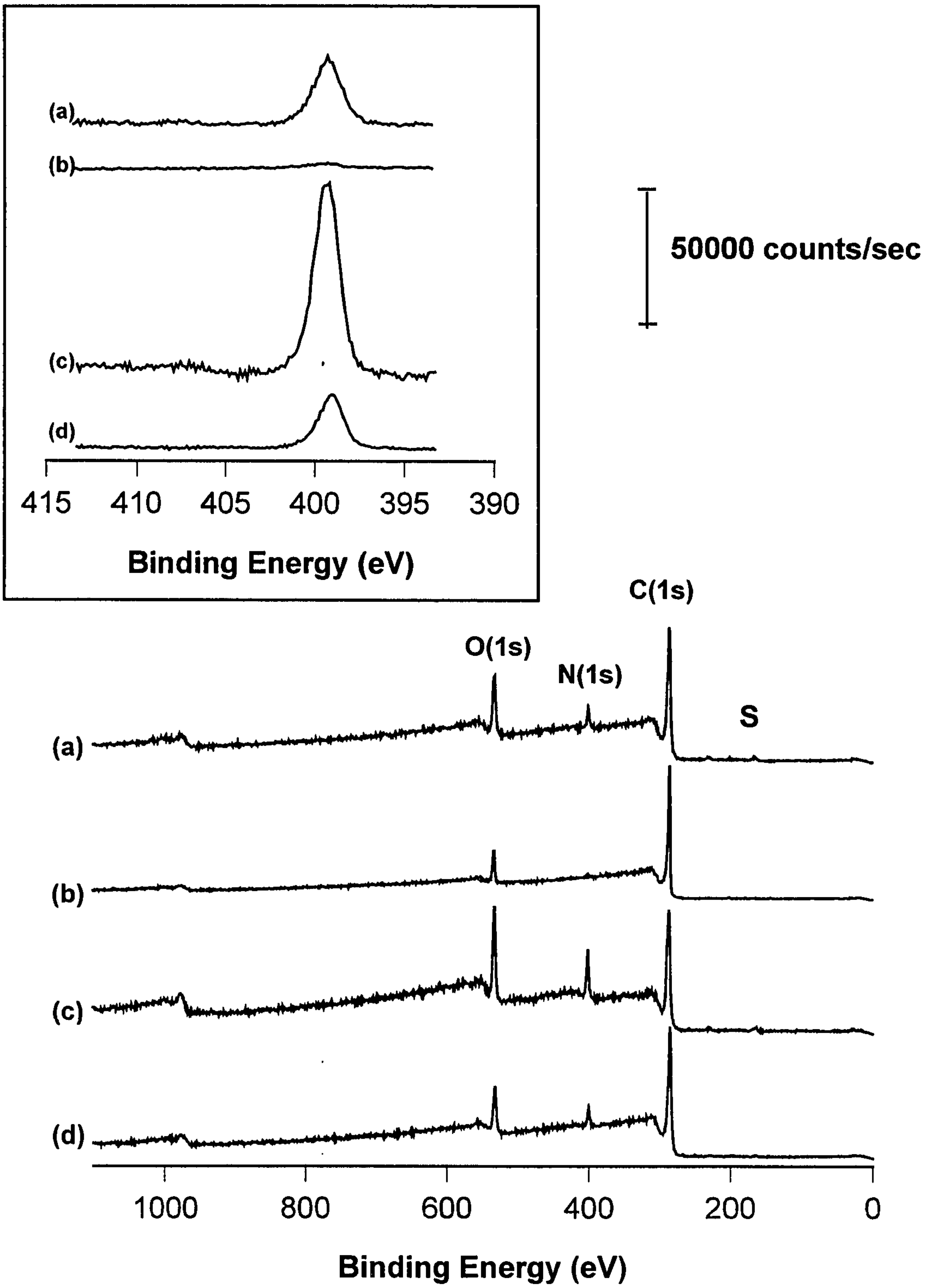
(a)
(b)
(c)
(d)
415
410
405
400
395
390
Binding Energy (eV)
50000 counts/sec
C(1s)
O(1s)
N(1s)
S
(a)
(b)
(c)
(d)
1000
800
600
400
200
0
Binding Energy (eV)

should greatly simplify the overall preparative procedure.

As a means of demonstrating further the utility of the biotin-coated GCEs for immobilizing proteins at the GCE surface, we attempted to complex the protein avidin with the surface-bound biotin using previously described procedures [18]. Parts c and d of Figure 6 show XPS survey spectra of a biotin-coated GCE and a freshly polished GCE that were exposed to an avidin-containing aqueous buffer solution, respectively [32]. Comparison of the relative intensities of the carbon, oxygen, and nitrogen peaks in Figure 6c to those for the biotin-coated GCE (Figure 6a) and a control sample (i.e., freshly polished GCE with adsorbed avidin (Figure 6d)) shows a large increase in the nitrogen and oxygen content at the biotin-coated GCE upon exposure to the avidin. This increase is consistent with the binding of avidin to surface-bound biotin. Although the N(1s) peak in Figure 6c is composed of signals from both the surface-bound biotin and avidin, the large diameter of the avidin protein molecule (4.5 nm [33]) combined with the small incident angle used for the XPS studies (e.g., 10°) likely results in a significant attenuation of the photoelectrons arising from the biotin moiety [23, 34]. Therefore, the N(1s) peak in Figure 6d can reasonably be compared to that in Figure 6d for adsorbed avidin, to assess the amount of avidin that is bound to the GCE surface through complexation with biotin. Together, these results confirm that biotin immobilized at the GCE surface via Scheme 1 can bind readily to avidin, thereby greatly simplifying the construction of biosensors based on biotin-avidin complexation.

Proposed Mechanism of Bonding.

In this section, we propose an extension of the mechanism outlined in Scheme I. This extension is based primarily on the combined weight of our experimental results and, to a lesser extent, on the literature concerning the solution phase reactions of amine cation radicals with substituted aromatic compounds [35,36]. Of particular importance is a comparison of the maximal surface coverage of the amine-containing compound DA ($\sim 1.8\times10^{-10}$ mol/cm^2) [23] that can be obtained via Scheme I to that expected for a closest packed monolayer [37] in which the catechol moieties are either perpendicular ($\sim 5.0\times10^{-10}$ mol/cm^2) or parallel ($\sim 2.4\times10^{-10}$ mol/cm^2) to the GCE surface. Though only a semiquantitative comparison at best [23], the differences in coverage argue that the immobilized DA is oriented with its ring parallel to the GCE surface. This conclusion, however, requires that the GCE reacts uniformly with the electrogenerated amine cation radicals. Thus, both the edge and basal planes of the GCE, which exist in roughly equal proportions [38, 39], must exhibit comparable reactivity in the immobilization of DA.

As a test for verification, we attempted to immobilize butylamine at the basal plane of HOPG electrodes via Scheme I. The CV curve obtained at such an electrode in an ethanolic solution containing 1 mM of butylamine and 0.1 M $LiClO_4$ showed a small wave with an E_p of +1.35 V indicative of amine oxidation. However, the total charge passed during this oxidation was significantly smaller than that passed for the analogous oxidation at a GCE (Figure 3a), suggesting that the kinetics of amine cation radical formation are much slower at HOPG electrodes. Importantly, the XPS spectrum in the N(1s) region for an HOPG electrode after attempting to immobilize butylamine was indistinguishable from that at a freshly polished GCE. To ensure that this inability to immobilize butylamine at HOPG was not simply due to insufficient amine cation radical generation, we tested the effects of multiple sweeps as well as of extending the positive limit of the sweep to +1.90 V. In each case, we found no evidence from an XPS characterization for immobilization. Therefore, although amine radicals are generated at an HOPG electrode, the basal plane of HOPG is not reactive towards the immobilization process of Scheme I. It then follows that immobilization via Scheme I takes place at the edge and not the basal plane of the GCE surface.

Since the edge planes of polished GCE surfaces are known to contain a significant amount of oxygen functional groups such as phenols, quinones, and carboxylic acids [5,40], the literature suggests that the amine radical coupling reactions may be directed and their rates affected, in part, by the different types of oxygen-containing groups at the edge planes. Such a possibility reflects the large body of literature concerning electrophilic substitution reactions of substituted aromatic compounds with amine radicals [35,36] as well as earlier arguments for free radicals reacting rapidly with the oxygen-containing edge planes on carbon electrodes [41,42]. In the former, studies have shown that amine radical-arene coupling reactions are strongly activated for ortho and para attack by electron releasing substituents such as hydroxyl groups and ketones, and strongly deactivated by electron withdrawing substituents such as carboxylic acids. By analogy, the phenol, quinone, and carboxylic acid functionalities at the edge plane of the GCE can either activate or deactivate the immobilization reaction. Experiments to test for contributions of this interesting possibility are presently being devised.

CONCLUSIONS

This paper has demonstrated the ability to create chemically modified GCEs for biosensor fabrication purposes via the electrooxidation of amine-containing compounds. The application of this method for the immobilization of dopamine for electrocatalytic purposes has been described elsewhere [23]. Importantly, this procedure dramatically simplifies the fabrication of modified electrodes, a process which often involves an extended series of pretreatment, activation, and functionalization steps. This procedure also provides a comparatively higher coverage of the immobilized species. In addition, we have found that the extent of immobilization is strongly dependent on the degree of substitution at the amine functionality, whereby the electrooxidation of primary amines yields the largest relative surface coverage and tertiary amines show no detectable surface coverage. The differences in the coverages are attributed primarily to a strong steric effect which hinders the accessibility of the amine cation radicals to binding sites at the GCE surface. Results further indicate that immobilization occurs at the edge vs basal plane sites of a GCE surface. Application of this method for the fabrication of biotin-containing biosensors is also underway in our laboratory. Studies focused on unraveling further the bonding mechanism are planned.

ACKNOWLEDGMENTS

R.S.D. gratefully acknowledges the support of an ACS Analytical Division Summer Fellowship sponsored by the Dow Chemical Corporation. This work was supported by the National Science Foundation (Grant CHE-9003308). The Ames Laboratory is operated for the U.S. Department of Energy under contract W-7405-eng-82.

REFERENCES AND NOTES

1. Murray, R. W. *Electroanalytical Chemistry: A Series of Advances*, Bard, A.J., Ed., Marcel Dekker: New York, 1984; vol. 13, p. 191.
2. Van Der Linden, W. E.; Dieker, J. W. *Anal. Chim. Acta* **1980**, *119*,1.
3. Kinoshita, K. *Carbon: Electrochemical and Physicochemical Properties*, Wiley: New York, 1988.
4. Dautartas, M. F.; Evans, J. F.; Kuwana, T. *Anal. Chem.* **1979**, *51*, 104.
5. Kepley, L. J.; Bard, A. J. *Anal. Chem.* **1988**, *60*, 1459.
6. Engstrom, R. W.; Strasser, V. A. *Anal. Chem.* **1984**, *56*, 136.
7. Watkins, B. F.; Behling, J. R.; Kariv, E.; Miller, L. L. *J. Am. Chem. Soc.* **1975**, *97*, 3549.
8. Firth, B. E.; Miller, L. L.; Mitani, M.; Rogers, T.; Lennox, J.; Murray, R. W. *J. Am. Chem. Soc.* **1976**, *98*, 8271.

9. Lin, A. W. C.; Yeh, P.; Yacynych, A. M.; Kuwana, T. *J. Electroanal. Chem.* **1977**, *84*, 411.

10. Pocard, N. L.; Alsmeyer, D. C.; McCreery, R. L.; Neenan, T. X.; Callstrom, M. R. *J. Am. Chem. Soc.* **1992**, *114*, 769.

11. Lennox, J. C.; Murray, R. W. *J. Electroanal. Chem.* **1977**, *78*, 395.

12. Tse, D. C. S.; Kuwana, T. *Anal. Chem.* **1978**, *50*, 1315.

13. Ueda, C.; Tse, D. C. S.; Kuwana, T. *Anal. Chem.* **1982**, *54*, 850.

14. Zak, J.; Kuwana, T. *J. Electroanal. Chem.* **1983**, *150*, 645.

15. Bourdillon, C.; Bourgeois, J.; Thomas, D. *J. Am. Chem. Soc.* **1980**, *102*, 4231.

16. Wieck, H. J.; Heider, G. H.; Yacynych, A. M. *Anal. Chim. Acta* **1984**, *158*, 137.

17. Pantano, P.; Morton, T. H.; Kuhr, W. G. *J. Am. Chem. Soc.* **1991**, *113*, 1832.

18. Pantano, P.; Kuhr, W. G. *Anal. Chem.* **1991**, *63*, 1413.

19. Pantano, P.; Kuhr, W. G. *Anal. Chem.* **1993**, *65*, 623.

20. Barbier, B.; Pinson, J.; Desarmot, G.; Sanchez, M. *J. Electrochem. Soc.* **1990**, *137*, 1757.

21. Deinhammer, R. S.; Shimazu, K.; Porter, M. D. *Anal. Chem.* **1991**, *63*, 1889.

22. Deinhammer, R. S.; Ting, E.; Porter, M. D. *J. Electroanal. Chem.* **1993**, *362*, 295.

23. Deinhammer, R. S.; Ho, M.; Anderegg, J. W.; Porter, M. D. *Langmuir* **1994**, *10*, 1306.

24. Bussing, T. D.; Holloway, P. H. *J. Vac. Sci. Tech. A* **1985**, *3*, 1973.

25. Scofield, J. H. *J. Elec. Spec.* **1976**, *8*, 129.

26. Masui, M.; Sayo, H.; Tsuda, Y. *J. Chem. Soc. (B)* **1968**, 973.

27. Mann, C. K. *Anal. Chem.* **1964**, *36*, 2424.

28. In addition to the lack of an oxidative wave for the N-propylacetamide, a characterization using XPS failed to detect the presence of the immobilized form of this amide.
29. Nordberg, R.; Albridge, R. G.; Bergmark, T.; Ericson, U.; Hedman, J.; Nordling, C.; Siegbahn, K.; Lindberg, B. J. *Arkiv for Kemi* **1968**, *28*, 257.
30. Wilchek, M.; Bayer, E. A. *Anal. Biochem.* **1988**, *171*, 1.
31. Attenuation of the photoelectrons arising from the carbon-bound nitrogen of the immobilized biotin moieties may also contribute to the higher N/C value [23].
32. In contrast to the alkylamine-, dopamine-, and biotin-coated GCEs, we found that the avidin-coated GCEs showed a positive shift in their N(1s) binding by ~0.7 eV. Since we suspected the presence of surface charging, we have corrected the positions of these bands by 0.7 eV.
33. Haussling, L.; Ringsdorf, H.; Schmitt, F. J.; Knoll, W. *Langmuir* **1991**, *7*, 1837.
34. Briggs, D.; Seah, M. P. *Practical Surface Analysis*; Wiley: Chichester, England, **1983**.
35. Minisci, F.; Galli, R.; Cecere, M. *Chim. Ind.* **1966**, *48*, 725.
36. Minisci, F. *Synthesis* **1973**, 1.
37. Soriaga, M. P.; Hubbard, A. T. *J. Am. Chem. Soc.* **1982**, *104*, 2735.
38. Bowling, R. J.; Packard, R. T.; McCreery, R. L. *J. Am. Chem. Soc.* **1989**, *111*, 1217.
39. Rice, R. J.; Pontikos, N. M.; McCreery, R. L. *J. Am. Chem. Soc.* **1990**, *112*, 4617.
40. Takahagi, T.; Ishitani, A. *Carbon* **1984**, *22*, 43.
41. Besenhard, J. O.; Fritz, H. P. *Angew. Chem. Int. Ed. Engl.* **1983**, *22*, 950.
42. Oyama, N.; Brown, A. P.; Anson, F. C. *J. Electroanal. Chem.* **1978**, *87*, 435.

CHAPTER 4. SURFACTANT MODIFIED EMLC PART I: EFFECT OF CATIONS ON SEPARATION

A paper to be submitted to Journal of Electroanalytical Chemistry (Preliminary Note)

Mankit Ho and Marc D. Porter

ABSTRACT

A novel approach for modification of electrochemically modulated liquid chromatography (EMLC)-based separations has been studied. The method is deriveed from the potential dependent differences in the electrical double layer structure that arise when a strongly adsorbed ionic species is present as an additive to the mobile phase. The viability of the approach was demonstrated by the comparison of the potential dependences of the separation of a ternary mixture of protonated alkyl aniline compounds in the presence of two different cation-containing supporting electrolytes in the mobile phase. This comparison uses a perchlorate-based supporting electrolyte with either lithium (Li^+) or tetraethylammonium ion (TEA^+) as the mobile phase cations. It was found that the response of the analytes to the E_{app} are much less at the negative potential of potential od zero charge (pzc) when TEA^+ was present. This is attributed the much higher surface excess of the TEA^+ at the stationary phase. Potential applications of the techniques are discussed.

INTRODUCTION

Several research groups [1-10], including our own [11-14], have been exploring the viability of a new form of liquid chromatography (LC). The heart of the technique, which we have dubbed electrochemically-modulated liquid chromatography (EMLC), is the transformation of the LC column into an electrochemical cell. Thus, electrochemically-induced alterations in the composition of a conductive stationary phase can be exploited for the manipulation of the efficiency of a separation.

Several EMLC-based separation formats have been described, including the use of stationary phases coated with conductive [4-9] and redox [3] polymer films, highly oxidized carbonaceous packings [1, 2], and unmodified carbonaceous packings [12, 14]. In each of these cases, elution profiles are affected by changes in a chemical property of the stationary phase. For example, electrochemically-driven transformations of coatings like polypyrrole [11, 13], polyaniline [8], and a ferrocene-containing polymer [3] can alter the ion exchange capacity [10] as well as the relative hydrophobicity of a stationary phase [13]. Changes in applied potential (E_{app}) can also be used to manipulate the effective donor-acceptor properties of a carbonaceous stationary phase [14].

In this preliminary report, we describe a novel strategy for EMLC-based separations. Our strategy is derived from the potential dependent differences in the electrical double layer structure that arise when a strongly adsorbed ionic species is present as an additive to the mobile phase. Scheme I presents a generalized depiction of the concept. Overall, when E_{app}

Scheme I. The effect of applied potential relative to pzc on the amount of cationic molecules adsorbed on the electrode surface.

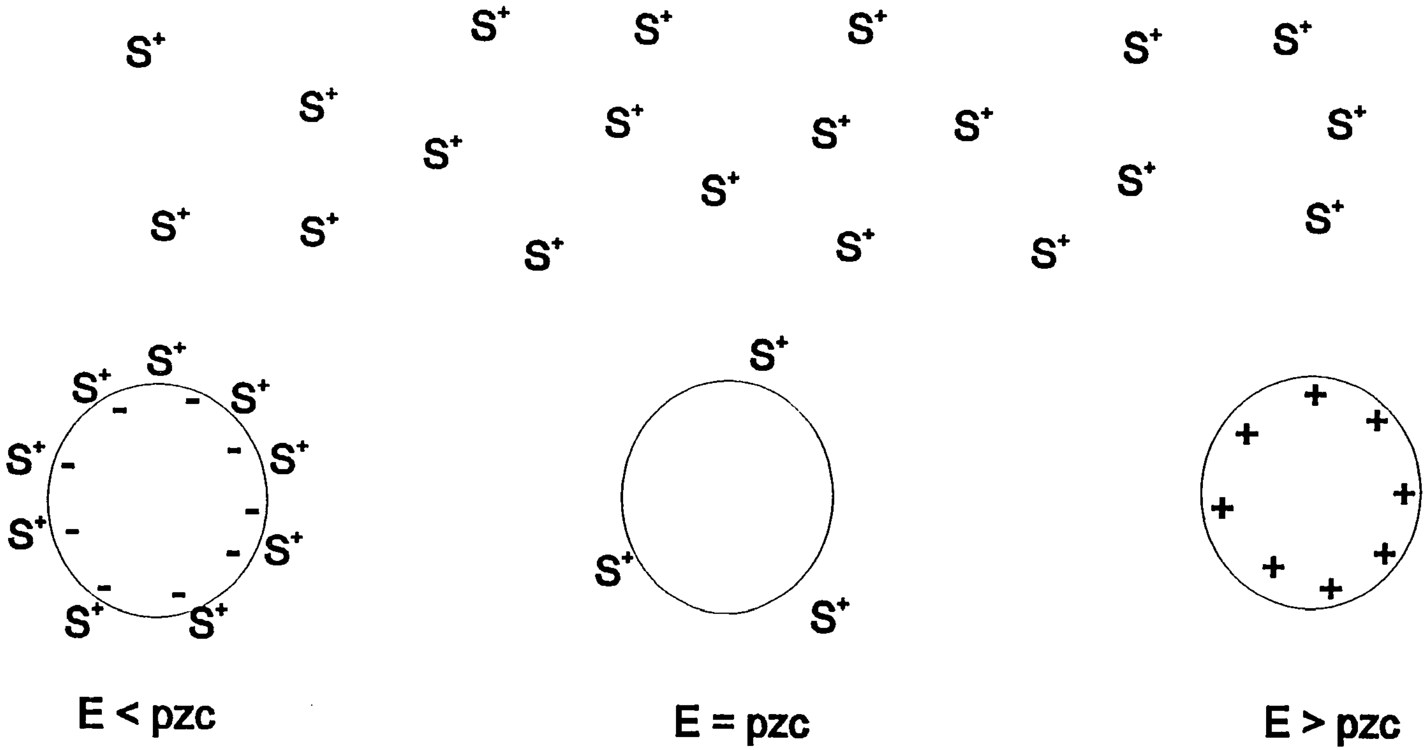
S+
-
+
E < pzc
E = pzc
E > pzc

is negative of the potential of zero charge (pzc), the excess of negative charge at the electrode surface leads to an interfacial excess of cationic species that increases the greater the excursion from the pzc [14]. Importantly, the interfacial excess is dominated by the cations that interact more strongly with the electrode surface. These differences in interactions reflect the combined effect of a complicated mixture of several chemical and physical considerations, including the ionic size, ionic charge, and extent of solvation of the solution species and the relative donor-acceptor properties of both the solution species, and the electrode [15]. It then follows that the effective capacity of a stationary phase for a cationic analyte will be strongly dependent on the competition for the surface from the cationic component of the supporting electrolyte present in the mobile phase. A parallel process can be envisioned for how the anionic component of the supporting electrolyte will affect the retention of anionic analytes.

We demonstrate herein the viability of the above approach through a comparison of the separations for a ternary mixture of protonated alkyl aniline compounds in the presence of two different cation-containing supporting electrolytes in the mobile phase. In one set of separations, a perchlorate-based supporting electrolyte with lithium (Li^+) is used. In the other case, Li^+ is replaced with tetraethylammonium ion (TEA^+), which is a more strongly adsorbed cation than Li^+ [16, 17], as the cation in the supporting electrolyte. Potential applications and extensions of this concept are discussed.

EXPERIMENTAL SECTION

Butylaniline (BA), hexylaniline (HA), octylaniline (OA), trifluoroacetic acid (TFA), and lithium perchlorate ($LiClO_4$) were from Aldrich; acetonitrile (HPLC grade) from Fisher, and $TEA^+ClO_4^-$ from GFS. All chemicals were used as received. Deionized water was obtained from a Millipore Milli-Q purification system.

The general design of the EMLC column and related instrumentation have been discussed elsewhere [14]. The conductive stationary phase consisted of uncoated porous graphitic carbon (PGC) spheres (Shandon Chromatography) that were dispersed in a dibromoethane/acetonitrile (10/7, v/v) slurry and subsequently packed at 5000 psi into the EMLC column. After packing, the EMLC column was equilibrated with degassed mobile phase at a flow rate 0.90 mL/min until a stable detector baseline was obtained. Equilibration times between experiments were ~30 min. The detection wavelength was 210 nm. Analyte concentrations were ~500 ppm, and the injection volume was 0.5 μL. All values of E_{app} are given with respect to a Ag/AgCl/sat'd (NaCl) electrode.

The mobile phase-supporting electrolyte was either 40% aqueous 0.1 M $LiClO_4$ (0.1% TFA, pH~2) and 60% 0.1 M $LiClO_4$ in acetonitrile or 40% aqueous 0.1 M $TEAClO_4$ (0.1% TFA, pH~2) and 60% 0.1 M $TEAClO_4$ in acetonitrile. Under these conditions, the amine functionalities of all three analytes are protonated. Additionally, the upper limit in E_{app} (+0.3 V) is defined by the susceptibility of the analytes to oxidation, and the lower limit (-0.8 V) by the reduction of solvent.

RESULTS AND DISCUSSION

The potential dependence of the separation of BA, HA, and OA is shown in Figure 1 at +0.30, +0.10, -0.20, -0.40, and -0.60 V using the mobile phase that contains Li^+ as the cationic component of the supporting electrolyte. Fully resolved elution bands are evident at each E_{app} for all three analytes, with elution times increasing with the length of the alkyl chain. Elution times also increase as E_{app} becomes more negative. For example, the elution of the mixture is completed in ~3 min at +0.30 V, but not until ~15 min at -0.60 V. This trend is *qualitatively* consistent with the differences in the excess charge at the surface of the stationary phase. That is, the greater the excess of negative charge at the surface of the stationary phase, the longer the elution time for each of the cationic analytes.

The separations in Figure 2 demonstrate the effect of a more strongly interacting cationic species in the mobile phase on the separation of the mixture by using the TEA^+-containing mobile phase as opposed to the Li^+-containing mobile phase. As found with the Li^+-containing mobile phase, the same general trend is evident in the separations of the mixture as a function of E_{app}. That is, elution times increase as E_{app} becomes more negative. In this case, however, the extent of the increase is not as large as observed with the Li^+-containing mobile phase. For example, the elution times at +0.30 V using Li^+ in the mobile phase are only marginally longer than those using TEA^+ in the mobile phase. In contrast, elution at -0.40 V requires ~8 min with Li^+, but only ~4 min with TEA^+. The difference in elution times at -0.60 V is even more notable.

Figure 1: Chromatograms of BA, HA, and OA at E_{app} (a) -0.60 V; (b) -0.40 V; (c) -0.20 V; (d) +0.10 V; (3) +0.30 V. The mobile phase consists of 60 % 0.1 M $LiClO_4$ in acetonitrile and 40 % aqueous with 0.1 M $LiClO_4$; 0.1 % TFA. Flow rate was 0.9 ml/min.

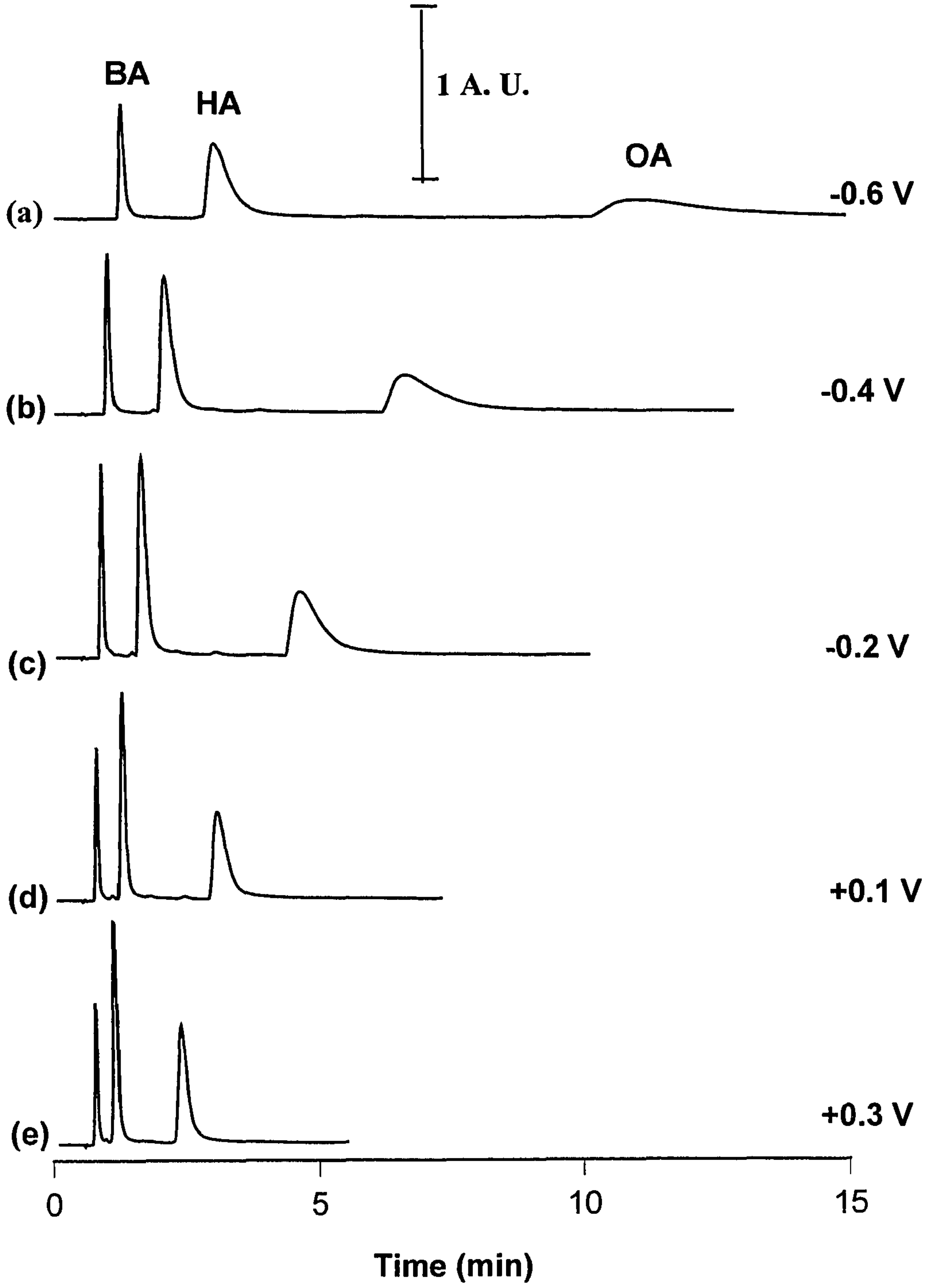
BA
HA
1 A. U.
OA
(a)
-0.6 V
(b)
-0.4 V
(c)
-0.2 V
(d)
+0.1 V
(e)
+0.3 V
0
5
10
15
Time (min)

Figure 2: Chromatograms of BA, HA, and OA at E_{app} (a) -0.60 V; (b) -0.40 V; (c) -0.20 V; (d) +0.10 V; (3) +0.30 V. The mobile phase consists of 60 % 0.1 M $TEAClO_4$ in acetonitrile and 40 % aqueous with 0.1 M $TEAClO_4$; 0.1 % TFA. Flow rate was 0.9 ml/min.

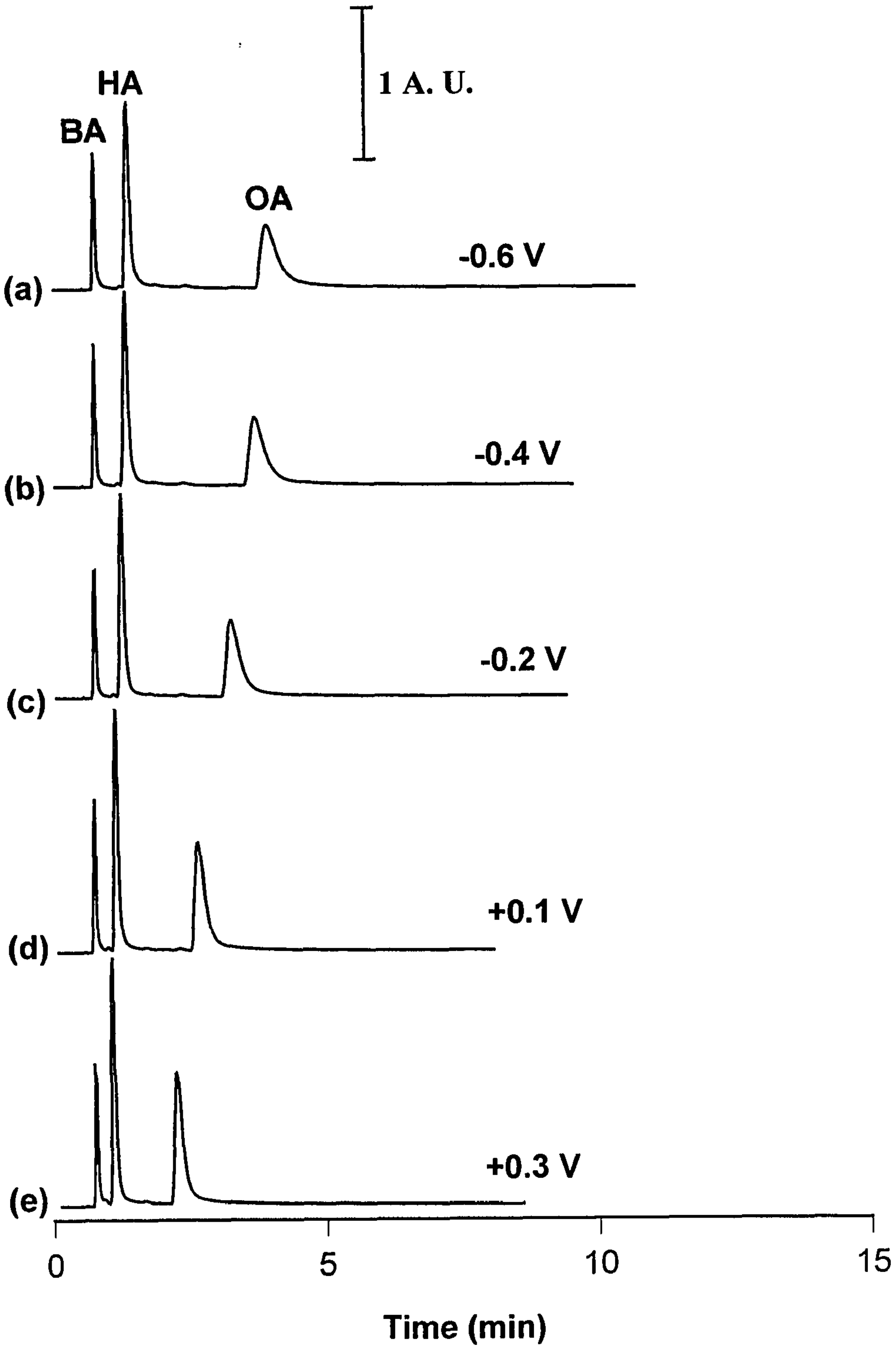
1 A. U.
HA
BA
OA
(a)
-0.6 V
(b)
-0.4 V
(c)
-0.2 V
(d)
+0.1 V
(e)
+0.3 V
0
5
10
15
Time (min)

A more detailed comparison of the two sets of separations is presented in Figure 3. This figure summarizes the separations at several values of E_{app} for each component in terms of capacity factors (k') values. As is evident, there is little difference in the retention for all of the analytes at the positive end of the potential window. However, as E_{app} becomes more negative, the difference in retention with the two phases increases. That is, with TEA^+ in the mobile phase, the retention of the analytes increases as E_{app} becomes more negative, but to a lesser extent than with Li^+ in the mobile phase. For example, at + 0.3 V, the difference for OA is only marginally detectable, whereas at -0.8 V the difference in log k' is ~0.7.

We attribute the above observations to the difference in the structures of the electrical double layer at the stationary phase at the negative values of E_{app}. When E_{app} is positive of pzc, the double layer structure is dominated by the presence of the anionic component of the mobile phase as well as by the solvent structure [15]. Since both mobile phases are composed of the same anion (i.e., $ClO4^-$), the double layer structures should be similar in both cases. The similarity of the separations for both systems at positive end of the potential window is consistent with this conclusion. In contrast, as E_{app} becomes more negative, the double layer structures formed from the two different mobile phases will reflect the difference in the interfacial excess of Li^+ (Γ_{Li+}) and TEA^+ (Γ_{TEA+}). The studies of cationic surface excess of both cations at mercury support the above assumption [16, 17]. It was shown that Γ_{TEA+} is more than 3 times than that of Γ_{Li+} at the same potential. Two possible ways can be envisioned to affect the separation of the cationic analytes as a result of large interfacial excess of TEA^+. Firstly, the adsorption of TEA^+ at the negative E_{app} blocks the

Figure 3: Plots of log k' vs. E_{app} for the (a) BA; (b) HA; (c) OA. Squares are data when $LiClO_4$ was used as supporting electrolyte. Circles are data from $TEAClO_4$ experiments.

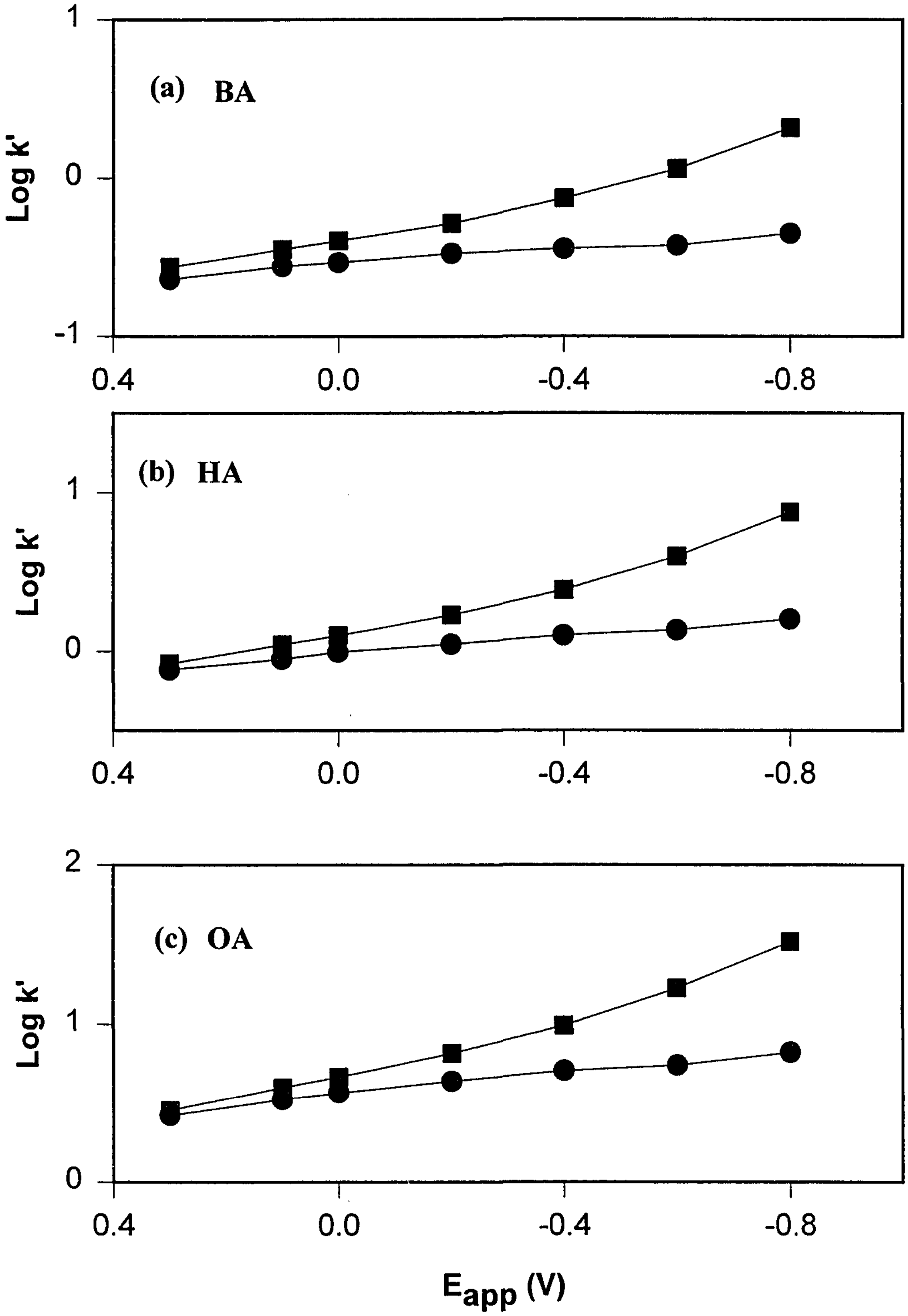
(a) BA
(b) HA
(c) OA
Log k'
Log k'
Log k'
1
0
-1
1
0
2
1
0
0.4
0.0
-0.4
-0.8
0.4
0.0
-0.4
-0.8
0.4
0.0
-0.4
-0.8
Eapp (V)

accessibility of the analytes to the surface. This has been shown by the inhibition of CrO_4^{2-} reduction in the presence of quaternary ammonium hydroxide [18]. Secondly, the higher surface excess will decrease the effective surface excess negative charges at the corresponding potential. For both cases, the analytes will stay less time at the stationary phase and consequently shorter retention. This is in agreement of the shorter retention time at negative E_{app} when compared to Li^+-containing mobile phase.

CONCLUSIONS

We have demonstrated in this preliminary note the ability to manipulate the EMLC-based separations with two different cation-supporting electrolyte mobile phase systems. It was shown that the protonated alkyl aniline compounds are less responsive to E_{app} at the negative of pzc. This is attributed to be the difference of the electrical double layer at the negative side of the potential window. The data indicate that the adsorption/desorption of the mobile phase additive can be manipulated by E_{app}. Thus, with this approach, one can envision the potential application to modify the selectivity of the stationary phase reversibly by careful selection of the mobile additive. Therefore, the selectivity of the stationary phase can be modified. Consequently, a wide range of compounds can be analyzed with just one type of column whereby the composition of the column is altered by an electrochemically-induced deposition/desorption of surfactant-like molecules at the surface of a conductive stationary phase. Further work on modifying the stationary phase with specific properties are in progress in our laboratory. The application of the method to modify the stationary phase with chiral additive will be reported elsewhere [19].

ACKNOWLEDGMENT

This work was supported by the National Science Foundation (Grant CHE-9003308) and by the Microanalytical Instrumentation Center at Iowa State University (ISU). The Ames Laboratory is operated for the U.S. Department of Energy by ISU under Contract W-7405-Eng-82.

REFERENCES

1. Antrim, R. F.; Scherrer, R. A. ; Yacynych, A. M. *Anal. Chim. Acta* **1984**, *164*, 283.
2. Antrim R. F.; Yacynych, A .M. *Anal. Lett.*, **1988** *21*, 1085.
3. Ghatak-Roy A. R.; Martin C. R. *Anal. Chem.* **1986**, *58*, 1574.
4. Ge, H.; Wallace G. G. *J. Liq. Chromatogr.* **1990**, *13*, 3245.
5. Ge, H.; Teasdale, P. R.; Wallace G. G. *J. Chromatogr.* **1991**, *544*, 305.
6. Ge, H.; Teasdale, P. R.; Wallace G. G. *Anal. Chem.* **1989**, *61*, 2391.
7. Nagaoka, T.; Fujimoto, M.; Uchida, Y.; Ogura K. *J. Electroanal. Chem.* **1992**, *336*, 45.

8. Nagaoka, T.; Fujimoto, M.; Nakao, H.; Kakuno, K.; Yano J. *J. Electroanal. Chem.* **1993**, *350*, 337.

9. Nagaoka, T.; Fujimoto, M.; Nakao, H.; Kakuno, K.; Yano J. *J. Electroanal. Chem.* **1994**, *364*, 179.

10. Hern, J. L.; Strohl, J. H. *Anal. Chem.* **1978**, *50*, 1954.

11. Deinhammer, R. S.; Shimazu, K.; Porter M. D. *Anal. Chem.* **1991**, *63*, 1889.

12. Deinhammer, R. S.;Ting, E.; Porter M. D. *J. Electroanal. Chem.* **1993**, *362*, 295.

13. Deinhammer, R. S.; Porter M. D.; Shimazu, K. *J. Electroanal. Chem.* **1995**, *387*, 35.

14. Deinhammer, R. S.;Ting, E.; Porter M. D. *Anal. Chem.* **1995**, *34*, 237.

15. Anson, F. C. *Acc. Chem. Res.* **1975**, 400.

16. Harrison, J. A.; Randles, J. E. B.; Schiffrin, D. J. *J. Electroanal. Chem.* **1970**, *25*, 197.

17. Devanathan,M. A. V.; Fernando, M. J. *J. Electroanal. Chem.* **1961**, *14*, 369.

18. Gierst, L.; Tondeur, J.; Nicolas,E. *J. Electroanal. Chem.* **1965**, *10*, 397.

19. Ho, M.; Porter, M. D. Manuscript in preparation.

CHAPTER 5. SURFACTANT MODIFIED EMLC PART II: MANIPULATION OF CHIRAL SEPARATION SELECTIVITY

A paper to be submitted to Science

Mankit Ho and Marc D. Porter

ABSTRACT

An approach for the modification of the selectivity of the stationary phase in electrochemically modulated liquid chromatography (EMLC)-based separation is described. The basis of the approach is that the amount of an organic additive adsorbed onto a stationary phase can be controlled by E_{app}. The viability of the method is demonstrated by the modification of the properties of an unmodified porous graphitic carbon (PGC) for the separation of optical isomers. In this report, β-cyclodextrin (CD) was used as the chiral selector and hexobarbital (HE) and mephenytoin (ME), two chiral pharmaceutical compounds, as the test molecules. The separation of the enantiomers of both HE and ME was realized with β-CD in the mobile phase. Moreover, the separation efficiency and the elution order of the enantiomers can be altered by E_{app}, which was affected by the dependence of the extent of immobilization of the additive onto the stationary phase. A model is then proposed for the mechanism of the separations.

INTRODUCTION

The separation of optical isomers is one of the most important tasks facing modern liquid chromatography [1-11]. Such separations are especially critical to pharmaceutical purposes because the therapeutic benefit of many compounds are enantiomerically specific. Most enantiomeric separations using liquid chromatography (LC) are performed at a stationary phase modified with a chiral selector [3-6]. However, because of the immense scope and the complexities of these separations, a wide variety of stationary-mobile phase combinations are required to meet the performance needs of this area.

Several groups [12-21] including ours [22-25] have recently been pursuing the development of a novel and versatile separation technique termed electrochemically-modulated liquid chromatography (EMLC). This technique allows the manipulation of the capacity factors of analytes by applying different potentials (E_{app}) to a conductive stationary phase [25]. We have further demonstrated that we can selectively and reversibly modify the properties of the stationary phase by the electrochemically induce deposition of an additive from the mobile phase [26]. The basis of the approach is that the amount of an organic additive adsorbed onto a stationary phase can be controlled by E_{app}, a process that in turn can be used to manipulate the surface properties of the stationary phase.

In this report, we extend the variants of EMLC by demonstrating how the properties of an unmodified porous graphitic carbon (PGC) column can be controlled with E_{app}, and how the deposition of a polar organic species onto the column can be used for the separation of optical isomers. For this purpose, we will use β-cyclodextrin (CD) as the chiral selector in the mobile phase and mephenytoin (ME) and hexobarbital (HE) as the test chiral molecules; two chiral pharmaceutical compounds that have been successfully separated at β-CD stationary phases [3-5]. Cyclodextrins are a family of oligomers that are composed of different numbers (6 for α-CD, 7 for β-CD, 8 for γ-CD and so on) of D(+)-glucopyranose units joined together through α(1', 4) linkages to form a donut-shaped structure. As a consequence of their structure, the cavities of the CDs are hydrophobic and the rim of the cavities are hydrophilic. Together, these two features facilitate the formation of inclusion complexes with a wide range of organic molecules. Furthermore, since CDs are optically active, the extent of binding within the cavity is dependent on the chirality of the guest. We will also show that the manipulation of E_{app} can be used to alter selectivity and to alter markedly the efficiency of the separation. A model is then proposed for the mechanism of the separations.

EXPERIMENTAL SECTION

Lithium perchlorate ($LiClO_4$) was from Aldrich, acetonitrile (HPLC grade), sodium phosphate and phosphoric acid (H_3PO_4) were from Fisher, α- and β-cyclodextrin were gifts from American Maize-Product Co, racemic mephenytoin (ME) was from U.S.P.C. Inc. and hexobarbital (HE) was from Sigma. The d-enantiomer of ME was from Toronto Research

Co. The d-enantiomer of HE was obtained by a separation of the racemate using a cyclodextrin stationary phase (Cyclobond 2000). All chemicals were used as received. Deionized water was obtained from a Millipore Milli-Q purification system.

The general design of the EMLC column and related instrumentation have been discussed elsewhere [25]. Briefly, the conductive stationary phase consisted of uncoated porous graphitic carbon (PGC) spheres (Shandon Chromatography) that were dispersed in a dibromoethane/acetonitrile (10/7, v/v) slurry and subsequently packed at 5000 psi into the EMLC column. After packing, the EMLC column was equilibrated with degassed mobile phase at a flow rate 0.90 mL/min until a stable detector baseline at 220 nm was obtained. Equilibration times between experiments were ~30 min. Analyte concentrations were ~500 ppm, and the injection volume was 0.5 µL.

THEORY/MODEL

As a basis for insight into these separations, Scheme 1 shows the range of equilibrium processes that are potentially involved in the separation of an analyte (A) with cyclodextrin (CD) as the mobile phase additive [27, 28], and how these processes may be affected by E_{app}.

Scheme I. Possible equilibria involved in the chromatographic

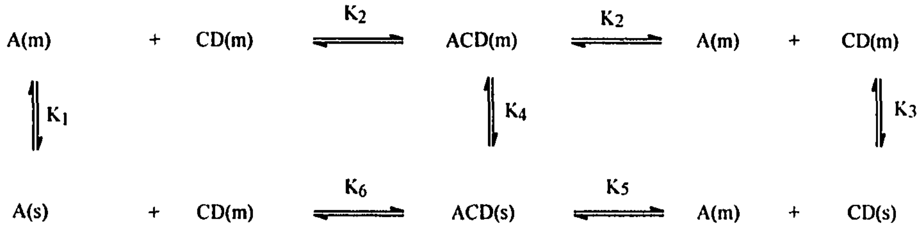
A(m)
+
CD(m)
K2
ACD(m)
K2
A(m)
+
CD(m)
K1
K4
K3
A(s)
+
CD(m)
K6
ACD(s)
K5
A(m)
+
CD(s)

The equilibrium constants for each process can be expressed as:

$$K_1 = \frac{[A(s)]}{[A(m)]} \qquad (1)$$

$$K_2 = \frac{[ACD(m)]}{[A(m)][CD(m)]} \qquad (2)$$

$$K_3 = \frac{[CD(s)]}{[CD(m)]} \qquad (3)$$

$$K_4 = \frac{[ACD(m)]}{[ACD(s)]} \qquad (4)$$

$$K_5 = \frac{[ACD(s)]}{[A(m)][CD(s)]} \qquad (5)$$

$$K_6 = \frac{[ACD(s)]}{[A(s)][CD(m)]} \qquad (6)$$

The capacity factor of (A) can be defined as:

$$k' = \phi \frac{[A(s)] + [ACD(s)]}{[A(m)] + [ACD(m)]} \qquad (7)$$

Where ϕ is the phase ratio, and equals the ratio of volume of stationary phase to that of mobile phase. Assuming that the uptake of ACD from the mobile phase is negligible, an assertion that reflects the preequilibration with CD prior to analyte injection, combination of equations (1)-(3) and (5), yields equation (8) as expression for the capacity factor:

$$k' = \phi \frac{K_1 + K_5 K_3 [CD(m)]}{1 + K_2 [CD(m)]} \qquad (8)$$

Importantly, the equilibrium processes for K_2 and K_5, which involve the complexation A with CD, will not be affected by E_{app}. In contrast, the processes in K_1 and K_3 will be dependent on E_{app}. The magnitude of K_1 and the effect of E_{app} will be dependent on the nature of the interactions between A and the stationary phase [29]. For cationic molecules, like the protonated forms of ME and HE, the value of K_1 increase as E_{app} becomes increasingly negative of the potential of zero charge (pzc) of the stationary phase, and decreases as E_{app} becomes increasingly positive of pzc. The same general trend is expected for the binding of CD to the stationary phase, based on the electron-donating properties of the hydroxyl functionalities of the CD, i.e., K_3 will increase above the pzc and decrease below the pzc.

RESULTS AND DISCUSSION

(A) Effect of E_{app} on the Retention of ME and HE. To evaluate the effect of E_{app} on the retention of ME and HE, separations were first performed without β-CD in the mobile phase. The mobile phase content is 80% aqueous 0.1 M $LiClO_4$ (20 mM phosphate buffer at pH ~ 2) and 20% acetonitrile. Figure 1 and 2 present the chromatograms of racemic mixtures of ME and HE, respectively, at E_{app} of -1.0 V, 0.0 V and +0.5 V (vs. Ag/AgCl (sat'd NaCl)). For both HE and ME, as E_{app} becomes increasingly negative, the retention of ME and HE increase. These trends are consistent with presence of the cationic forms of the analytes under these elution conditions. These dependences indicate that K_1 for both ME and HE becomes smaller as E_{app} becomes more positive. The retention dependences also reveal that ME is more strongly retained than HE at all values of E_{app}. For example, the retention time of ME at -1.0 V is ~10 min, whereas that of HE is ~8 min. The chromatograms also show that there is no detectable separation of the racemic mixtures.

(B) Effect of the Addition of β-CD in the Mobile Phase. Dramatic differences in the above separations are observed when β-CD is present as an additive in the mobile phase.

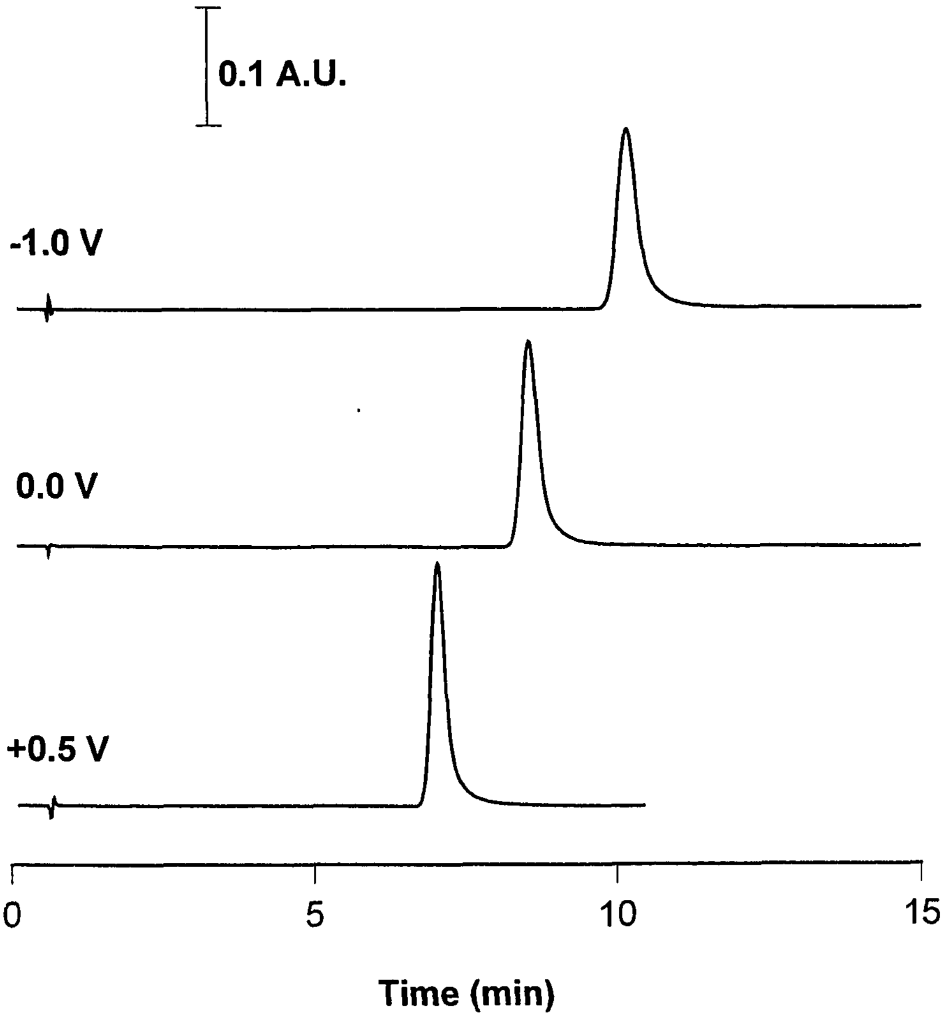

Figure 1: Chromatograms of ME at E_{app} -1.0 V, 0.0 V, and +0.5 V. The mobile phase consists of 20 % 0.1 M $LiClO_4$ in acetonitrile and 80 % aqueous with 0.1 M $LiClO_4$; 20 mM phosphate buffer. Flow rate was 0.9 ml/min. The detection wavelength is 220 nm.

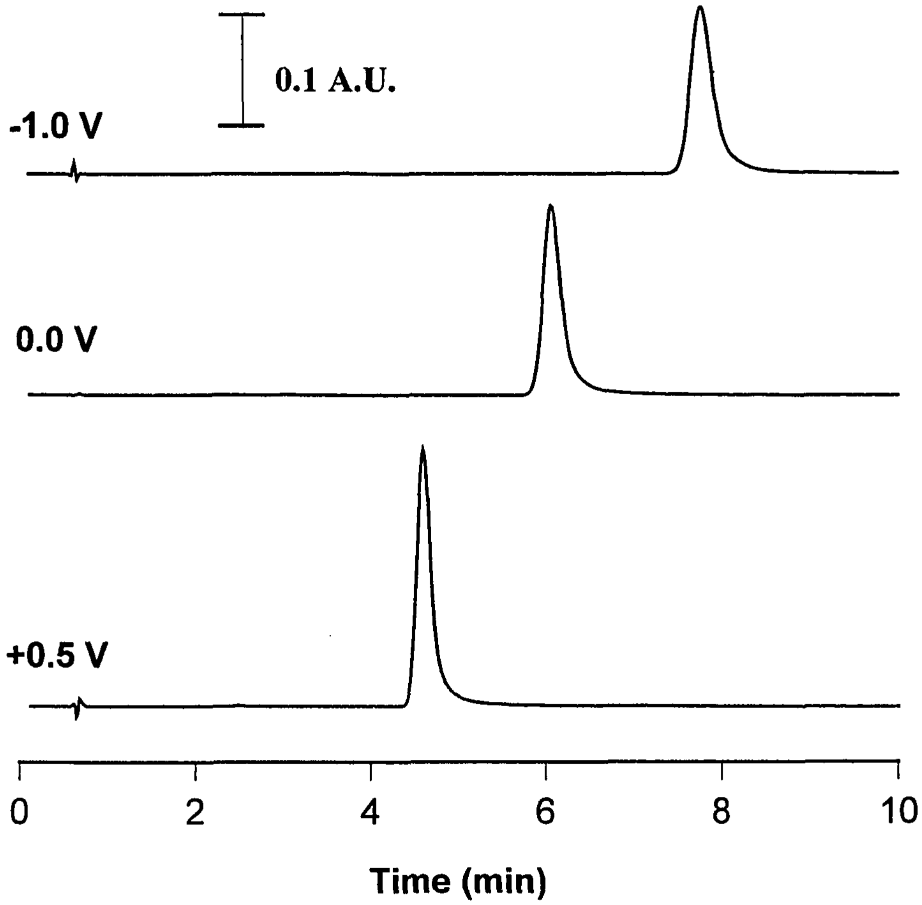

Figure 2: Chromatograms of HE at E_{app} -1.0 V, 0.0 V, and +0.5 V. The mobile phase consists of 20 % 0.1 M $LiClO_4$ in acetonitrile and 80 % aqueous with 0.1 M $LiClO_4$; 20 mM phosphate buffer. Flow rate was 0.9 ml/min. The detection wavelength is 220 nm.

Figure 3 shows the chromatograms of a mixture of the two enantiomeric forms of ME with the addition of a chiral selector (β-CD) to the mobile phase at several values of E_{app}. The mobile phase content is 80% aqueous 0.1 M $LiClO_4$ (20 mM phosphate buffer at pH ~ 2), 15 mM β-CD and 20% acetonitrile. The mixture contains an excess amount of the d-enantiomer of ME for the determination of the elution order. Under these conditions, the separation of the enantiomers is observed with the efficiency dependent on E_{app}. Importantly, the elution order of the two enantiomers is altered by E_{app}. The l-enantiomer of ME is retained longer when a negative potential (-1.0 V) is applied to the column, whereas the d-enantiomer of ME is retained longer at a more positive potential (+0.5 V). In comparison to the separations without β-CD (see Figure 1), the dependence of k' on the E_{app} follows the same general trend when β-CD is present, but the overall retention times are smaller. For example, the separation takes more than 10 min at an E_{app} of -1.0 V without β-CD, but only ~8 min with β-CD.

The same experiments were performed for the separation of a racemic mixture of HE. Figure 4 presents the chromatograms of HE with β-CD in the mobile phase. As found for ME, the separation of the two enantiomers of HE are realized. Though not shown, we find that elution order of the two enantiomers occurs for much more dilute mixtures where the d-enantiomer is present in a slight excess. At positive E_{app} (+0.5 V), the l-enantiomer is retained longer, whereas the d-enantiomer is retained longer at negative E_{app} (-1.0 V). Furthermore, the separation efficiency of the enantiomers is very high (α is 1.24 when E_{app} is +0.5 V). The chromatograms also show that, in opposition to that found for ME, the

Figure 3: Chromatograms of ME at E_{app} -1.0 V, -0.5 V, 0.0 V, and +0.5 V. The mobile phase consists of 20 % 0.1 M $LiClO_4$ in acetonitrile and 80 % aqueous with 0.1 M $LiClO_4$; 15 mM β-cyclodextrin; 20 mM phosphate buffer. Flow rate was 0.9 ml/min. The detection wavelength was 220 nm.

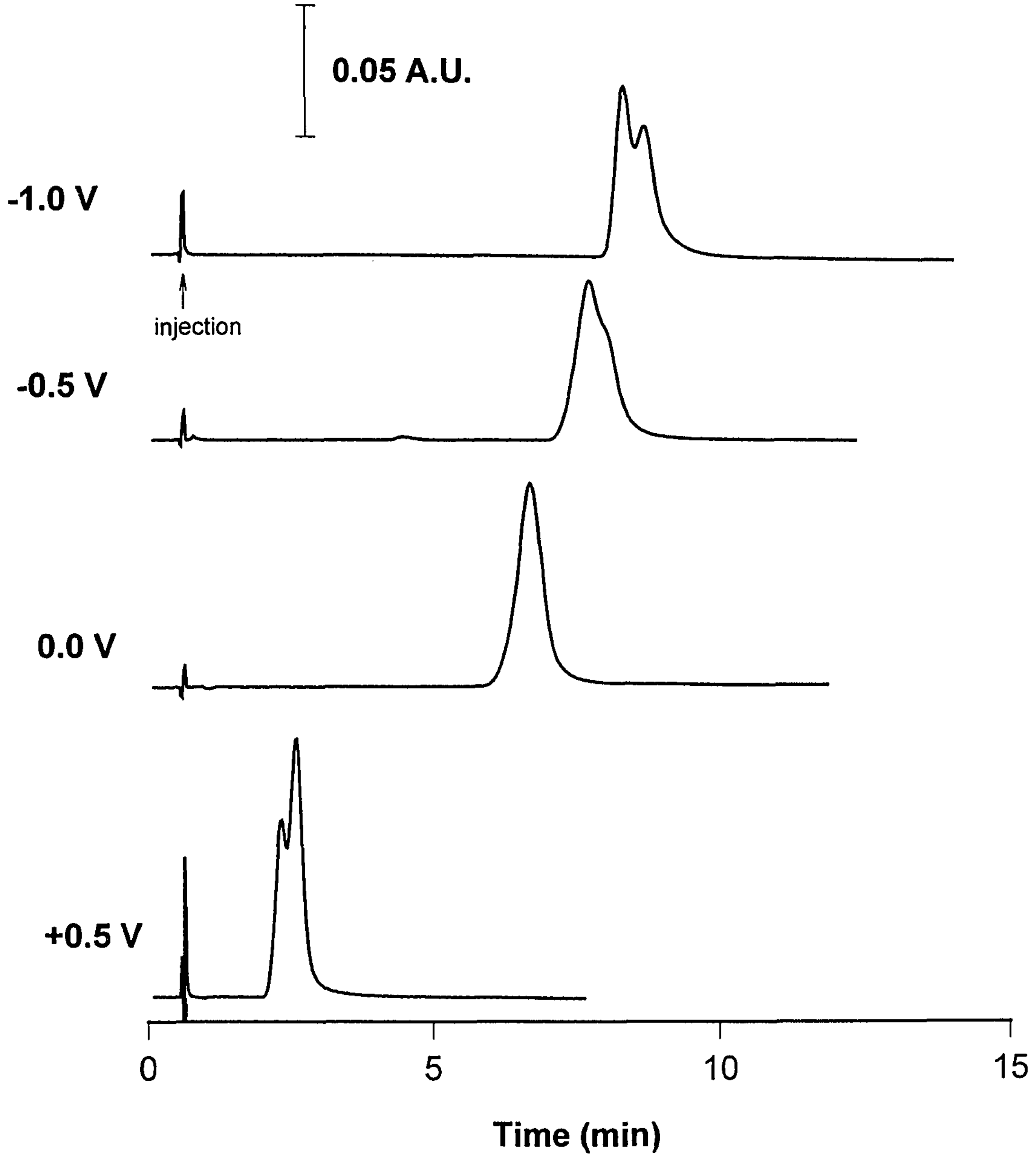
0.05 A.U.
-1.0 V
injection
-0.5 V
0.0 V
+0.5 V
0
5
10
15
Time (min)

Figure 4: Chromatograms of HE at E_{app} -1.0 V, -0.5 V, 0.0 V, and +0.5 V. The mobile phase consists of 20 % 0.1 M $LiClO_4$ in acetonitrile and 80 % aqueous with 0.1 M $LiClO_4$; 15 mM β-cyclodextrin; 20 mM phosphate buffer. Flow rate was 0.9 ml/min. The detection wavelength was 220 nm.

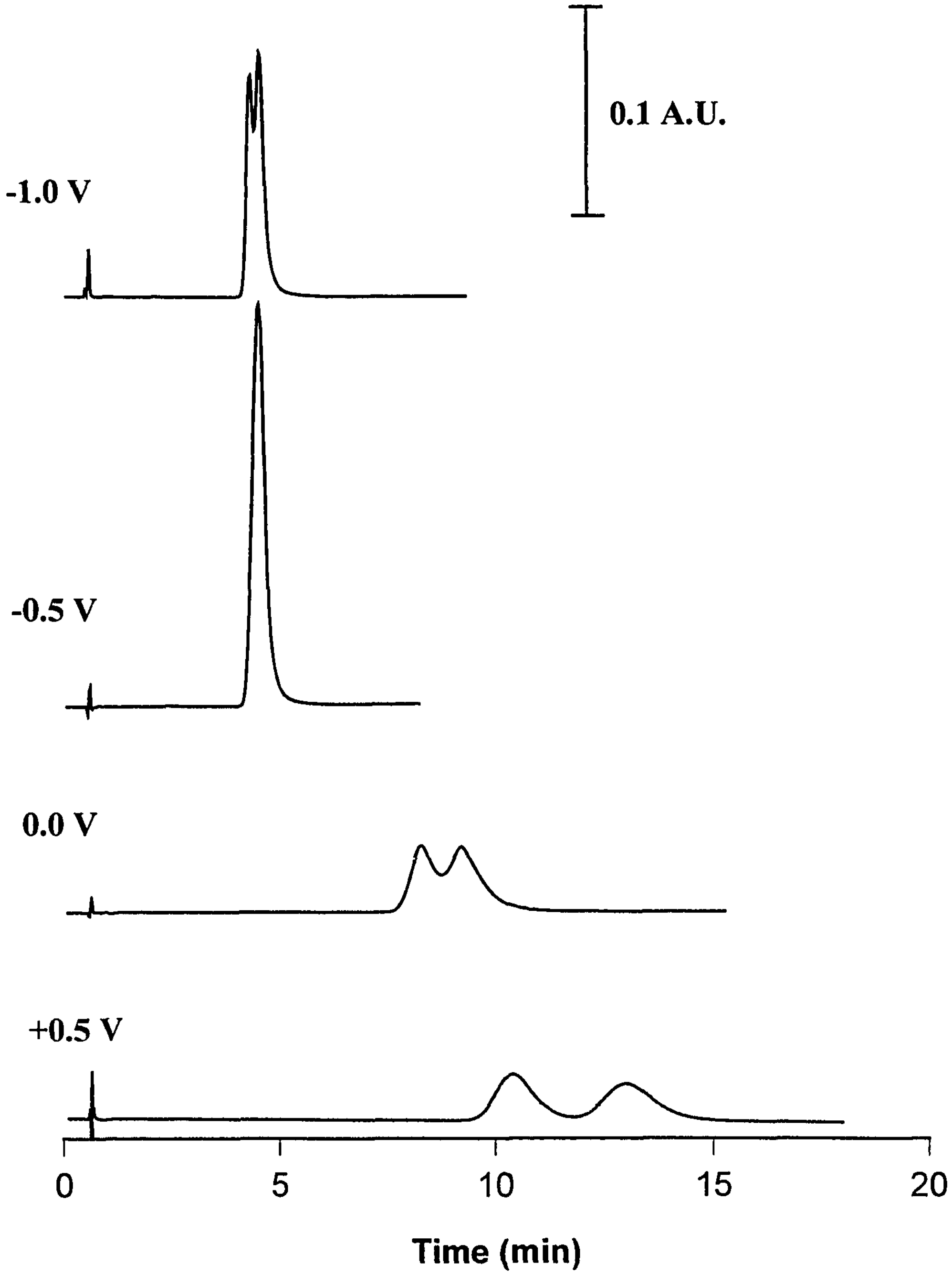
0.1 A.U.
-1.0 V
-0.5 V
0.0 V
+0.5 V
0
5
10
15
20
Time (min)

retention of HE exhibits a completely different dependence on E_{app}. That is, the retention is shorter at negative E_{app} (-1.0 V) than at more positive E_{app} (+0.5 V). The next section examines these observations within the context of a preliminary retention mechanism view of the equilibria given in Scheme 1 and summarized in equation (8).

(C) Discussion of the Separation Mechanism. As illustrated in the above section, the presence of β-CD has dramatic but differing effects on the retention of ME and HE. For ME, although the retention decreases in the presence of β-CD, the dependence of k' on E_{app} still follows the same trend as found without β-CD. In contrast the retention of HE shows a completely opposite dependence on E_{app} in the presence of β-CD. These observations can be explained by the difference in the relative magnitudes of K_1 and K_5 for ME and HE. As summarized by equation (8), the dependence of k' arises from the effect of E_{app} on K_1 and/or K_3. The data in Figures 1 and 2 show that K_1 increases at more negative values of E_{app}. The binding of β-CD, however, increases at more positive E_{app}, with K_3 then decreases as E_{app} becomes more negative. The effect of K_3 on k' is therefore through the formation of the complex via K_5. As such, the overall effect of E_{app} will be realized through the relative magnitudes of K_1 and K_5. If $K_1 > K_5$, the effect of the E_{app} will be dominated by variation of K_1, which is the case for the separation of ME. Therefore, the dependence of k' on E_{app} will be qualitatively the same with or without β-CD in the mobile phase. On the other hand if $K_5 > K_1$, the magnitude of K_3 will determine the change in k'. We therefore view the retention of HE as following the dependence of k' through the manipulation of K_3 by E_{app}.

To verify the above explanation, separations were performed with α-CD, the cyclodextrin with a smaller complexation constant with both ME and HE (i.e., small K_5 value), in the mobile phase. The mobile phase content is 80% aqueous 0.1 M $LiClO_4$ (20 mM phosphate buffer at pH ~ 2), 15 mM α-CD and 20% acetonitrile. Figures 5 and 6 present the chromatograms of racemic mixtures of ME and HE, respectively, at several values of E_{app}. As expected, the chromatograms show that there is no detectable separation of the racemic mixtures. More importantly, the dependences of k' on E_{app} for both ME and HE follow the same general trend as found for the separation of ME with β-CD in the mobile phase. The observations are in agreement with the trends predicted by the model when $K_1 > K_5$.

For the separation of the enantiomers, there are two key but opposing factors that are involved. As shown in Scheme 1, the preferential complexation of one of the enantiomers with β-CD will decrease its k', whereas the preferential complexation at the surface immobilized β-CD will increase the k' of the same enantiomer. The overall retention therefore will be the result of the combination of the two opposing complexation processes. We therefore can manipulate the extent of the complexation of the enantiomers at the surface of the carbonaceous stationary phase (K_5) by controlling the amount of immobilized β-CD (K_3). For example, as E_{app} becomes increasingly negative, the amount of immobilized β-CD will decrease. In this case, the effect of the preferential of one of the enantiomers with β-CD

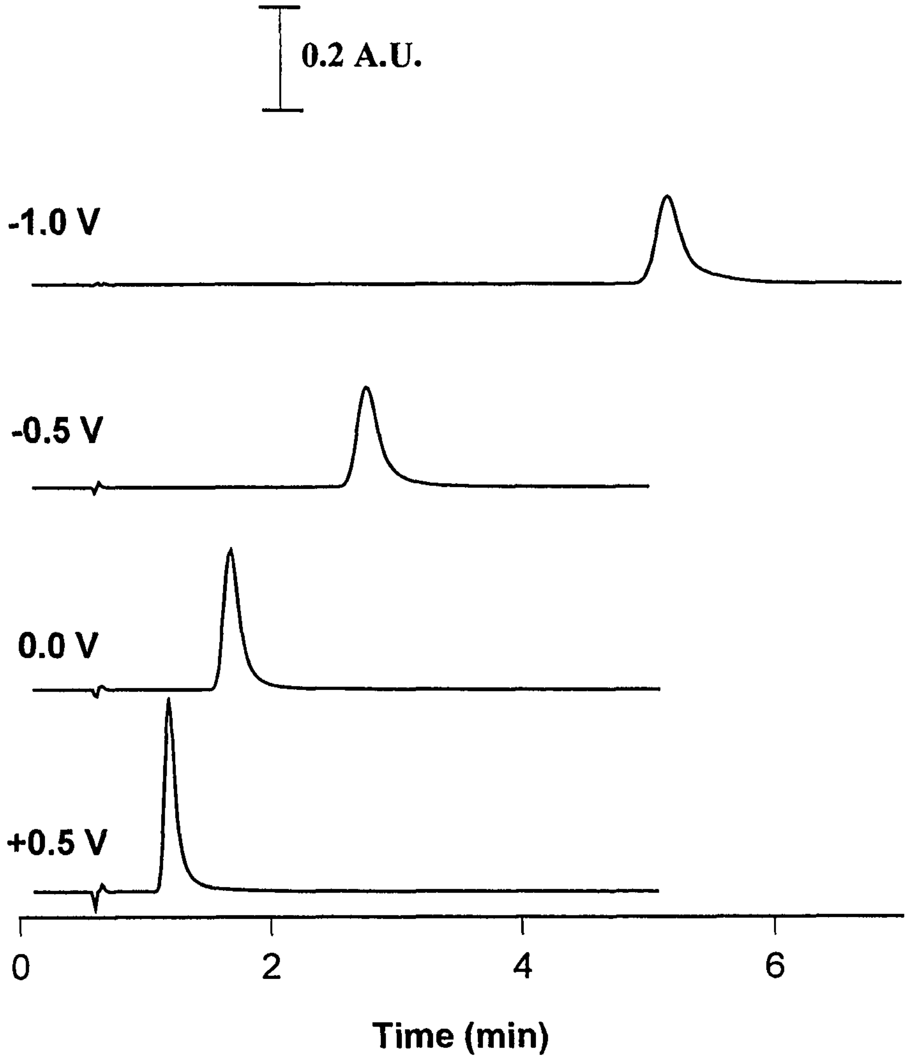

Figure 5: Chromatograms of ME at E_{app} -1.0 V, -0.5 V, 0.0 V, and +0.5 V. The mobile phase consists of 20 % 0.1 M $LiClO_4$ in acetonitrile and 80 % aqueous with 0.1 M $LiClO_4$; 15 mM α-cyclodextrin; 20 mM phosphate buffer. Flow rate was 0.9 ml/min.

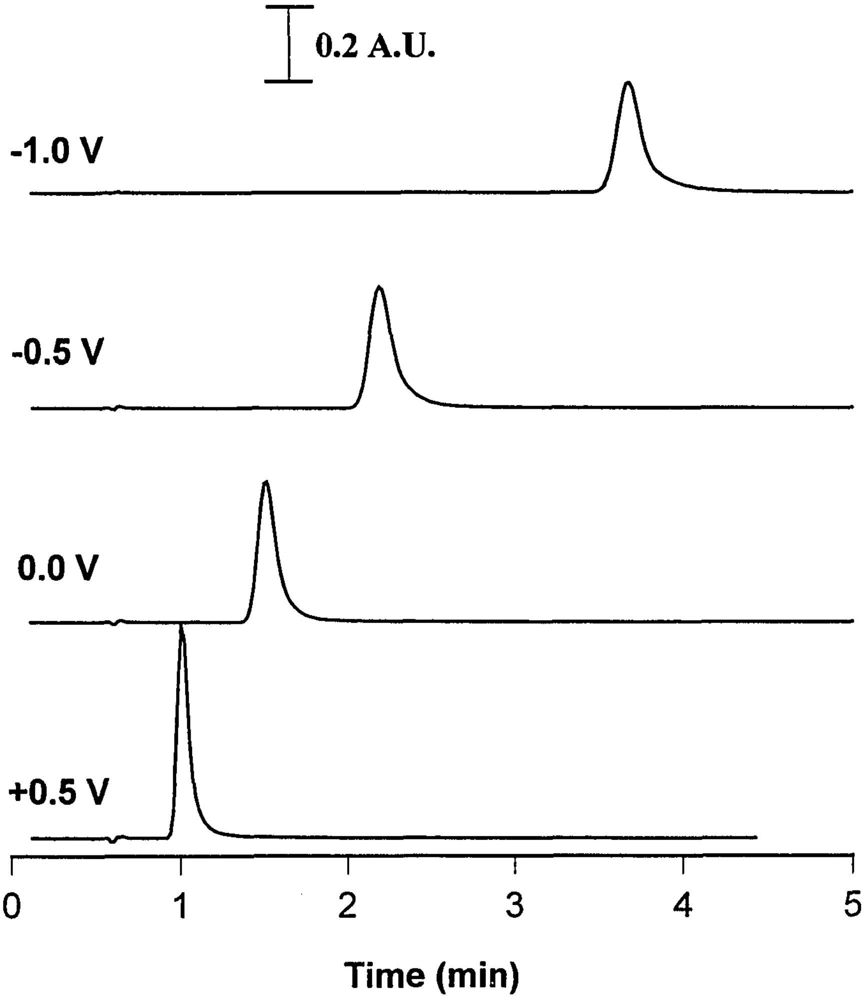

Figure 6: Chromatograms of HE at E_{app} -1.0 V, -0.5 V, 0.0 V, and +0.5 V. The mobile phase consists of 20 % 0.1 M $LiClO_4$ in acetonitrile and 80 % aqueous with 0.1 M $LiClO_4$; 15 mM α-cyclodextrin; 20 mM phosphate buffer. Flow rate was 0.9 ml/min.

in solution complexation will become increasingly important. In contrast, as E_{app} becomes more positive, the amount of immobilized β-CD will increase, and the effect of preferential complexation of one of the enantiomers at the stationary phase will become dominant.

The above analysis predicts that changes in E_{app} can alter the elution order of a pair of optical isomers, offering a viable explanation of the results in Figures 3 and 4. Thus, when a positive potential is applied (e.g., +0.5 V) to the stationary phase, the amount of immobilized β-CD increases, and the enantiomer that has the larger complexation constant with β-CD (i.e., the d-enantiomer of ME and l-enantiomer of HE) will be more strongly retained on the column. In the same way, if a more negative potential is applied to the column, the β-CD concentration at the surface of the stationary phase decreases. The enantiomer that has a larger complexation constant with β-CD will spend more time in the mobile phase and will elute before the more weakly complexed enantiomer.

CONCLUSION

This report has demonstrated the ability to modify and manipulate the chromatographic selectivity of a stationary phase by the electrochemically induced deposition of an organic additive to the mobile phase. The viability of the approach was demonstrated by the enantiomeric separation of two optical isomers of ME and HE using β-CD as the mobile phase additive. Moreover, the separation efficiency and the elution order of the enantiomers can be altered by E_{app}, which was affected by the dependence of the extent of immobilization of the additive onto the stationary phase. Thus, by carefully selecting the mobile phase additive, our approach offers the possibility of requiring only one column for the separation of a wide range of complex mixtures. Further experiments to explore the other potential applications of this new variant of EMLC are underway in our laboratory.

ACKNOWLEDGMENT

This work was supported by the National Science Foundation (Grant CHE-9003308) and by the Microanalytical Instrumentation Center at Iowa State University (ISU). The Ames Laboratory is operated for the U.S. Department of Energy by ISU under Contract W-7405-Eng-82.

REFERENCES

1. Davankov, V. A. *Adv. Chromatogr.* **1980**. *18*, 139-195.
2. Davankov, V. A.; Kurganov, A. A.; Bochkov, A. S. *Adv. Chromatogr.* **1980**, *22*, 71.
3. Armstrong, D. W.; Ward, T. J.; Armstrong, R. D.; Beesley, T. E. *Science* **1986**, *232*, 1132.
4. Armstrong, D. W.; Demond, W.; Alak, A.; Hinze, W. L.; Riehl, T. E.; Bui, K. *Anal. Chem.* **1985**, *57*, 234.

5. Hinze, W. L.; Riehl, T. E.; Armstrong, D. W.; Demond, W.; Alak, A.; Wrad, T. *Anal. Chem.* **1985,** *57,* 237.

6. Stalcup, A. M.; Chang, A.-C.; Armstrong, D. W. *J. Chromatogr.* **1991,** *540,* 113.

7. Sybilska, D.; Zukowski, J.; Bojarski, J. *J. Liq. Chromatogr.* **1986,** *9,* 591.

8. Gazda, M.; Szepesi, G.; Huszar, L. *J. Chromatogr.* **1988,** *436,* 31.

9. Armstrong, D. W. *J. Liq. Chromatgr.* **1984,** *7,* 591.

10. Ward, T. J. *Anal. Chem.* **1994,** *66,* 633A.

11. Novotny, M.; Soini, H.; Stefansson, M. *Anal. Chem.* **1994,** *66,* 646A.

12. Antrim R. F.; Yacynych, A .M. *Anal. Lett.* **1988,** *21,* 1085.

13. Ghatak-Roy A. R.; Martin C. R. *Anal. Chem.* **1986,** *58,* 1574.

14. Ge, H.; Wallace G. G. *J. Liq. Chromatogr.* **1990,** *13,* 3245.

15. Ge, H.; Teasdale, P. R.; Wallace G. G. *J. Chromatogr.* **1991,** *544,* 305.

16. Ge, H.; Teasdale, P. R.; Wallace G. G. *Anal. Chem.* **1989,** *61,* 2391.

17. Nagaoka, T.; Fujimoto, M.; Uchida, Y.; Ogura K. *J. Electroanal. Chem.* **1992,** *336,* 45.

18. Nagaoka, T.; Fujimoto, M.; Nakao, H.; Kakuno, K.; Yano J. *J. Electroanal. Chem.* **1993,** *350,* 337.

19. Nagaoka, T.; Fujimoto, M.; Nakao, H.; Kakuno, K.; Yano J. *J. Electroanal. Chem.* **1994,** *364,* 179

20. Hern, J. L.; Strohl, J. H. *Anal. Chem.* **1978,** *50,* 1954.

21. Antrim, R. F.; Scherrer, R. A. ; Yacynych, A. M. *Anal. Chim. Acta.* **1984,** *164,* 283.

22. Deinhammer, R. S.; Shimazu, K.; Porter M. D. *Anal. Chem.* **1991**, *63*, 1889.

23. Deinhammer, R. S.; Ting, E.; Porter M. D. *J. Electroanal. Chem.* **1993**, *362*, 295.

24. Deinhammer, R. S.; Porter M. D.; Shimazu, K. *J. Electroanal. Chem.* **1995**, *387*, 35.

25. Deinhammer, R. S.; Ting, E.; Porter M. D. *Anal. Chem.* **1995**, *34*, 237.

26. Ho, M.; Porter, M. D. To be submitted to *J. Electroanal. Chem.*.

27. Horvath, C.; Melander, W.; Molnar, I.; Molnar, P. *Anal. Chem.* **1977**, *49*, 2295.

28. Horvath, C.; Melander, W. *J. Chromatogr.* **1979**, *186*, 371.

29. Deinhammer, R. S. *Ph. D. Dissertation* **1994**, Iowa State University.

SUMMARY, DISCUSSION, AND PERSPECTIVE

This dissertation has examined several approaches for the manipulation of interfacial structures for the application to chemical analysis. Chapter 1 opens the possibility of the creation of interfacial structures with molecular recognition properties. We have synthesized two new thiol-containing cyclodextrins derivatives. The unique feature of the derivatives is the use of ethylene spacer groups that increase the flexibility for the thiol moieties to achieve registry with the preferred binding sites at the gold surface. Detailed studies to assess the effect of solvent and immersion time on monolayer formation were carried out. Characterizations by different surface sensitive techniques showed that the monolayers have an orientation with the cyclodextrin cavity along the surface normal when DMF is used as the solvent for monolayer formation. The molecular recognition properties of the monolayers were demonstrated by QCM experiments using hexane and tetrachloroethylene as probe molecules. However, several developmental issues need to be addressed to advance the fabrication of highly selective interfaces. First, the coverage data indicated that the surface is not covered with densely packed monolayers of the thiol-containing cyclodextrin. Defects in the monolayers will result in a nonspecific interaction and degrade performance in terms of selectivity. The co-adsorption of bulky alkylsulfur compounds (e.g., the dialkydisulfur) may be useful as a route to fill in the defect sites. Second, the derivatization of the cyclodextrin layer at the secondary hydroxyl groups along the rim of the cyclodextrin provides an accessible path for the construction of more chemically complex structures. It has been shown that the terminal hydroxyl group of monolayers can be easily modified by several reaction pathways (e.g., the reactions with acid chloride [50], acid anhydride [51] and epichlorohydrin [52]). Finally, another interesting structure modification would be the attachment of an electroactive moiety (e.g., ferrocene moieties [53, 54]) to the rim of the cyclodextrin cavity. Thus, the accessibility of ionic species to the cavity of the cyclodextrin could be controlled electrostatically by the oxidation and reduction of the ferrocenyl moiety.

Chapter 2 demonstrated that the interfacial structure can also play an important role in the potency of an immobilized catalysis. Two thiol-derivatized cobalt-porphyrins with different "expected" orientations at gold were synthesized. Voltammetric data showed that both monolayers catalyze the two-electron reduction of O_2 to H_2O but with different efficiencies. This difference was attributed to the result of the coplanar, inclined π-π interaction between adsorbates of the "one-legged" precursor, the structure of which hindered the accessibility of O_2 to the catalytically active sites. In order to unravel the viability of this assertion further, however, more definitive characterization of the interfacial structures of the two types monolayers are needed. In addition to the use of infrared, Raman, and visible spectroscopy, the use of scanning tunneling microscopy to image the two dimensional spatial arrangement of the layers may prove valuable. Another important issue is the effect of the micro-environment surrounding the immobilized metalloporphyrins. The micro-environment can , for example, be systematically manipulated through the construction of two-component monolayers containing the porphyrin adsorbate and various organosulfur compounds. The end-group and the length of the alkyl chain could be used to alter the hydrophobicity, hydrophility, and ionic nature of the micro-environments. Lastly, the fabrication of a co-facial type of metalloporphyrin monolayer may improve the catalytic potency of the monolayers [36, 37]. This exploration could be accomplished either by using a mixed monolayer to control the intermolecular distance between the porphyrin adsorbates or by the synthesis of thiol-derivatized cofacial porphyrins. Such a study should provide valuable insight into the construction of high efficiency fuel cells.

In Chapters 4 and 5, the feasibility of manipulating the selectivity of the stationary phase through the control of the adsorption/desorption of surfactant-like molecules in the mobile phase by the alteration of applied potential (E_{app}) was investigated. These studies are part of broad program in our group that investigates an electrochemical approach to manipulate the effective composition of the stationary phase and to fine-tune the resolution of liquid chromatographic separations. Although we have demonstrated in earlier work that capacity factors can be manipulated by E_{app} [47, 49], the separation of many classes of compounds (e.g., optical isomers) requires an extension of selectivity of the interaction available at the column. To modify the selectivity of the stationary phase, we investigated an approach using mobile phase modifiers. In these two chapters, we demonstrated the potential of an approach for the manipulation of the selectivity of the stationary phase by the electrosorption of surfactant-like species. In addition to the separation of a wide variety of complex mixtures, the method can also be used to study important fundamental phenomena in electrochemistry, such as the double layer structure at the electrode-solution interface [55, 56], the retention mechanism in EMLC [57-59], and the interaction between bound moieties and solution phase species [60].

In Chapter 4, the effect of different supporting electrolyte in the mobile phase was explored. The response of three alkylanilines (cationic molecules) to E_{app} was studied under two different cation-containing mobile phase systems. It was shown that the electrosorption of the alkylanilines behave differently at the negative end of the potential window. This difference was explained via the difference in the electrical double layer formed at the stationary phase. Detailed investigations of the role of the supporting electrolyte on the retention of different analtyes will undoubtedly be fruitful for the studies of the electrical double layer structures as well as the retention mechanism in EMLC-based separations. Such studies can be conducted by examining the retention behavior of wide variety of probe molecules (e.g., cationic, anionic, and neutral molecules) with systematic changes of the mobile phase composition (e.g., the composition and concentration of the supporting electrolyte).

Chapter 5 demonstrated the viability of a surfactant-modified EMLC column for the separation of optical isomers. Enantiomeric separations of two chiral pharmaceutical compounds (i.e., mephenytoin and hexobarbital) were realized using β-cyclodextrin as an additive in the mobile phase. Moreover, the elution order of the enantiomers were manipulated by E_{app}, a process not possible via conventional liquid chromatography. A simple model was proposed as a mechanistic explanation of the results based on the various interactions between the stationary phase, analytes, and the cylcodextrin. This work clearly demonstrated the potential application of EMLC as an approach to the separation of optical isomers. However, for such methods to become widely adopted, a considerable amount of developmental work remains. For chiral separations with β-cyclodextrin in the mobile phase, efforts to unravel the separation mechanism more quantitatively are needed. Such experiments include (1) the study of the retention of β-cyclodextrin as a function of E_{app}; (2) separations at different concentrations of cyclodextrin in the mobile phase; and (3) studies of the separation of structurally different chiral compounds. Work aimed at further expanding the role of E_{app} will also prove fruitful, and may include the synthesis of charge-containing cylcodextrin derivatives, since the effect of E_{app} on the immobilization of a charged species is greater than that on neutral species [57]. Besides using cyclodextrin as the chiral selector in the mobile phase, investigations of various different types of chiral selectors [61, 62] (for example bile salts [63, 63] and surfactant amino acids [65, 66]) would also be of clear interest. Together, the above studies should prove valuable in development of surfactant-modified EMLC, expanding the range and scope of this exciting new separation technique.

REFERENCES

1. Mallouk, T. E. and Harrison, D. J. Eds., *Interfacial Design and Chemical Sensing,* ACS Symposium Series 561, American Chemical Society, Washington, **1994.**
2. Ulman, A., *Introduction of Thin Organic Films: From Langmuir-Blodgett to Self-Assembly.* Academic Press, Boston, **1991**.
3. Bard, A. J.; Abruna, H. D.; Chidsey, C. E.; Faulkner, L. R.; Feldberg, S. W.; Itaya, K.; Majda, M.; Melroy, O.; Murray, R. W.; Porter, M. D.; Soriaga, M. P.; White, H. S. *J. Phys. Chem.* **1993**, *97,* 7147.
4. Steinberg, S.; Tor, Y.; Sabatani, E.; Rubinstein, I. *J. Am., Chem., Soc.* **1991**, *113*, 5176.
5. Sagiv, J. *J. Am. Chem. Soc.* **1980**, *102*, 92.
6. Kim, J. -H.; Cotton, T. M.; Uphaus, R. A. *J. Phys. Chem.* **1988**, *92*, 5575.
7. Porter, M. D. *Chem. Eng. News* **1989** (May 1), 32.
8. Rojas, M. T.; Koniger, R.; Stoddart, J. F.; Kaifer, A. E. *J. Am. Chem. Soc.* **1995**, *117*, 336.
9. Chailapakul, O.; Crooks, R. M. *Langmuir* **1995**, *11*, 1329.
10. Bilewicz, R.; Sawaguchi, T.; Chamberlain, R. V.; Majda, M. *Langmuir* **1995**, *11*, 2256.
11. Wang, J.; Wu, H.; Angnes, L. *Anal. Chem.* **1993**, *65*, 1893.
12. Kepley, L. J. Crooks, R. M.; Ricco, A. J. *Anal. Chem.* **1992**, *64*, 3191.

13. Schierbaum, K. D.; Weiss, T.; Thoden van Velzen, E. U.; Engbersen, J. F. J.; Reinhoudt, D. N.; Goepel, W. *Science* **1994,** *265*, 1413.

14. Carron, K. T.; Pelterson, L.; Lewis, M.; *Environ. Sci. Technol.* **1992**, *26*, 1950.

15. Fairbank, R. P.; Xiang, Y.; Wirth, M. J. *Anal. Chem.,* in press.

16. Nuzzo, R. G.; Allara, D. L. *J. Am. Chem. Soc.* **1983**, *105*, 4481.

17. Porter, M. D.; Bright, T. B.; Allara, D. L.; Chidsey, C. E. D. *J. Am. Chem. Soc.* **1987**, 8 *109*, 3559.

18. Bain, C. D.; Troughton, E. B.; Tao, Y. -T; Evall, J.; Whitesides, G. M.; Nuzzo, R. G. *J. Am. Chem. Soc.* **1989**, *111*, 321.

19. Biebuyck, H. A.; Whitesides, G. M. *Langmuir* **1993**, *9*, 1766.

20. Zhong, C. J.; Porter, M. D. *J. Am. Chem. Soc.* **1994**, *116*, 11616.

21. Whitesides, G. M.; Laninis, P. E. *Langmuir* **1990**, *6*, 87

22. Bain, C. D.; Whitesides, G. M. *J. Am. Chem. Soc.* **1989**, *111*, 7164.

23. Li, T. -T.; Weaver, M. J. *J. Am. Chem. Soc.* **1984**, *106*, 6107.

24. Chidsey, C. E. *Science* **1991**, *251*, 919

26. Rowe, G. K.; Creager, S. E. *Langmuir* **1991**, *7*, 2307.

27. Sun, L.; Kepley, L. J.; Crooks, R. M. *Langmuir* **1992**, *8*, 2101.

28. Sun, L.; Johnson, B.; Wade, T.; Crooks, R. M. *J. Phys. Chem.* **1990**, *94*, 8869.

29. Bilewicz, R.; Madja, M. *Langmuir* **1991**, *7*, 2794.

30. Bilewicz, R.; Madja, M. *J. Am. Chem. Soc.* **1991**, *113*, 5464.

31. Schierbaum, K. D.; Weiss, T.; Thoden van Velzen, E. U.; Engbersen, J. F. J.; Reinhoudt, D. N.; Goepel, W. *Science* **1994,** *265*, 1413.

32. Murray, R. E. *Electroanalytical Chemistry: A Series of Advances*; Bard, A. J., Ed.; Marcel Dekker: New York, 1984; Vol. 13, p. 191.

33. Forshey, P. A.; Kuwana, T. *Inorg. Chem.* **1983**, *22*, 699.

34. Van Galen, D. A.; Majda, M. *Anal. Chem.* **1988,** *60*, 1549.

35. Hutchison, J. E.; Postlethwaite, T. A.; Murray, R. W. *Langmuir* **1993**, *9*, 3277.

36. Durand, R. R.; Bencosme, C. S.; Collman, J. P.; Anson, F. C. *J. Phys. Chem.* **1987**, *217*, 271.

37. Ni, C. L.; Abdalmuhdi, I.; Chang, C. K.; Anson, F. C. *J. Phys. Chem.* **1987**, *91*, 1158.

38. Antrim, R. F.; Scherrer, R. A. ; Yacynych, A. M. *Anal. Chim. Acta.* **1984**, *164*, 283.

39. Antrim R. F.; Yacynych, A .M. *Anal. Lett.* **1988,** *21*, 1085.

40. Ghatak-Roy A. R.; Martin C. R. *Anal. Chem.* **1986,** *58*, 1574.

41. Ge, H.; Wallace G. G. *J. Liq. Chromatogr.* **1990**, *13*, 3245.

42. Ge, H.; Teasdale, P. R.; Wallace G. G. *J. Chromatogr.* **1991**, *544*, 305.

43. Nagaoka, T.; Fujimoto, M.; Uchida, Y.; Ogura K. *J. Electroanal. Chem.* **1992**, *336*, 45.

44. Nagaoka, T.; Fujimoto, M.; Nakao, H.; Kakuno, K.; Yano J. *J. Electroanal. Chem.* **1993**, 357.

45. Nagaoka, T.; Fujimoto, M.; Nakao, H.; Kakuno, K.; Yano J. *J. Electroanal. Chem.* **1994**, 364, 179

46. Deinhammer, R. S.; Shimazu, K.; Porter M. D. *Anal. Chem.* **1991,** *63,* 1889.

47. Deinhammer, R. S.; Ting, E.; Porter M. D. *J. Electroanal. Chem.* **1993,** *362,* 295.

48. Deinhammer, R. S.; Porter M. D.; Shimazu, K. *J. Electroanal. Chem.* **1995,** *387,* 35.

49. Deinhammer, R. S.; Ting, E.; Porter M. D. *Anal. Chem.* **1995,** *34,* 237.

50. Bertilsson, L.; Liedberg, B. *Langmuir* **1993,** *9,* 141.

51. Keller, H.; Schrepp, W; Fuchs, H. *Thin Solid Films* **1992,** *210/211,* 799.

52. Lofas, S.; Johnsson, B. *J. Chem. Soc., Chem. Commu.* **1990,** 1526.

53. Breslow, B.; Trainor, G.; Ueno, A. *J. Am. Chem. Soc.* **1983,** *105,* 2739.

54. Noble, W. J. le; Srivastava, S.; Breslow, B.; Trainor, G. *J. Am. Chem. Soc.* **1983,** *105,* 2745.

55. Tobias, H.; Soffer, A. *J. Electroanal. Chem.* **1983,** *148,* 221.

56. Oren, Y.; Tobias, H.; Soffer, A. *J. Electroanal. Chem.* **1984,** *162,* 87.

57. Deinhammer, R. S. *Ph. D. Dissertation* **1994,** Iowa State University.

58. Dill, K. A. *J. Phys. Chem.* **1987,** *91,* 1980.

59. Horvath, C.; Melander, W.; Molnar, I. *J Chromatogr.* **1976,** *125,* 129.

60. Horvath, C.; Melander, W.; Nahum, V *J Chromatogr.* **1979,** *186,* 371.

61. Ward, T. J. *Anal. Chem.* **1994,** *66,* 633A.

62. Novotny, M.; Soini, H.; Stefansson, M. *Anal. Chem.* **1994,** *66,* 646A.

63. Cole, R. O.; Sepaniak, M. J.; Hinze, W. L.; Gorse, J.; Oldiges, K. *J. Chromatogr.* **1991,** *557,* 113.

64. Nishi, H.; Fukuyama, T.; Matsuo, M.; Terabe,, S. *J Chromatogr.* **1990,** *515,* 233.

65. Cohen, A. S.; Paulus, A.; Karger, B. L. *Chromatographia* **1987**, *24*, 15.

66. Otsuka, K.; Terabe, S. *J. Chromatogr.* **1990,** *515*, 221.